INFORMATION TO USERS

This manuscript has been reproduced from the microfilm master. UMI films the text directly from the original or copy submitted. Thus, some thesis and dissertation copies are in typewriter face, while others may be from any type of computer printer.

The quality of this reproduction is dependent upon the quality of the copy submitted. Broken or indistinct print, colored or poor quality illustrations and photographs, print bleedthrough, substandard margins, and improper alignment can adversely affect reproduction.

In the unlikely event that the author did not send UMI a complete manuscript and there are missing pages, these will be noted. Also, if unauthorized copyright material had to be removed, a note will indicate the deletion.

Oversize materials (e.g., maps, drawings, charts) are reproduced by sectioning the original, beginning at the upper left-hand corner and continuing from left to right in equal sections with small overlaps. Each original is also photographed in one exposure and is included in reduced form at the back of the book.

Photographs included in the original manuscript have been reproduced xerographically in this copy. Higher quality 6" x 9" black and white photographic prints are available for any photographs or illustrations appearing in this copy for an additional charge. Contact UMI directly to order.

A generalized, parametric PR-QMF /wavelet transform design approach for multiresolution signal decomposition

Çağlar, Hakan, Ph.D.

New Jersey Institute of Technology, 1992

A Generalized, Parametric PR-QMF/Wavelet Transform
Design Approach for Multiresolution Signal Decomposition

by

Hakan Çağlar

Dissertation submitted to the Faculty of the Graduate School

of the New Jersey Institute of Technology in partial fulfillment

of the requirements for the degree of

Doctor of Philosophy

1991

APPROVAL SHEET

Title of Thesis: A Generalized, Parametric PR-QMF/Wavelet Transform
Design Approach for Multiresolution Signal Decomposition

Name of Candidate: Hakan Çağlar
Doctor of Philosophy, 1991

Thesis and Abstract Approved_____Date _____
Dr. Ali N. Akansu
Assistant Professor
Department of Electrical and Computer Engineering

Signature of other members   _____Date _____
of the thesis committee.   Dr. Rashid Ansari
Bell Communications Research
Morristown, New Jersey

_____Date _____
Dr. Yeheskel Bar-Ness
Professor
Department of Electrical and Computer Engineering

_____Date _____
Dr. Erdal Panayırcı
Professor
Department of Electrical and Computer Engineering

_____Date _____
Dr. John Tavantzis
Professor
Mathematics Department

VITA

Name: Hakan Çağlar

Degree and date to be conferred: Ph.D. Dec 6. 1991.

Secondary education: Izmit Lisesi.
                     Turkey. 1980

Collegiate institutions attended:	Date	Degree	Date of Degree
New Jersey Institute of Technology	1/88-12/91	Ph.D	Dec. 1991
Polytechnic University	1/86-12/87	M.Sc	Dec. 1987
Istanbul Technical University	9/80-5/84	B.Sc.	May 1984

Major: Electrical Engineering.

ABSTRACT

Title of Thesis: A Generalized, Parametric PR-QMF/Wavelet Transform
Design Approach for Multiresolution Signal Decomposition

Hakan Çağlar Doctor of Philosophy, 1991
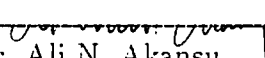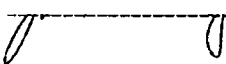
Thesis directed by: Dr. Ali N. Akansu

This dissertation aims to emphasize the interrelations and the linkages
of the theories of discrete-time filter banks and wavelet transforms. It is
shown that the Binomial-QMF banks are identical to the interscale coeffi-
cients or filters of the compactly supported orthonormal wavelet transform
bases proposed by Daubechies.

A generalized, parametric, smooth 2-band PR-QMF design approach
based on Bernstein polynomial approximation is developed. It is found that
the most regular compact support orthonormal wavelet filters, coiflet filters
are only the special cases of the proposed filter bank design technique.

A new objective performance measure called Non-aliasing Energy Ra-
tio(NER) is developed. Its merits are proven with the comparative per-
formance studies of the well known orthonormal signal decomposition tech-
niques.

This dissertation also addresses the optimal 2-band PR-QMF design prob-
lem. The variables of practical significance in image processing and coding
are included in the optimization problem. The upper performance bounds of
2-band PR-QMF and their corresponding filter coefficients are derived.

It is objectively shown that there are superior filter bank solutions avali-
able over the standard block transform, DCT. It is expected that the theo-

retical contributions of this dissertation will find its applications particularly in Visual Signal Processing and Coding.

Acknowledgement

I would like to express my apprecation to Dr. Ali N. Akansu for his support, knowledge and insight during my research at N.J.I.T. far in excess of reasonable expectations.

I would also like to express my thankfulness to Dr. Richard Haddad for contributing his knowledge.

Many thanks are due to the distinguished members of the committee: Dr. Rashid Ansari, Dr. Yeheskel Bar-Ness and Dr. John Tavantzis. Their encouragement and valuable discussion have improved the quality of this dissertation.

The author would also like to thank the valuable members of the electrical and the computer engineering deparment for their help and continuous support.

I would also like to extend a special thanks to my sister and my family. Many thanks go to my friends, Kemal Sis and all my friends, for their selfless dedication and generous support.

Sevgili anneme, babama

ve kardeşime

To my Parents

Contents

List of Figures

List of Tables

Chapter 1

Introduction

Recent advances in semiconductor devices have made visual communications a reality. It is predicted that this technological advance will find most of its commercial applications within this decade along with the extensive provision of ISDN services to the customers.

The concept of multiresolution has been widely recognized as a useful tool in Machine Vision. More recently, this signal processing technique has also been studied for Image-Video Coding applications. It is commonly agreed that standards of the next generation Image-Video Codecs will provide this desired feature inherently. Two-band filter banks have been employed in the literature as the basic component of hierarchical filter banks, particularly for Visual Signal Processing. This dissertation studies the filter bank theory in depth, and proposes several novel filter bank design approaches. It also examines their practical merits.

We first describe a class of orthogonal binomial filters which provide a set of basis functions for a bank of perfect reconstruction finite impulse response quadrature mirror filters(PR-QMF FIR). These Binomial QMFs are shown to be the same filters as those derived from a discrete orthonormal wavelet approach by Daubechies. These filters are the unique maximally-flat magnitude square PR-QMFs. We emphasize the strong linkage between the popular wavelet transform theory and the

well established filter banks theory.

A generalized, parametric PR-QMF design technique based on Bernstein polynomial approximation is developed in the next chapter. The parametric nature of this solution provides useful insights to the PR-QMF problem. Several well-known orthonormal wavelet filters, most regular filters, Coiflet filters, Daubechies wavelet filters, PR-QMFs, are all shown to be the special cases of the proposed technique. Any orthonormal PR-QMF can be designed with this technique. The filter examples we considered are smooth and ripple-free. This approach can also be easily applied for rippled QMF design problems. This design technique yields a simple tool to relate the features of the filter bank to be designed and its corresponding wavelet transform basis.

Furthermore we present an analysis of band energy distributions in perfect reconstruction(PR) multirate systems and evaluates the effects of aliasing. A performance measure called Non-Aliasing Energy Ratio(NER) is defined. The merit of the new measure is emphasized with the performance comparisons of the popular block transforms and 2-band PR-QMF based filter banks. It is shown that the new measure complements the energy compaction measure used widely in the literature.

A multivariable optimization problem is formulated to design optimum 2-band PR-QMFs in the last part of this dissertation. The energy compaction, aliasing energy, step response, zero-mean high-pass filter, uncorrelated subband signals, constrained nonlinearity of the phase-response, and the given input statistics are simultaneously considered in the proposed optimal filter design technique. A set of optimal PR-QMF solutions and their optimization criteria along with their objective performance are given for comparison. This PR-QMF design approach leads to an input-driven adaptive subband filter bank structure. It is shown that these optimal filters objectively outperform the well-known fixed PR-QMFs and the standard

Discrete Cosine Transform, DCT, in the literature. It is expected that these new PR-QMFs are also subjectively superior to the latter in image and video coding applications and will be used in practice.

Chapter 2

Subband Signal Decomposition

2.1 Introduction

In many signal processing applications which involve storage and transmission of digital signal there is a need for source compression. Subband coding has emerged as one of the suitable techniques for satisfying these needs[1][2][3]. The principles of subband coding have been successfully applied first in one-dimensional signals like speech, and then 2-D signals like still images and video, at the medium and low bit rates[4][5][6].

The subband signal decomposition has become a very popular transform recently, because of its mathematical flexibity. Its main advantage over the block transforms comes from the arbitrary duration of its basis functions or band-pass filters compared to the fixed duration in block transforms or block filter banks. This fact will be exploited later in Chapter 7 for the optimal design of PR-QMFs.

The most meaningful application of subband coding is in visual signal processing, since it provides the multiresolution signal representation inherently. Subband image coding decomposes the input image into relatively narrow subbands where each of these subband signals are decimated and encoded. The bit allocation among subband signals are accurately matched to the statistics of subbands[7]. At the receiver side, these subbands are decoded, interpolated, and added together to

4

obtain the reconstructed image. The underlying principle for the coder is that the bit allocation can be optimized such that those subbands with more significance get more bits allocated. The advantages of subband coding can be viewed from several different points of view. The most common one focuses on the perceptual merits of this technique. Since the human visual system (HVS) responds differently to the quantization noise in different spectral subbands, it is clearly advantageous to be able to control the spectral shape of the noise. This is achievable by coding the signal in independent subbands. Another aspect of the subband technique is more fundamental from data compression point of view. This method transforms the signal into subband domain in which the energy of the signal is distributed unevenly among subbands. This energy pattern is used efficiently for controlling the allocation of available bits[7]. If the adjacent subbands have small or negligible energy leakage, then the noise introduced with the quantization will be confined to that band. This allows to control the spectral shape of the quantization noise in the reconstructed signal. Waveform coding techniques such as PCM, DPCM, or vector quantization are used for coding of subbands.

In this chapter, we first present the downsampling and upsampling operations which are the basic building blocks of multirate digital signal processing. This is followed by polyphase signal representation and its application in multirate filter banks. Then, we derive the two-channel Perfect Reconstruction Quadrature Mirror Filter (PR-QMF) bank requirements. In the next section, we extend the subband idea for 2-D signals with separable and non-separable filter banks. The following section derives the equivalent parallel realization of cascaded tree structures, and discusses different subband trees. Then, the last section of this chapter explains the idea of Laplacian Pyramid for signal decomposition and derives the necessary and sufficient conditions on filters in order to achieve the critical sampling rate.

5

This new pyramidal structure with critical sampling is called Modified Laplacian Pyramid and its relations with the biorthogonal 2-band filter banks are also shown in this section.

2.2 Multirate Digital Signal Processing

In recent years, there has been tremendous progress in multirate processing of digital signals which found its applications, in communications, speech and image processing, spectral analysis, radar systems, antenna systems and others[8][9][10][11][12]. Unlike the single-rate systems, the sample spacing varies in multirate systems from point to point. That is why more efficient processing of signals can be achieved with this approach. Unfortunately, the change of sample rate results with the introduction of a new type of error, i.e., aliasing. The aliasing error should somehow be cancelled since the perfect reconstruction of the signal is the main objective of filter bank structure[10][11][12][13][14].

The basic building blocks in a multirate digital signal processing are downsampling and upsampling operations. In the next section, we introduce these basic multirate building blocks, along with their time and frequency domain characterizations, and their interrelations[10][11]. Fig. 2.1 displays two-channel QMF bank and implies the functions of downsampling and upsampling operations.

2.2.1 Downsampling and Upsampling

The process of down-sampling by an integer factor of M is characterized by the input output relation in time domain

$$y_D(n) = x(Mn) \tag{2.1}$$

The relation indicates that the output at time n is equal to the input at time Mn. As a consequence of this, only the input samples with the indices equal to the

6

multiples of M are retained. A downsampler takes sequence $x(n)$ as input and outputs time-compressed sequence $y_D(n)$. The compression ratio M is an integer. This operation is denoted by the downward arrow (indicative of down sampling). The sampling rate reduction of $M = 2$ is demonstrated as an example in Fig. 2.2.
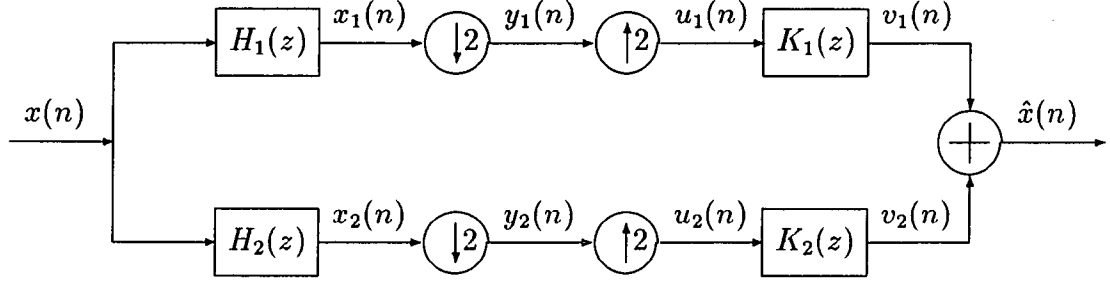
Fig. 2.1 Two-Channel QMF Bank.

Since the downsampling corresponds to a compression in time domain, one should expect a stretching effect in frequency domain. The Fourier domain description of downsampler is given as

$$Y_D(e^{j\omega}) = \frac{1}{M} \sum_{k=0}^{M-1} X(e^{j(\frac{\omega-2k\pi}{M})}) \tag{2.2}$$

It can also be expressed in z domain as

$$Y_D(z) = \frac{1}{M} \sum_{k=0}^{M-1} X(z^{1/M}W^k) \tag{2.3}$$

where $W = e^{-j\frac{2\pi}{M}}$. $X(e^{j\omega})$ and $Y_D(e^{j\omega})$ are the Fourier transforms of the input signal $x(n)$ and the downsampled output signal $y_D(n)$, respectively. The term with $k = 0$ is indeed the M-fold stretched version of $X(e^{j\omega})$. $M - 1$ terms for $k > 0$ are uniformly frequency shifted versions of this stretched spectrum. These M terms together make up a function with period of 2π in ω. The sum of terms with $k > 0$ are called the aliasing. The overlapping areas of the bottom part of Fig. 2.2 indicate the aliasing error due to subsampling. As long as the input signal $x(n)$ has a

bandwidth of $[\frac{-\pi}{M}, \frac{\pi}{M}]$ no aliasing errors will occur[11].

$$x(n) \longrightarrow \boxed{\downarrow M} \longrightarrow y_D(n) = x(Mn)$$
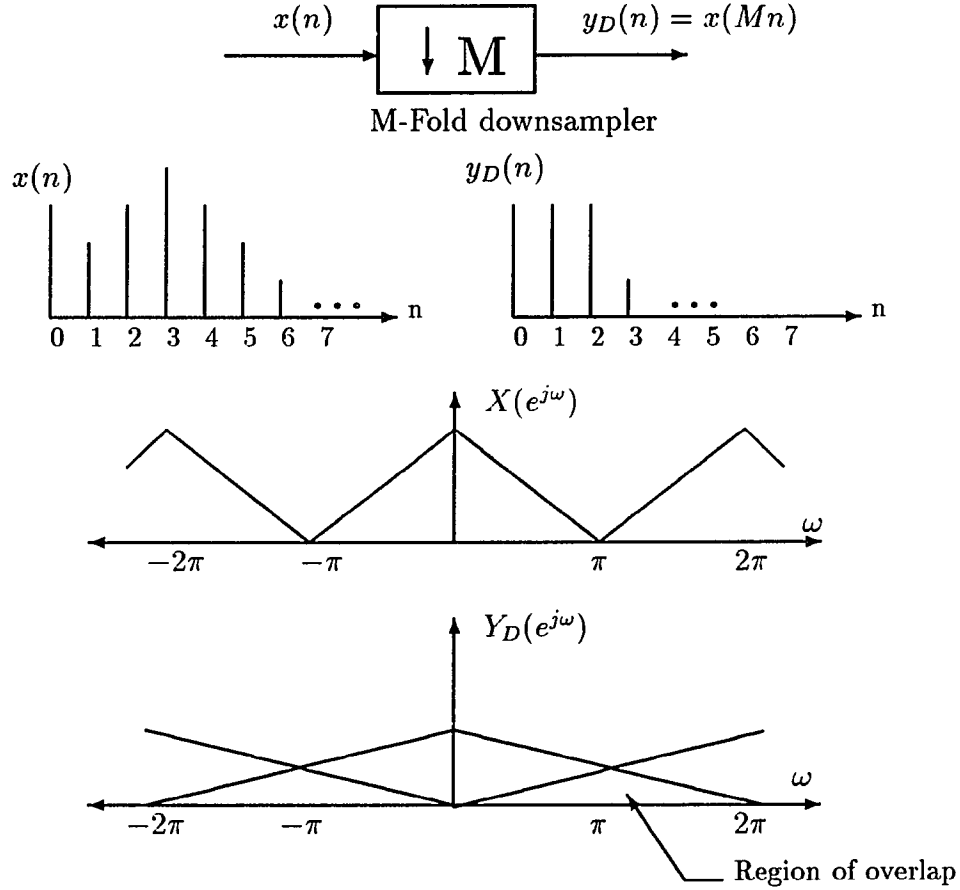
M-Fold downsampler

Fig. 2.2. Downsampler operation for $M = 2$.

Similarly, an L-fold upsampling is characterized by the input output time relation

$$y_I(n) = \begin{cases} x(\frac{n}{L}) & \text{if n is a multiple of L} \\ 0 & \text{otherwise} \end{cases} \tag{2.4}$$

That is, the output signal is obtained by inserting $L-1$ zero valued samples between adjacent samples of $x(n)$. An upsampler is given in Fig. 2.3 for $L = 2$. The input output relation of an upsampler in Fourier domain is shown as

$$Y_I(e^{j\omega}) = X(e^{j\omega L}) \quad \text{and}$$

8

$$Y_I(z) = X(z^L) \quad \text{in z-domain} \qquad (2.5)$$

i.e $Y_I(e^{j\omega})$ is an L-fold compressed version of $X(e^{j\omega})$. The multiple copies of the basic spectrum, called imaging effect and its extra copies are created by the upsampler. An upward arrow with L indicates L-fold upsampler. The effect of stretching in time is a compression in frequency domain. Thus, $L - 1$ images of the original spectrum are caused with this operation. The imaging effect is the dual of aliasing effect caused by the downsampler. The images in the output of the upsampler are usually removed by the properly chosen interpolation filter.
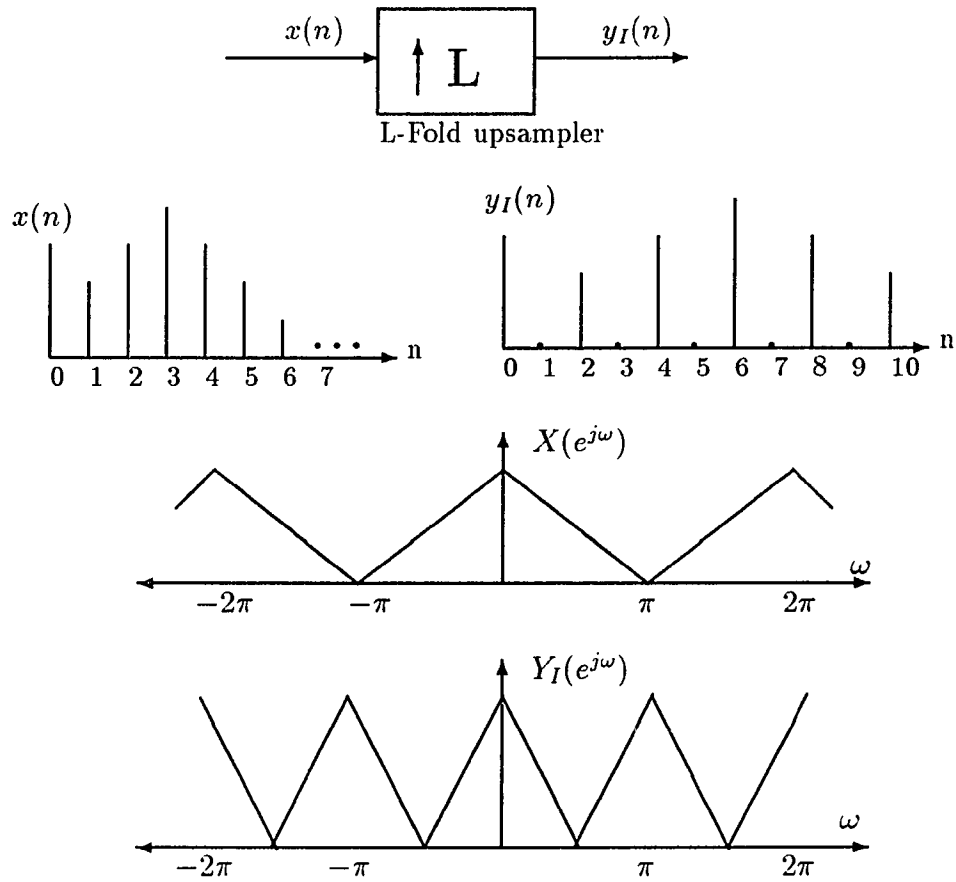
Fig. 2.3. Upsampler operation for $L = 2$.

Even though downsampler and upsampler are linear systems, they are time varying. Accordingly, they can not be represented by transfer function[10][11].

The fundamental difference between aliasing and imaging is important. Aliasing can cause loss of information because of the possible overlapping of the spectra. Imaging, on the other hand, does not lead to any loss of information. This is consistent with the fact that no time domain samples are lost.
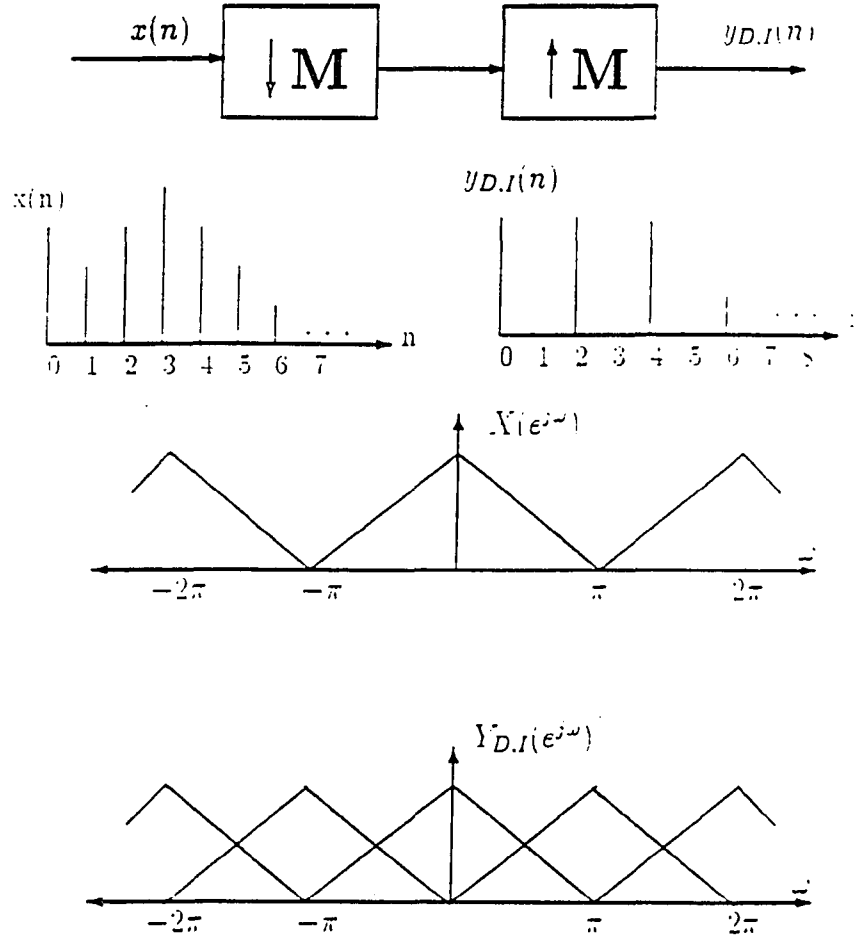
Fig. 2.4. Downsampler followed by upsampler for $M = 2$.

It is important to analyze the multirate structure where a downsampler and an upsampler are cascaded. The downsampler causes aliasing. whereas the upsampler causes imaging. all in frequency domain. Fig. 2.4 shows a cascade connection of down upsampler which is encountered in a typical filter bank. The signal $y_{D.I}(n)$ is equal to $x(n)$ whenever n is a multiple of M. and zero otherwise

$$y_{D.I}(n) = \begin{cases} x(n) & \text{if } n \text{ is a multiple of } M \\ 0 & \text{otherwise} \end{cases} \qquad (2.6)$$

10

The input-output relation of this cascaded down upsampler structure is found in z domain as

$$Y_{D,I}(z) = \frac{1}{M} \sum_{k=0}^{M-1} X(zW^k) \qquad (2.7)$$

This means that $MY_{D,I}(e^{j\omega})$ is the sum of $X(e^{j\omega})$ and its $M-1$ uniformly frequency shifted versions $X(e^{j(\omega - \frac{2\pi k}{M})})$ $k = 1, 2, \cdots, M-1$. From Fig. 2.4 we see that $x(n)$ can be recovered from $y_{D,I}(n)$ if there is no frequency overlapping. If the anti-aliasing filter which precedes the downsampler is not proper (i.e. the Nyquist condition for the rate change is not met), aliasing occurs at the output of downsampler. Therefore $x(n)$ can not be recovered perfectly. Notice that the $x(n)$ can be recovered perfectly if the total band with of $X(e^{j\omega})$ be less than $2\pi/M$. It is not necessary for $X(e^{j\omega})$ to be restricted to $|\omega| < \pi/M$.

A different type of cascade down/upsampler structure is shown in Fig. 2.5. It should be noticed that the two building blocks in Fig. 2.5.a and Fig. 2.5.b are not equivalent in general. For example, for $M = L$, the system of Fig. 2.5.a is an identity system, whereas the system of Fig. 2.5.b causes a loss of $M-1$ samples out of M samples. It can be shown that these systems are identical if and only if L and M are relatively prime numbers[10][11].
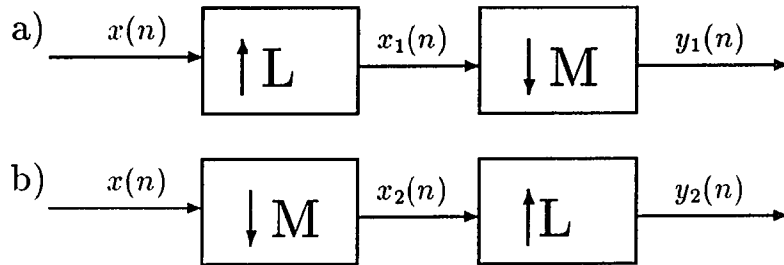
Fig. 2.5. Two different structures to cascade downsampler and upsampler

a) Identity system.

b) Loss of $M-1$ samples of M input samples.

11

2.3 Polyphase Decomposition

The polyphase decomposition, first introduced by Bellanger[12], is fundamental to many applications in multirate digital signal processing. A few examples of these efficient real time applications of decimation-interpolation are in fractional sampling rate transformers, uniform DFT filter banks, and perfect reconstruction analysis/synthesis systems.

It is possible to represent the system function of a digital filter, $H(z) = \sum_n h(n)z^{-n}$ in M component polyphase form as

$$H(z) = \sum_{k=0}^{M-1} G_k(z^M)z^{-k} \qquad (2.8)$$

where $\{G_k(z)\}$ are called the polyphase components and defined by

$$G_k(z) = h(k) + h(k+M)z^{-1} + h(k+2M)z^{-2} + \cdots \qquad (2.9)$$

The impulse response of the kth polyphase filter is simply an M-fold downsampled version of $h(n)$,

$$g_k(n) = h(Mn+k), \qquad k = 0, 1, ..., M-1 \qquad (2.10)$$

Note that for a given $H(z)$, the polyphase components, $G_k(z)$, depend on M. In most of the applications M is fixed, therefore we will not use M as the second subscript in notation (such as $G_{k,M}(z)$).

Since $g_0(n)$ is the M-fold downsampled version of $h(n)$, from Eq.(2.2) we can write it in z domain

$$G_0(z) = \frac{1}{M} \sum_{k=0}^{M-1} H(z^{1/M}W^k) \qquad (2.11)$$

or equivalently,

$$G_0(z^M) = \frac{1}{M} \sum_{k=0}^{M-1} H(zW^k) \qquad (2.12)$$

12

This is an important property of M component polyphase form. Note that the representation of Eq.(2.8) holds whether $H(z)$ is FIR or IIR. Additionally, it is important to note that the polyphase decomposition can be applied to any sequence $x(n)$.

2.4 Two-Channel Filter Banks

The spectrum of input signal $X(e^{j\omega})$, $0 \leq \omega \leq \pi$, is divided into two equal bandwidth sub-spectra or subbands in this filter bank structure given in Fig. 2.1. The filters $H_1(z)$ and $H_2(z)$ of Fig. 2.1 function as anti-aliasing filters, while $K_1(z)$ and $K_2(z)$ function as interpolation filters. Since the whole spectrum is divided into two equal bands, from Nyquist theorem the signals $x_1(n)$ and $x_2(n)$ are down sampled by two which yield subband signals $y_1(n)$ and $y_2(n)$. In turn, the synthesis stage starts with the upsampling of subband signals by two and interpolating these signals, $u_1(n)$ and $u_2(n)$, with the interpolation filters $K_1(z)$ and $K_2(z)$ respectively. The interpolated subband signals $v_1(n)$ and $v_2(n)$ are added to obtain the reconstructed signal $\hat{x}(n)$. The down/upsamplers cause aliasing and imaging effects respectively as discussed earlier. Therefore the synthesis filters $K_1(z)$ and $K_2(z)$ should be chosen such that the imaging terms cancel the aliasing terms for the perfect reconstruction. In fact, this is possible.

The conditions for perfect reconstruction in the prototype two-channel FIR-QMF banks have been studied extensively in the literature[10][11][12][13][14][15]. These conditions will be re-derived here in the frequency domain and also their time domain relations will be found. Time domain PR conditions are more tractable than the frequency domain versions especially in M-band filter bank design problems.

Tracing the signals with the help of Fig. 2.1 through the top branch in z

domain gives

$$X_1(z) = H_1(z)X(z)$$

$$V_1(z) = K_1(z)U_1(z) \tag{2.13}$$

as the outputs of the decimation and interpolation filters respectively. The down-sampler and upsampler impose

$$Y_1(z) = \frac{1}{2}[X_1(z^{1/2}) + X_1(-z^{1/2})]$$

$$U_1(z) = Y_1(z^2) \tag{2.14}$$

Combining all these yields the interpolated subbands

$$V_1(z) = \frac{1}{2}K_1(z)[H_1(z)X(z) + H_1(-z)X(-z)] \tag{2.15}$$

$$V_2(z) = \frac{1}{2}K_2(z)[H_2(z)X(z) + H_2(-z)X(-z)] \tag{2.16}$$

The z-transform of the reconstructed signal, is then the summation of these as

$$\begin{aligned}
\hat{X}(z) &= \frac{1}{2}[H_1(z)K_1(z) + H_2(z)K_2(z)]X(z) \\
&\quad + \frac{1}{2}[H_1(-z)K_1(z) + H_2(-z)K_2(z)]X(-z) \\
&= T(z)X(z) + S(z)X(-z)
\end{aligned} \tag{2.17}$$

Perfect reconstruction requires:

(i) $\quad S(z) = 0, \quad$ for all z

(ii) $\quad T(z) = cz^{-n_0}, \quad c$ is a constant $\tag{2.18}$

The term containing $X(-z)$ which is the alias component, vanishes if one chooses

$$K_1(z) = H_2(-z)$$

$$K_2(z) = -H_1(-z) \tag{2.19}$$

14

then

$$S(z) = 0 \quad \text{for all } z \tag{2.20}$$

the first requirement is satisfied, $S(z) = 0$. Since aliasing is cancelled then the linear time-varying(LTV) system becomes a linear time-invariant(LTI) system with the transfer function

$$T(z) = \frac{\hat{X}(z)}{X(z)} = \frac{1}{2}[H_1(z)K_1(z) + H_2(z)K_2(z)] \tag{2.21}$$

which represents the distortion caused by the QMF bank. If

$$T(z) = cz^{-n_0} \quad c \text{ is a constant}$$

then equivalently

$$\hat{x}(n) = cx(n - n_0)$$

Hence, the reconstructed signal is a delayed version of input signal $x(n)$. Therefore this system is called perfect reconstruction.

If $T(z)$ is not a pure delay, the reconstructed signal $\hat{x}(n)$ may suffer from

• amplitude distortion(AMD) if $|T(e^{j\omega})| \neq c$ for all ω where c is a constant.

• phase distortion(PHD) if $T(z)$ does not have a linear phase or equivalently $arg[T(e^{j\omega})] \neq K\omega$ where K is a constant.

To eliminate the amplitude distortion it is necessary to have $T(z)$ as an all-pass function. On the other hand, $T(z)$ has to be FIR with linear phase to eliminate the phase distortion(PHD).

Summary: The reconstructed signal, $\hat{x}(n)$ may suffer from three different kinds of distortions in general[10][11]

• aliasing distortion(ALD)

• amplitude distortion(AMD)

• phase distortion(PHD)

15

with the proper choice of synthesis filters as in Eq.(2.19) aliasing is cancelled, then we have

$$T(z) = \frac{1}{2}[H_1(z)H_2(-z) - H_1(-z)H_2(z)] \tag{2.22}$$

It is easy to have $T(z)$ with the linear phase FIR by simply choosing $H_1(z)$ and $H_2(z)$ functions to be linear phase FIR. In the earliest known QMF banks, analysis and synthesis filters were chosen as[18]

$$
\begin{aligned}
H_2(z) &= H_1(-z) \\
K_1(z) &= H_1(z) \\
K_2(z) &= -H_2(z) = -H_1(-z)
\end{aligned}
\tag{2.23}
$$

then we have

$$T(z) = \frac{1}{2}[H_1^2(z) - H_1^2(-z)] \tag{2.24}$$

It is clear that aliasing is cancelled. By choosing $H_1(z)$ to be linear phase FIR, PHD is also eliminated. But we are still left with the AMD.

It is a well known fact that linear phase two-channel FIR QMF bank with the filters chosen as in Eq.(2.23) can have PR property if and only if $H_1(z)$ is in the simple 2-tap form[11]

$$H_1(z) = h_1(0)z^{-2n_0} + h_1(1)z^{-(2n_0+2k_0+1)} \tag{2.25}$$

with $h_1(0) = h_1(1)$. Then, we have the magnitude squares

$$|H_1(e^{j\omega})|^2 = cos^2(k_0 + 1/2)\omega$$

and the high-pass function

$$|H_2(e^{j\omega})|^2 = sin^2(k_0 + 1/2)\omega$$

We can conclude that with the choice of filters as in Eq.(2.23), there is not any linear phase transfer function except the 2-tap case such that the phase and

amplitude distortions are simultaneously eliminated. After eliminating ALD and PHD, it is however possible to minimize AMD. To be more specific, one optimizes the coefficients of $H_1(z)$ such that $|T(e^{j\omega})|$ is made as close to a constant as possible while minimizing the stop band energy of $H_1(z)$ in order to have a good low pass characteristic. Such an optimization has been suggested by Johnston[18]. and Jain and Crochiere[19] with the objective function

$$J = \alpha \int_{\omega_s}^{\pi} |H_1(e^{j\omega})|^2 d\omega + (1 - \alpha) \int_{0}^{\pi} (1 - |T(e^{j\omega})|^2) d\omega \qquad (2.26)$$

minimized where ω_s is the cutoff frequency of the filter.

It is worth noting that N, the length of the low pass filter $H_1(z)$. should be chosen to be even. Odd values of N will force $T(e^{j\omega})$ to be zero at $\omega = \pm\pi/2$. Fig. 2.6 shows the magnitude distortion of the optimal filters driven by Johnston. with respect to criteria defined in Eq.(2.26). Since $|T(e^{j\omega})|$ is not constant for all ω. it demonstrates the existence of AMD. The coefficients of Johnston filters for $N = 6, 8, 12, 16, 32$ are given in Table 2.3 with different α weighting factors.
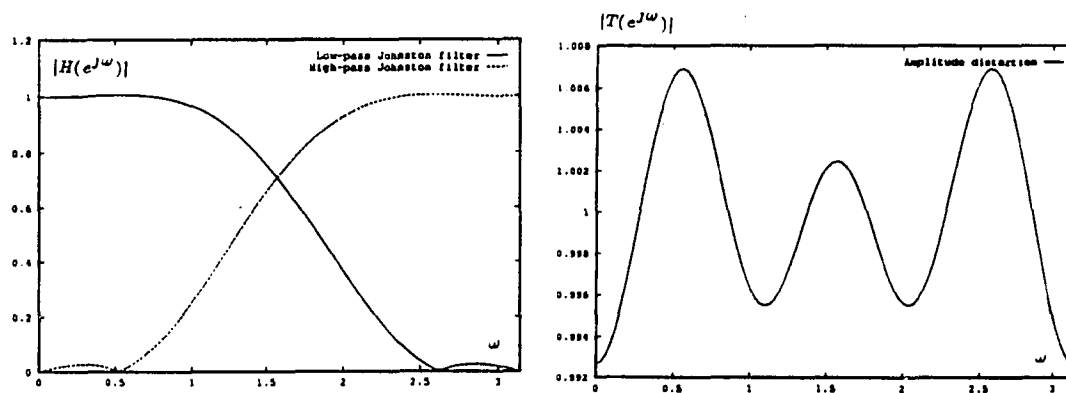
Fig. 2.6 a) Frequency response of Johnston QMF filters for $N = 8$. b) Amplitude distortion of Johnston filter given in a).

In this approach, the choice of filters eliminates ALD and PHD completely. The AMD is then minimized by the optimization. A complementary approach to this problem would be to choose the filters to eliminate ALD and AMD, and then minimize the PHD. Again, the choice of synthesis filters as in Eq.(2.19) will eliminate the AMD. One way of doing this is to choose $H_1(z)$ as a low pass IIR filter. Let us define a high pass IIR function $H_2(z)$ such that[20][21][22][23][24]

$$|H_1(e^{j\omega})|^2 + |H_2(e^{j\omega})|^2 = 1 \quad \text{for all} \quad \omega \tag{2.27}$$

Such a filter pair $\{H_1(z), H_2(z)\}$ is called the power complementary pair.

Let the low-pass IIR transfer function $H_1(z)$ be in the form

$$H_1(z) = \frac{N_1(z)}{D_1(z)} = \frac{\sum_{n=0}^{N} a_1(n) z^{-N}}{\sum_{n=0}^{N} b_1(n) z^{-N}} \tag{2.28}$$

where $N_1(z)$ is the numerator polynomial and $D_1(z)$ is the denominator polynomial of order N. Then the high-pass IIR function

$$H_2(z) = \frac{N_2(z)}{D_2(z)} = \frac{\sum_{n=0}^{N} a_2(n) z^{-N}}{\sum_{n=0}^{N} b_2(n) z^{-N}} \tag{2.29}$$

Since they are power complementary pair, $N_2(z)$ should satisfy

$$|N_2(e^{j\omega})|^2 = |D_1(e^{j\omega})|^2 - |N_1(e^{j\omega})|^2 \tag{2.30}$$

The zeros of $H_1(z)$ and $H_2(z)$ are on the unit circle and $N_1(z)$, $N_2(z)$ are symmetric or antisymmetric polynomials (if $H_1(z)$ is a digital Butterworth, Chebyshev or elliptic filter, this is always the case). To eliminate the magnitude distortion, they must be of the form

$$H_1(z) = \frac{A_0(z) + A_1(z)}{2}$$

and

$$H_2(z) = \frac{A_0(z) - A_1(z)}{2}$$

18

$A_0(z)$ and $A_1(z)$ should be chosen as all pass functions. Additionally, $H_1(z)$ satisfies the mirror condition as

$$H_2(z) = H_1(-z)$$

and we end up with the distortion function

$$T(z) = \frac{A_0(z)A_1(z)}{2}$$

which is all pass.

In other words, aliasing distortion is cancelled, amplitude distortion is completely eliminated but the phase distortion is created by the nonlinear phase of $T(e^{j\omega})$ which can be compensated by the all-pass phase equalization. Interested readers are directed to the references [21][22][23][24] for subband coding with IIR filter banks.

2.4.1 Two-Channel Perfect Reconstruction QMF Banks

Up to now, we have seen that the filter choice of Eq.(2.19) allows the aliasing to be cancelled and either phase distortion or magnitude distortion is eliminated completely. The remaining distortion can either be minimized by using optimization techniques, or equalized by cascading with another filter.

Smith and Barnwell[13], and Mintzer[15] have shown first time in the literature that, aliasing, amplitude distortion, and phase distortion can be completely eliminated in a two-channel filter bank. They proved that if the linear phase requirement on the analysis and synthesis filters are relaxed then 2-band PR filter bank solution exists. Such a filter bank is said to have perfect reconstruction property since $\hat{x}(n)$ is a replica of $x(n)$ except with a delay. They called it the Conjugate Quadrature Filter(CQF) bank. Filter coefficients of Smith-Barnwell CQFs are tabulated in Table 2.4 for $N = 8, 16, 32$.

Perfect reconstruction requires

(i) $S(z) = 0$, for all z

(ii) $T(z) = cz^{-n_0}$, c a constant

As discussed earlier, if one chooses

$$
\begin{aligned}
K_1(z) &= -H_2(-z) \\
K_2(z) &= H_1(-z)
\end{aligned}
\tag{2.31}
$$

the first requirement is met, $S(z) = 0$, and aliasing is eliminated. This leaves us with

$$
T(z) = \frac{1}{2}[H_1(-z)H_2(z) - H_1(z)H_2(-z)]
$$

Next, with N odd integer(even length filter), one selects

$$
H_2(z) = z^{-N}H_1(-z^{-1})
\tag{2.32}
$$

This choice forces

$$
H_2(-z) = -K_1(z)
$$

so that

$$
T(z) = \frac{1}{2}z^{-N}[H_1(z)H_1(z^{-1}) + H_1(-z)H_1(-z^{-1})]
\tag{2.33}
$$

Therefore, the perfect reconstruction requirement reduces to finding a prototype low-pass filter $H(z) = H_1(z)$ such that[17]

$$
\begin{aligned}
Q(z) &= H(z)H(z^{-1}) + H(-z)H(-z^{-1}) = \text{constant} \\
&= R(z) + R(-z)
\end{aligned}
\tag{2.34}
$$

This selection implies that all four filters are causal whenever $H(z)$ is causal. The PR requirement, Eq.(2.34), can be readily recast in an alternate, time domain

form. First, one notes that $R(z)$ is the autocorrelation sequence of $h(n)$ and is representable by a finite series of the form

$$R(z) = \rho(N)z^N + \rho(N-1)z^{N-1} + \cdots + \rho(0)z^0 + \cdots + \rho(N-1)z^{-N-1} + \rho(N)z^{-N} \quad (2.35)$$

Then,

$$R(-z) = -\rho(N)z^N + \rho(N-1)z^{N-1} - \cdots + \rho(0)z^0 - \cdots + \rho(N-1)z^{-N-1} - \rho(N)z^{-N}$$

$$(2.36)$$

Therefore, $Q(z)$ consists only of even powers of z. To force $Q(z) = $ constant, it suffices to make all even indexed coefficients in $R(z)$ equal to zero except $\rho(0)$.

The coefficients in $R(z)$ are simply the samples of the autocorrelation sequence $\rho(n)$ given by

$$
\begin{aligned}
\rho(n) &= \sum_{k=0}^{N} h(k)h(k+n) = \rho(-n) \\
&\stackrel{\text{def}}{=} h(n) \odot h(n)
\end{aligned}
\quad (2.37)
$$

where $\odot$ indicates a correlation operation. This follows from the z-transform relationships

$$R(z) = H(z)H(z^{-1}) \longleftrightarrow h(n) \star h(-n) = \rho(n) \quad (2.38)$$

Hence, we need to set $\rho(n) = 0$ for n even, and $n \neq 0$. Therefore,

$$\rho(2n) = \sum_{k=0}^{N} h(k)h(k+2n) = 0, \qquad n \neq 0 \quad (2.39)$$

If the normalization is imposed,

$$\sum_{k=0}^{N} |h(k)|^2 = 1 \quad (2.40)$$

one obtains the PR requirement

$$\sum_{k=0}^{N} h(k)h(k+2n) = \delta_n \quad (2.41)$$

21

The 2-band, equal bandwidth perfect reconstruction filter bank described above consists of, analysis and synthesis filters $\{H_1(z), H_2(z)\}$ which do not have linear phase except the 2-tap solution. If we give up the power complementary or energy preserving requirement of the analysis filters, we can obtain perfect reconstruction FIR QMF banks with linear phase. These filters have unequal bandwidths. It is seen from Eq.(2.17) that the output of the two-channel critically sampled analysis/synthesis system can be written as[25][26]

$$\hat{X}(z) = \frac{1}{2}[K_1(z) K_2(z)] \begin{bmatrix} H_1(z) & H_1(-z) \\ H_2(z) & H_2(-z) \end{bmatrix} \begin{bmatrix} X(z) \\ X(-z) \end{bmatrix} \qquad (2.42)$$

Let us call the above 2×2 matrix as $\mathcal{H}(z)$. For the perfect reconstruction it is necessary and sufficient that the synthesis filters satisfy

$$\begin{bmatrix} K_1(z) \\ K_2(z) \end{bmatrix} = \frac{z^{-N_1}}{det[\mathcal{H}(z)]} \begin{bmatrix} H_2(-z) \\ -H_1(-z) \end{bmatrix} \qquad (2.43)$$

Clearly, in order to have perfect reconstruction with FIR synthesis filters after FIR analysis filters, the necessary and sufficient condition is

$$det[\mathcal{H}(z)] = cz^{-2N_2-1}$$

where c is a constant. In other words, $det[\mathcal{H}(z)]$ must be a pure delay. Note that

$$\begin{aligned} det[\mathcal{H}(z)] &= H_1(z)H_2(-z) - H_1(-z)H_2(z) \\ &= P(z) - P(-z) = cz^{-2N_2-1} \end{aligned} \qquad (2.44)$$

where $P(z) = H_1(z)H_2(-z)$. Obviously, Eq.(2.44) implies that since $P(z)$ can have arbitrary number of even indexed coefficients but there must be only one non-zero coefficient of an odd power of z. It is worth noting that for the power complementary filter (orthonormal case)

$$H_1(z)H_2(-z) = -z^{2N-1}H_1(z)H_1(z^{-1}) \qquad (2.45)$$

then,

$$P(z) = -z^{2N-1}R(z) \qquad (2.46)$$

Therefore, instead of factorizing $R(z)$ for orthonormal (or paraunitary) filter banks where

$$R(z) = H(z)H(z^{-1})$$

One chooses any valid factorization of the form

$$P(z) = P_1(z)P_2(z)$$

There are many possible solutions of perfect reconstruction FIR QMF banks with

$$H_1(z) = P_1(z)$$

and

$$H_2(z) = P_2(-z)$$

It is important to emphasize that we give up the orthonormality condition in this most general 2-band filter bank case. Then the synthesis filters are not the time-reversed versions of the analysis filters. In the literature these are called biorthogonal FIR QMF banks[26][27][28]. These filter banks satisfy PR but their filters do not consider Nyquist conditions of the rate change operations. These filter banks, as expected, have more significant aliasing after the analysis. Therefore their performance expected to be inferior to the unitary filter banks. Table 2.1 summarize the different 2-band QMF design approaches.

For signal coding applications one would like to have the subband signals be independent or uncorrelated. A weaker condition which does not depend on the source is the orthogonal filters where at least uncorrelated input data will be decomposed into uncorrelated subbands[32]. In filter terms and for two-band system, this means that $H_1(z)$ and $H_2(z)$ should be orthogonal. Since our interest

is limited to the orthogonal systems we shall not discuss the biorthogonal systems further in this thesis. Interested readers are suggested to the references which deal with the subject in great detail[26][27][28][29].

2.4.2   Two-Dimensional PR-QMF Filter Banks

The extension of QMF to multi-dimensional signals was first introduced by Vetterli in 1984[4]. The image processing and coding applications have proven their merits. Similar to 1-D case, a fundamental subband splitting scheme is considered for 2-D signals, where the input signal is divided into four subbands.

Considering a 2-D input signal $x(m, n)$ and a 2-D output signal $y(m, n)$ with downsampling and upsampling, it can be shown that

Downsampling:

$$y(m, n) = x(2m, 2n)$$

Upsampling:

$$
\begin{array}{rcl}
y(2m, 2n) & = & x(m, n) \\
y(2m, 2n + 1) & = & 0 \\
y(2m + 1, 2n) & = & 0 \\
y(2m + 1, 2n + 1) & = & 0
\end{array}
$$

Then 2-D 2-band QMF bank input output relation which consists of downsampling, upsampling and decimation-interpolation filtering operations for 2-D signal is given as

$$\hat{X}(e^{j\omega_1}, e^{j\omega_2}) = \frac{1}{4} \sum_{k=0}^{1} \sum_{l=0}^{1} X(e^{j\omega_1 + k\pi}, e^{j\omega_2 + l\pi}) \sum_{m=0}^{1} \sum_{n=0}^{1} H_{mn}(e^{j\omega_1 + k\pi}, e^{j\omega_2 + l\pi}) K_{mn}(e^{j\omega_1}, e^{j\omega_2})$$

$$(2.47)$$

In a fashion similar to 1-D case, the output of 2-D analysis/synthesis system can be rewritten as

$$\hat{X}(z_1, z_2) = \frac{1}{2} \left[K_1(z_1, z_2) K_2(z_1, z_2) \right] \begin{bmatrix} H_1(z_1, z_2) & H_1(-z_1, -z_2) \\ H_2(z_1, z_2) & H_2(-z_1, -z_2) \end{bmatrix} \begin{bmatrix} X(z_1, z_2) \\ X(-z_1, -z_2) \end{bmatrix}$$

$$(2.48)$$

where $z_1 = e^{j\omega_1}$ and $z_2 = e^{j\omega_2}$.

To cancel the aliased version of the input signal $X(-z_1, -z_2)$ at the output, we choose the synthesis filters as

$$
\begin{aligned}
K_1(z_1, z_2) &= H_2(-z_1, -z_2) \\
K_2(z_1, z_2) &= -H_1(-z_1, -z_2)
\end{aligned}
\tag{2.49}
$$

With

$$
H_2(z_1, z_2) = -\tilde{H}_1(-z_1, -z_2)
$$

where $\tilde{H}$ represents the complex conjugate. The requirement for the orthonormal perfect reconstruction filter bank reduces to

$$
H_1(z_1, z_2)\tilde{H}_1(z_1, z_2) + H_1(-z_1, -z_2)\tilde{H}_1(-z_1, -z_2) = 2
\tag{2.50}
$$

The similarities of these results with the 2-band 1-D case is obvious. Therefore these result can be extended easily to 2-D M-band systems[4][6][25].

When 2-D filters are separable, the resulting system is a trivial extension of the one dimensional case. It is a tensor product of one dimensional system. All the properties follow from the properties of each dimensions. It was shown by Vetterli[4] by using separable 2-D filters

$$
\begin{aligned}
H_{mn}(e^{j\omega_1}, e^{j\omega_2}) &= H_m(e^{j\omega_1})H_n(e^{j\omega_2}) \\
K_{mn}(e^{j\omega_1}, e^{j\omega_2}) &= K_m(e^{j\omega_1})K_n(e^{j\omega_2})
\end{aligned}
\tag{2.51}
$$

filter design problem is reduced to one dimensional case. When separable filters in each dimension are chosen according to Eq.(2.31) as discussed earlier, all three aliasing terms completely vanish and we have the expression

$$
\begin{aligned}
T(e^{j\omega_1}, e^{j\omega_2}) &= \frac{\hat{X}(e^{j\omega_1}, e^{j\omega_2})}{X(e^{j\omega_1}, e^{j\omega_2})} \\
&= \left[|H(e^{j\omega_1})|^2 + |H(e^{j(\omega_1+\pi)})|^2 \right] \times \left[|H(e^{j\omega_2})|^2 + |H(e^{j(\omega_2+\pi)})|^2 \right]
\end{aligned}
$$

25
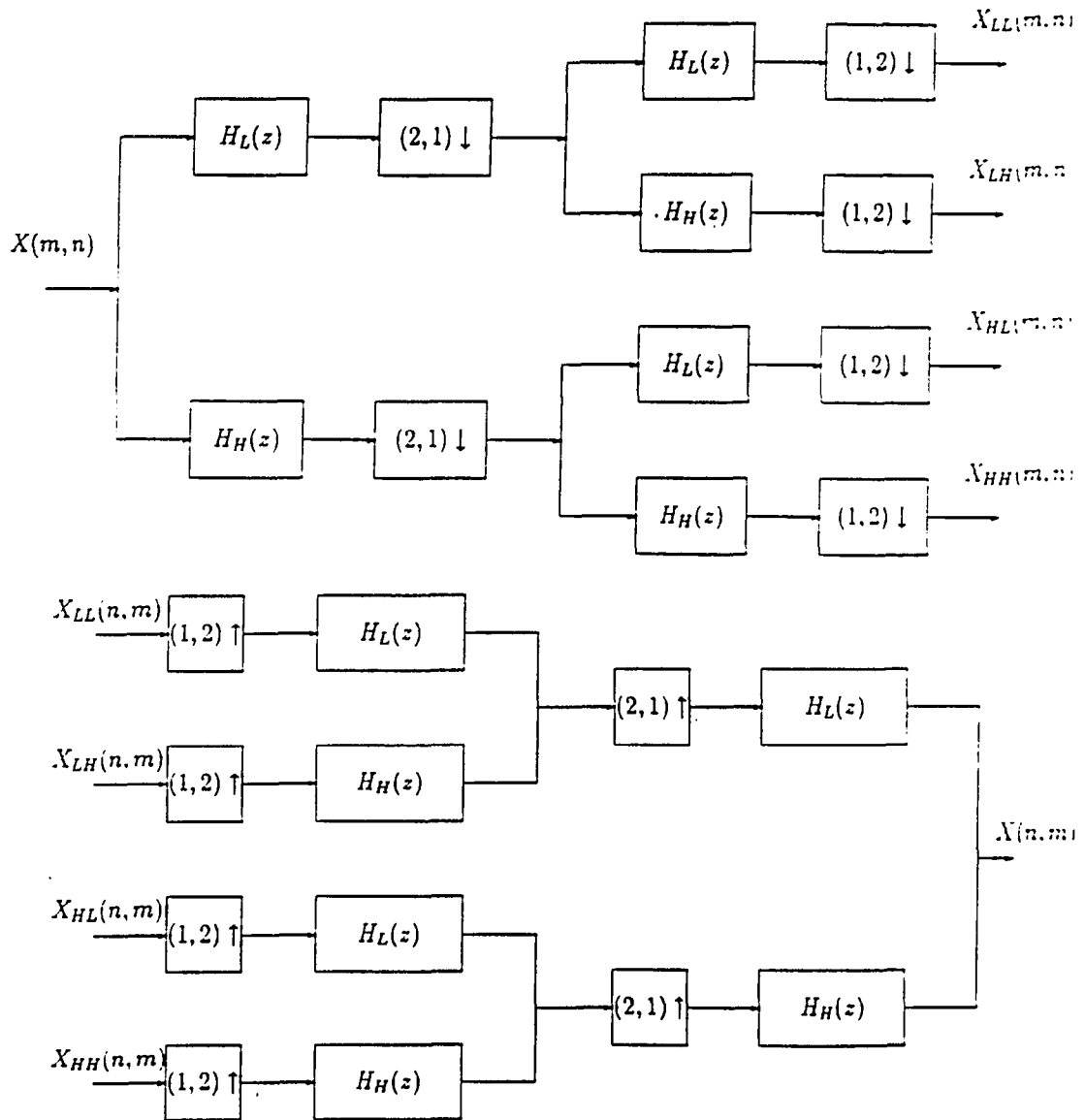
Fig. 2.7. Two dimensional subband decomposition by using one dimensional separable filters.

It is seen from this relation that we can employ conventional 1-D QMFs along one dimension at a time. This is decipted in Fig. 2.7 where 2-band split as described earlier has been applied in 2-D signal. Two subbands are denoted as "L" and "H" (low pass and high pass respectively) and thus "LH" denotes the band which is low-pass filtered and downsampled in one dimension, and high pass filtered and downsampled in the other.

In addition to the advantages of easier design, the computational complexity of separable FIR filters is also much less than the non-separable ones. On the other hand, it is clear that separable filters are the special case of non-separable filters. Even if the computational complexity is increased in non-separable case, one gains additional freedom in the design. There exist linear phase orthonormal 2-D non-separable FIR filter solutions which provide perfect reconstruction (remember there is no separable solution with the linear phase except the 2-tap case)[25][26].

2.4.3 Equivalent Parallel Realization of Cascaded Sub-band Tree Structures

In subband image coding, it is usually not sufficient to divide an image into only four subbands, further band splitting is desired. As discussed later, it has been a common practice to use a hierarchical subband tree structure of two-band filter banks, i.e. successive splits of subbands. Instead of using cascaded tree structures, it will be shown that such designs can also be readily implemented in terms of parallel integer band filter bank structures. Because of its structural simplicity this direct approach may be preferred for low order designs[9].

To show this parallel structural relationship, let us first look at some of the useful identities in multirate signal processing ($H(z)$ is rational), given in Fig. 2.8.[25][26]

I) The order of upsampling by L and downsampling by M can be interchanged if

and only if L and M are relative prime.

II) A filter after downsampling by M can be represented identically with its up-sampled version followed by downsampling

III) A filter in front of an upsampling by L can be equivalently represented with its upsampled version preceded by upsampling.

I)

$$\longrightarrow \boxed{\uparrow L} \longrightarrow \boxed{\downarrow M} \longrightarrow \quad \equiv \quad \longrightarrow \boxed{\downarrow M} \longrightarrow \boxed{\uparrow L} \longrightarrow$$

II)

$$\longrightarrow \boxed{\downarrow M} \longrightarrow \boxed{H(z)} \longrightarrow \quad \equiv \quad \longrightarrow \boxed{H(z^M)} \longrightarrow \boxed{\downarrow M} \longrightarrow$$

III)

$$\longrightarrow \boxed{H(z)} \longrightarrow \boxed{\uparrow L} \longrightarrow \quad \equiv \quad \longrightarrow \boxed{\uparrow L} \longrightarrow \boxed{H(z^L)} \longrightarrow$$
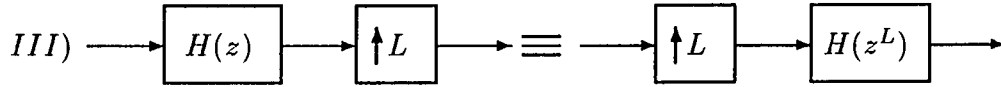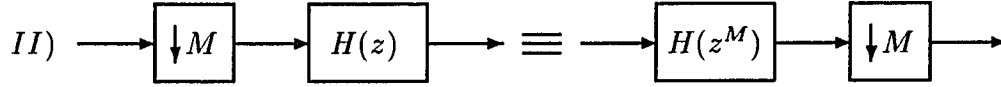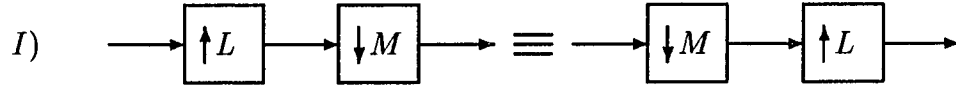
Fig. 2.8. Some useful identities in multirate signal processing.

Use of identity III provides the equivalent single stage interpolator of a multi stage interpolator as shown in Fig. 2.9 where $x(n)$ is the input, and $y(m)$ is the output signal, and $X(z)$, $Y(z)$ are their z- transforms respectively.

$$x(n) \longrightarrow \boxed{\uparrow L_1} \longrightarrow \boxed{H_1(z)} \longrightarrow \boxed{\uparrow L_2} \longrightarrow \quad \ldots \quad \longrightarrow \boxed{\uparrow L_i} \longrightarrow \boxed{H_i(z)} \longrightarrow y(m)$$

$$x(n) \longrightarrow \boxed{\uparrow L} \longrightarrow \boxed{H(z)} \longrightarrow y(m)$$
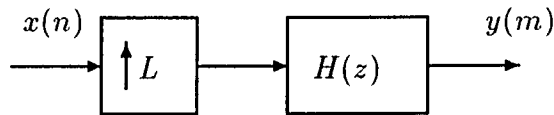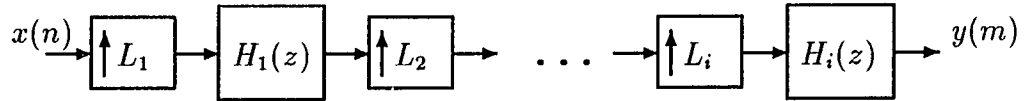
Fig. 2.9. a) Multistage interpolator b) Equivalent single stage interpolator.

28

Also let $H_1(z)$, $H_2(z)$,..., $H_i(z)$ be their interpolation filters and L_1, L_2, ..., L_i be the upsamplig ratios. Then, it can be shown from identity III that

$$Y(z) = H(z)X(z^L)$$

where

$$H(z) = H_1(z^{\prod_{n=2}^{i} L_n})H_2(z^{\prod_{n=3}^{i} L_n})...H_i(z)$$

and

$$L = \prod_{n=1}^{i} L_n$$

This form suggests the equivalent single stage interpolator model to replace an i-stage cascade interpolator.
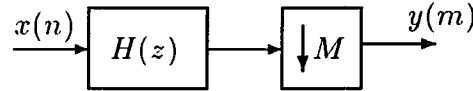
Fig. 2.10. a) Multistage cascade decimator b) Equivalent single stage decimator.

A similar identity can also be derived for the case of cascaded decimators by applying property II as

$$Y(z) = \frac{1}{M} \sum_{k=0}^{M-1} X(z^{1/M}W^k)H(z^{1/M}W^k) \qquad (2.52)$$

where

$$H(z) = H_1(z)H_2(z^{M_1})...H_i(z^{\prod_{n=1}^{i-1} M_n})$$

and

$$M = \prod_{n=1}^{i} M_n$$

Therefore multistage integer decimators can be replaced by a single stage integer decimator, as demonstrated in Fig. 2.10.

The conversion of a hierarchical tree structure to an equivalent parallel filter bank structure can now be achieved by simply applying the identities derived above for each branch of the structure. For example, two-stage, 4 band hierarchical subband tree structure will now be translated into the equivalent parallel 4 band structure. Let $H_L(z)$ and $H_H(z)$ be the low and high pass-filters respectively. Also note that if these are QMF filter bank designs, they satisfy the mirror property

$$H_H(z) = H_L(-z^{-1})$$

Then, these equivalent band pass filters $H_1(z)$, $H_2(z)$, $H_3(z)$, $H_4(z)$ for one stage parallel filter bank structure have the forms as in Fig. 2.11

$$
\begin{aligned}
H_1(z) &= H_L(z)H_L(z^2) \\
H_2(z) &= H_L(z)H_H(z^2) \\
       &= H_L(z)H_L(-z^{-2}) \\
H_3(z) &= H_H(z)H_H(z^2) \\
       &= H_L(-z^{-1})H_L(-z^{-2}) \\
H_4(z) &= H_H(z)H_L(z^2) \\
       &= H_L(-z^{-1})H_L(z^2)
\end{aligned}
\tag{2.53}
$$

These filters are based on iterated low and high pass filters, derived from the regular binary subband tree. In practice, these product band-pass filters often has very long impulse responses. That is why this design technique is usually preferred for low order filters[9].
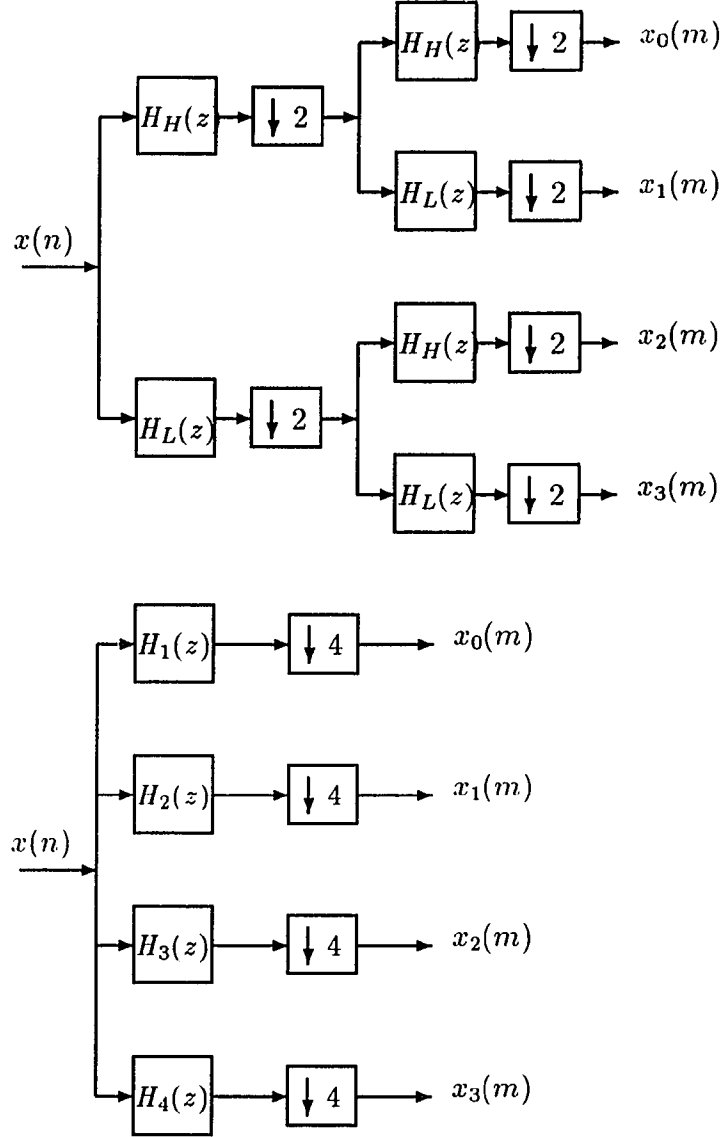
Fig. 2.11 Two stage 4 band hierarchical structure translated into parallel 4 band parallel structure.

2.5   Subband Tree Structures

2.5.1   Regular Binary Subband Tree Structure

The multirate techniques are very useful tools for multi-resolution spectral analysis. In this group, the PR-QMF bank is the most efficient one. As shown in
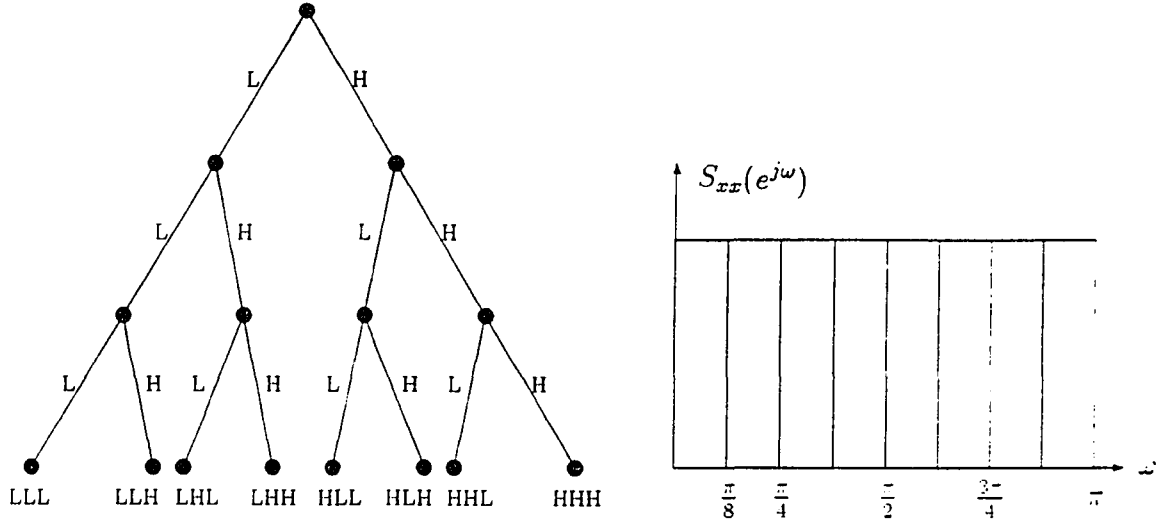
Fig. 2.12. A regular tree structure for L=3 and its frequency band split
assuming ideal 2-band PR-QMFs employed.

the previous section. these filter banks divide the input spectrum into two equal subbands yielding low(L) and high(H) bands. This two-band split PR-QMF operation can again be applied to (L) and (H) half bands and the quarter width bands (LL)-(LH)-(HL)-(HH) are obtained. When this procedure is repeated L times. 2^L equal width bands are obtained. This approach provides the maximum possible frequency resolution of $\pi/2^L$. This spectral analysis structure is called an L-level regular binary subband tree. For $L = 3$ the regular binary tree structure and its frequency band split is given in Fig. 2.12. This figure assumes that the ideal filters are employed.

This time-frequency based structure is a very useful vehicle to decompose the signals or their spectra into subbands or subspectra. When PR-QMFs are employed. the synthesis tree replicates the analysis operations and the input signal

is perfectly reconstructed.

In practice, finite length filters are replaced with the ideal filters. Therefore the interband aliasing or leakage exists. In a multilevel tree structure this frequency leakage can cause some degradation in the frequency bands of finer frequency resolutions. This is a disadvantage of the regular binary subband tree over a direct M-band(equal) frequency split since the M-band approach provides better way of monitoring the frequency split. On the other hand, the multilevel analysis/synthesis trees are much simpler to implement and provide a coarse-to-fine(multiresolution) signal decomposition as a byproduct.

2.5.2   Irregular Binary Subband Tree Structure

Almost all of the practical signal sources concentrate significant portions of their energies in subregions of their spectra. This indicates that some intervals of overall signal spectrum are more significant or important than the others. Therefore all subbands of the regular binary tree may not be equally needed. Since we also aim to minimize the computational complexities of the spectral analysis/synthesis operations, some of the finest frequency resolution subbands are combined to yield larger bandwidth frequency bands. This implies the irregular termination of the tree branches. Hence, it is expected that the frequency bands of the irregular tree have unequal bandwidths. Fig. 2.13 displays an arbitrary irregular binary subband tree structure with the maximum tree level $L = 3$ and its frequency band split. This figure assumes that the ideal filters are employed.

The number of bands in this irregular spectral decomposition structure is less than the regular tree case, $M \leq 2^L$. The regular tree provides the best possible frequency resolution for a fixed L. It has equal width frequency bands while the irregular tree provides unequal bandwidths. Both of these subband tree structures split the spectrum as a power of two frequency resolutions since they employ a
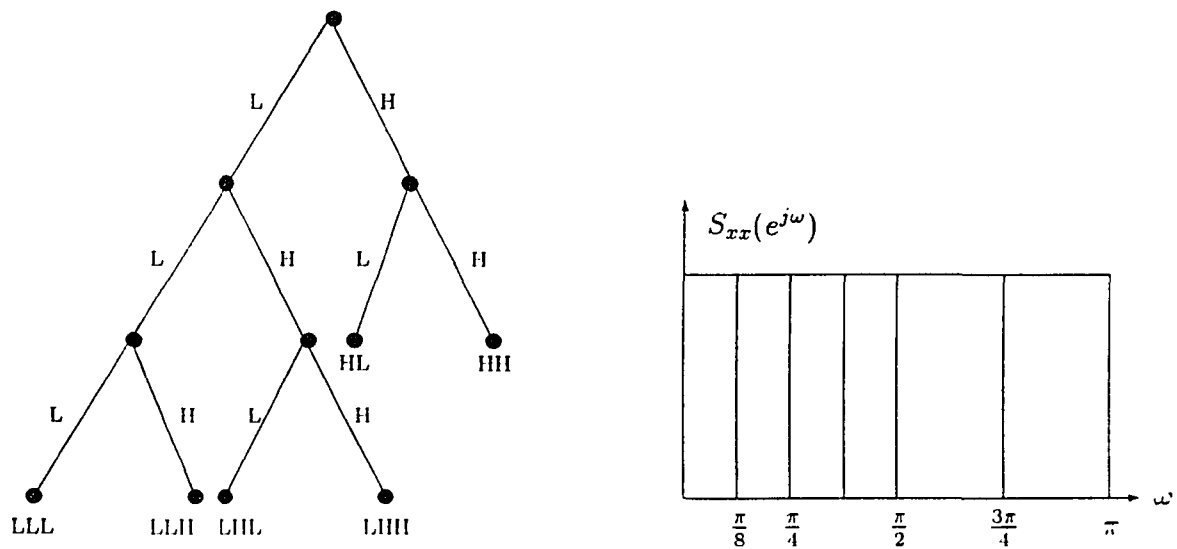
Fig. 2.13. An irregular tree structure and its frequency band split assumming ideal 2-band PR-QMFs employed.
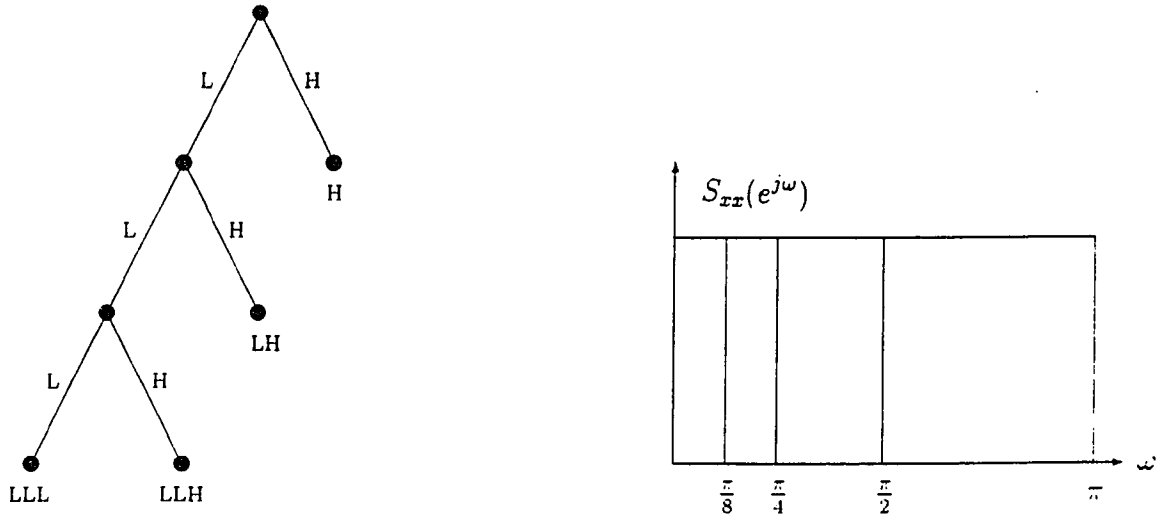
Fig. 2.14 A dyadic (octave band) tree structure and its frequency band
split assuming ideal 2-band PR-QMFs employed.

two-band frequency split algorithm repeatedly.

2.5.3   Dyadic Subband Tree Structure

The dyadic tree is a special binary irregular tree structure. It splits only the low half
of the spectrum into the new two equal bands in any level of the tree. Therefore the
detail or higher half frequency components of the signal at any level of the tree is
not decomposed anymore. The dyadic tree in time and its corresponding frequency
resolution for $L = 3$ is given in Fig. 2.14.

A simple examination of this analysis/synthesis structure shows that half-
resolution frequency splitting steps on low bands are performed. Therefore. it is also
called the octave-band or constant-Q subband tree structures. First, low(L) and
high(H) signal bands are obtained here. While band (L) provides a coarser version

35

of the original signal and band (H) contains the detail information. It is also known from the theory of multirate signal processing that these bands have decimated signal durations in time. Therefore the total number of coefficients or subband samples is equal to the the number of input samples. If the low spectral component or band (L) is interpolated by two, the detail information or the interpolation error is compensated by the interpolated version of band (H). Hence the original signal is perfectly recovered in this one step dyadic tree structure. The procedure is repeated L times onto only lower spectral half component of the higher level node in the tree. This multiresolution(coarse-to-fine) signal decomposition idea has been first proposed in 2-D by Burt and Adelson[33] for vision and image coding problems. This popular decomposition technique is called the Laplacian pyramid. The celebrated orthonormal wavelet transform also utilizes this dyadic subband tree as fast transform algorithm. The wavelet transforms are studied in detail in Chapter 3. We will now present briefly the Laplacian pyramid signal decomposition technique and discuss its similarities with a dyadic tree structure PR filter bank

2.6 Laplacian Pyramid for Signal Decomposition

The coarse-to-fine hierarchical or progressive signal representation concepts has been of great interest in computer vision and image coding fields. An image frame and its coarser, decimated in time, versions are interrelated in a progressive manner. Burt and Adelson[33], proposed this concept for image coding applications.

The basic idea of this approach is actually to perform a dyadic tree-like spectral or subband analysis. The idea will be explained with a 1-D example and the connections to a dyadic PR subband tree are set. This idea was first proposed by Veterli[26] as a special case of unequal bandwidth 2-band filter banks, lately,

Kim and Ansari also derived the the extension of Laplacian pyramid for special filter bank cases[36].

The signal in Fig. 2.15 $x(n)$ is low-pass filtered and downsampled by 2. Let us denote this signal as $x_D^1(n)$. Then upsample $x_D^1(n)$ by 2, interpolate it and denote the interpolated signal as $x_I^1(n)$. The corresponding interpolation error of stage 1 is expressed as

$$x_L^1(n) = x(n) - x_I^1(n) \qquad (2.54)$$

where L stands for Laplacian since this interpolation error has a Laplacian-shaped pdf for most of the image sources considered by Burt and Adelson. To obtain $x(n)$ perfectly one should sum

$$x(n) = x_I^1(n) + x_L^1(n) \qquad (2.55)$$

Since $x_I^1(n)$ is obtained from $x_D^1(n)$; $x_L^1(n)$ and $x_D^1(n)$ are sufficient to represent $x(n)$ perfectly. The duration of $x_D^1(n)$ is half the duration of $x(n)$. This provides a multiresolution or coarse-to-fine signal representation in time. The decimation and interpolation steps on the higher level low-pass signal are repeated until the desired level, L, of the dyadic-like(since we call dyadic tree with the PR conditions) tree structure is reached. For $L = 3$, Fig. 2.15 indicates that the signals $x_D^3(n)$, $x_L^3(n)$, $x_L^2(n)$, and $x_L^1(n)$ are required to recover $x(n)$ perfectly. It is seen here again that the number of coefficients or subband samples needed to represent $x(n)$ perfectly is larger than the number of samples in $x(n)$. Therefore this structure does not satisfy the orthonormality conditions of a general transform concept.

This weakness of the Laplacian pyramid scheme can be easily fixed if the proper anti-aliasing and interpolation filters are employed. These filters also provide the conditions for the decimation and interpolation of high-frequency or detail signal. Therefore the number of coefficients needed for a complete representation is equal to the number of signal samples. This enhanced pyramidal signal repre-
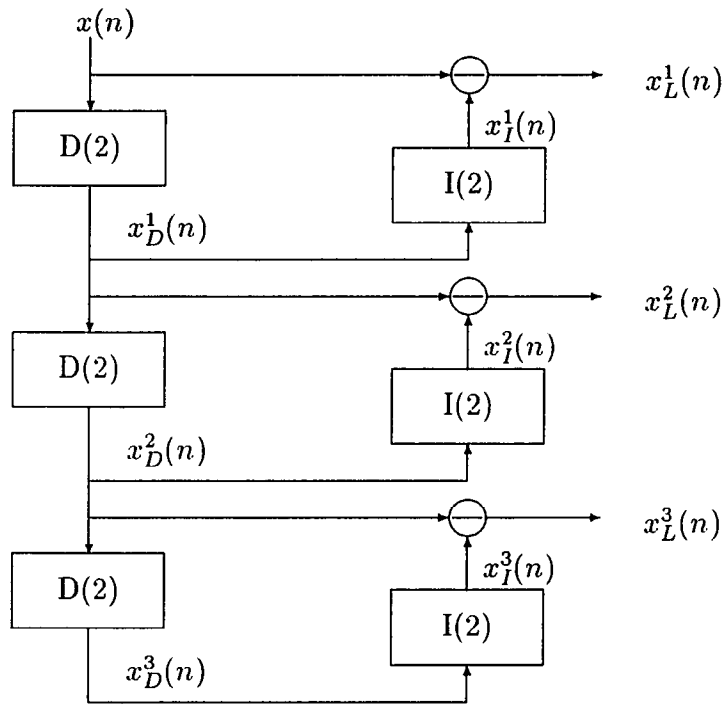
Fig. 2.15 Laplacian pyramid structure.

sentation scheme is practically much more valuable than the Laplacian pyramidal decomposition and indeed identical to the dyadic subband tree concept.

2.6.1 Modified Laplacian Pyramid for Critical Sampling

The oversampling nature of the Laplacian pyramid is undesirable particularly for signal coding applications. Obviously, this signal decomposition technique requires more number of coefficients or subband samples than the input signal. We should notice that the Laplacian pyramid does not put any constraint on low-pass anti-aliasing and interpolation filters although it changes the rate of the signal by 2. This is the questionable point of this approach. The Nyquist condition is not imposed in the structure.

We modify the Laplacian pyramid structure in this section to achieve the critical sampling. In other words, the filter conditions to decimate also the Laplacian or interpolation error signal by 2 and to reconstruct the input signal perfectly are derived in this section. Then, we will point out the similarities between the Modified Laplacian Pyramid and two-band PR-QMF banks.

Fig. 2.16 displays one level of a Modified Laplacian Pyramid. It is traced from this figure that the error signal $X_L(z)$ is filtered by $H_2(z)$ and down upsampled by 2, then interpolated by $K_2(z)$. The resulting branch output signal $V_2(z)$ is added to the low-pass decimated interpolated version of the input signal, $V_1(z)$, to obtain the reconstructed signal $\hat{X}(z)$. We keep the analysis in the z-domain for simplicity.

We can write the low-pass decimated interpolated version of the input signal from Fig. 2.16 similar to 2-band PR-QMF case analyzed earlier

$$V_1(z) = \frac{1}{2}K_1(z)[H_1(z)X(z) + H_1(-z)X(-z)] \qquad (2.56)$$

39
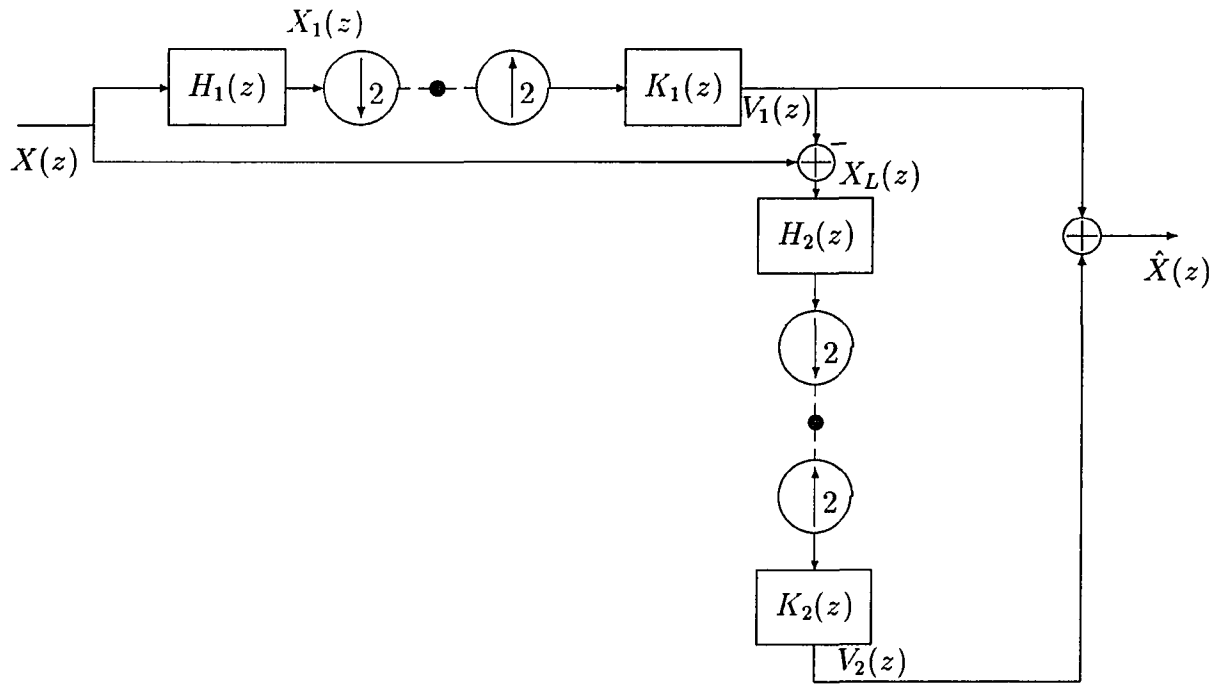
Fig. 2.16. Modified Laplacian pyramid structure allowing perfect reconstruction with critical number of samples.

and the Laplacian interpolation error signal

$$X_L(z) = X(z) - V_1(z) \tag{2.57}$$

is obtained. As stated earlier $X_L(z)$ has the full resolution of the input signal $X(z)$. Therefore the decomposition structure oversamples the input signal. Now, let us decimate and interpolate the error signal. We can write the resulting signal of these procedure from Fig. 2.16 as

$$V_2(z) = \frac{1}{2}K_2(z)[H_2(z)X_L(z) + H_2(-z)X_L(-z)] \tag{2.58}$$

If we put Eqs.(2.56) and (2.57) in this equation

$$
\begin{aligned}
V_2(z) &= \frac{1}{2}[H_2(z)K_2(z) - \frac{1}{2}H_1(z)K_1(z)H_2(z)K_2(z) \\
&\quad -\frac{1}{2}H_1(z)K_1(-z)H_2(-z)K_2(z)]X(z) \\
&\quad +\frac{1}{2}[H_2(-z)K_2(z) - \frac{1}{2}H_1(-z)K_1(z)H_2(z)K_2(z) \\
&\quad -\frac{1}{2}H_1(-z)K_1(-z)H_2(-z)K_2(z)]X(-z)
\end{aligned} \tag{2.59}
$$

We can now write the reconstructed signal as

$$
\begin{aligned}
\hat{X}(z) &= V_1(z) + V_2(z) \\
&= T(z)X(z) + S(z)X(-z)
\end{aligned} \tag{2.60}
$$

where

$$
\begin{aligned}
T(z) &= \frac{1}{2}[H_1(z)K_1(z) + H_2(z)K_2(z)] - \frac{1}{4}[H_1(z)K_1(z)H_2(z)K_2(z) \\
&\quad +H_1(z)K_1(-z)H_2(-z)K_2(z)]
\end{aligned} \tag{2.61}
$$

and

$$
\begin{aligned}
S(z) &= \frac{1}{2}[H_1(-z)K_1(z) + H_2(-z)K_2(z)] - \frac{1}{4}[H_1(-z)K_1(z)H_2(z)K_2(z) \\
&\quad +H_1(-z)K_1(-z)H_2(-z)K_2(z)]
\end{aligned} \tag{2.62}
$$

41

If we choose the synthesis or interpolation filters as

$$K_1(z) = -z^{-1}H_2(-z)$$

$$K_2(z) = z^{-1}H_1(-z) \tag{2.63}$$

the aliasing terms are cancelled and

$$S(z) = 0$$

$$T(z) = \frac{1}{2}z^{-1}[-H_1(z)H_2(-z) + H_2(z)H_1(-z)] \tag{2.64}$$

Now the perfect reconstruction requirements reduce to

$$\frac{\hat{X}(z)}{X(z)} = T(z) = cz^{-n_0} \tag{2.65}$$

where c is a constant and the reconstructed signal is identical to the input signal with the shift of n_0.

It is observed from Eq.(2.65) that the magnitude of $T(z)$ must be constant for perfect reconstruction. This implies so called biorthogonal 2-band filter banks in the literature. As mentioned earlier, one should be careful about the filters of a multi-rate structure. These filters should function as anti-aliasing filters. This requirement indicates that the filters $H_1(z)$ and $H_2(z)$ should be low-pass and high-pass respectively. This also implies that the orthonormality condition is satisfied. It is clear that this Modified Laplacian structure with

$$H_2(z) = z^{-N}H_1(-z^{-1}) \tag{2.66}$$

becomes identical to the orthonormal or unitary 2-band PR-QMF banks of Section 2.4 where

$$T(z) = \frac{1}{2}z^{-(N+1)}[H_1(z)H_1(z^{-1}) + H_1(-z)H_1(-z^{-1})] = cz^{-(N+1)} \tag{2.67}$$

with N (even length filter) odd integer. This derivation shows that the Modified Laplacian Pyramid emerges as a biorthogonal 2-band filter bank, or more desirably

as an orthonormal 2-band PR-QMF based dyadic subband tree structure if one employs the proper filters. This Modified Laplacian Pyramid concept is also identical to biorthogonal or orthonormal wavelet transform algorithms[26][36].

	Method I Johnston's Filter	Method II PR-QMF's (paraunitary filters) Smith-Barnwell Vaidyanatan-Hong	Method III Biorthogonal Filters Vetterli Vaidyanatan Ansari	Method IV IIR Filters
Relation between filters	$H_2(z) = H_1(-z)$ $K_1(z) = H_1(z)$ $K_2(z) = -H_1(-z)$	$H_2(z) = z^{-N}H_1(-z^{-1})$ $K_1(z) = -H_2(-z)$ $K_2(z) = H_1(-z)$	$P(z) = H_1(z)H_2(-z)$ $K_1(z) = z^{-n_0}H_2(z)$ $K_2(z) = -z^{-n_2}H_1(-z)$ with $det[\mathcal{H}(z)] = z^{-n}$	$H_2(z) = H_1(-z)$ $K_1(z) = H_1(z)$ $K_2(z) = -H_1(-z)$
Phase response of analysis filter	linear	non-linear	linear	non-linear
Distortion in QMF bank	ALD cancelled AMD minimized PHD eliminated	ALD cancelled AMD eliminated PHD eliminated	ALD cancelled AMD eliminated PHD eliminated	ALD cancelled AMD eliminated PHD equilazed

Table 2.1. Two band QMF bank design approaches.

Transition Code Letter	Normalized Transition Band
A	0.14
B	0.1
C	0.0625
D	0.043
E	0.023

Table 2.2. Normalized transition bands and their code letters for Johnston QMFs.

8 TAP		
0.48998080		
0.06942827		
-0.07065183		
0.00938715		
12 TAP(A)	**12 TAP(B)**	
0.48438940	0.4807962	
0.08846992	0.0980852	
-0.08469594	-0.0913825	
-0.00271032	-0.0075816	
0.01885659	0.0274553	
-0.00380969	-0.0064439	
16 TAP(A)	**16 TAP(B)**	**16 TAP(C)**
0.4810284	0.4773469	0.4721122
0.0977981	0.1067987	0.1178666
-0.0903922	-0.0953023	-0.0992955
-0.0096663	-0.0161186	-0.0262756
0.0276414	0.0359685	0.0464768
-0.0025897	-0.0019209	0.0019911
-0.0050545	-0.0099722	-0.0204875
0.0010501	0.0028981	0.0065256

24 TAP(B)	24 TAP(C)	24 TAP(D)
0.4731289	0.4686479	0.4654288
0.1160355	0.1246452	0.1301121
-0.0982978	-0.0998788	-0.0998442
-0.0256153	-0.0346414	-0.0408922
0.0442397	0.0508816	0.0540298
0.0038915	0.0100462	0.0154739
-0.0190199	-0.0275519	-0.0329583
0.0014464	-0.0006504	-0.0040137
0.0064858	0.0135401	0.0197638
-0.0013738	-0.0022731	-0.0015714
-0.0013929	-0.0051829	-0.0106140
0.0003833	0.0023292	0.0046984

32 TAP(C)	32 TAP(D)	32 TAP(E)
0.46640530	0.46367410	0.45964550
0.12855790	0.13297250	0.13876420
-0.09980243	-0.09933859	-0.09768379
-0.03934878	-0.04452423	-0.05138257
0.05294745	0.05481213	0.05570721
0.01456844	0.01947218	0.02662431
-0.03123862	-0.03496440	-0.03830613
-0.00418748	-0.00796173	-0.01456900
0.01798145	0.02270415	0.02812259
-0.00013038	0.00206947	0.00737988
-0.00945831	-0.01422899	-0.02103823
0.00141424	0.00084268	-0.00261204
0.00423419	0.00818194	0.01568082
-0.00126830	-0.00196967	-0.00096245
-0.00140379	-0.00397155	-0.01127565
0.00069105	0.00225513	0.00512322

Table 2.3. Johnston QMF coefficients(coefficients are listed from center to end).

8 TAP	16 TAP	32 TAP
0.034897558217851	0.021935982030043	0.008494372478233
-0.010983019462528	0.001578616497663	-0.000099617816873
-0.062864539349519	-0.060254491028752	-0.008795047132402
0.223907720892568	-0.011890659620534	0.000708779549084
0.556856993531445	0.137537915636625	0.012204201560354
0.357976304997285	0.057454500563909	-0.001762639314795
-0.023900270561131	-0.321670296165893	-0.015584559035738
-0.075940963791882	-0.528720271545339	0.004082855675060
	-0.295779674500919	0.017652220240893
	0.000204311084517	-0.003835219782884
	0.029066997894467	-0.016747613884736
	-0.035334860887081	0.018239062108698
	-0.006821045322743	0.005781735813341
	0.026066784682641	-0.046926740909076
	0.001033363491944	0.057250054450731
	-0.014359309574775	0.354522945953839
		0.504811839124518
		0.264955363281817
		-0.083290951611400
		-0.139108747584926
		0.033140360806591
		0.090359384220331
		-0.014687917291347
		-0.061033358867071
		0.006606122638753
		0.040515550880356
		-0.002631418173168
		-0.025925804761497
		0.000931953235019
		0.015356389599161
		-0.000119683269332
		-0.010570322584723

Table 2.4. 8, 16, 32 tap PR-CQF coefficients with 40 dB stopband attenuation.

Chapter 3

Wavelet Transform

3.1 Introduction

The wavelet transforms, particularly the orthonormal wavelet transforms have been popular recently as a new tool for the multiresolution signal decomposition[37][38][39]. It has also been realized that the orthonormal wavelet transforms are very closely linked to the well-known orthonormal Perfect Reconstruction Quadrature Mirror Filter(PR-QMF) based dyadic subband filter banks which was introduced in Chapter 2. The purpose of this chapter is to introduce the wavelet transforms and to emphasize their links with PR-QMF banks. We also present the unique features of the compactly supported Orthonormal Wavelet transforms and their connections and interpretations with the conventional FIR PR-QMF banks. In this category, particularly the impact of regularity of the wavelet function on PR-QMF will be examined in detail[40].

Most of the material in this chapter is of tutorial value and provides the summary of the wavelet transform theory. Since one of the contribution of this dissertation is to emphasize and highlight the connections of wavelet transform and filter bank theories, this chapter serves as the vehicle to link the contributions of this dissertation to the wavelet transforms proposed earlier in the literature.

After defining the continuous wavelet transforms, the discrete wavelet trans-

forms will be discussed. Their significance from signal processing point of view will be interpreted. The orthonormal wavelet bases, which are very important in signal analysis/synthesis, will be presented next. The orthonormal wavelet filters will be emphasized and their connections with the wavelet function will be shown. We will mention wavelet regularity and Daubechies wavelet bases and their time-frequency localization features. Next section will deal with the generalization of compactly supported orthonormal wavelet bases and their connections to the M-band PR-QMF filter banks. The theoretical proofs and rigorous derivations of the topics covered in this chapter are not in the focus of this dissertation and will be omitted often but the references will be provided.

3.2 Wavelet Transforms

Analysis of signals using appropriate basis functions is one of the fundamental problems in signal processing field. J.B.J. Fourier proposed the complex sinusoids as the basis functions for signal decomposition[34]. The Fourier transform of a finite energy continuous time signal $f(t)$, (i.e. $f(t) \in L^2$) is defined as

$$F(\Omega) = \int_{-\infty}^{\infty} e^{-j\Omega t} f(t) dt \qquad (3.1)$$

The strength of the standard Fourier analysis is that it allows the decomposition of a signal into its individual frequency components and establishes the relative intensity of each frequency component. Because of the infinite durations of these basis functions, any time-local information (e.g. an abrupt change in the signal) is spread over the whole frequency spectrum. Therefore, this transform can not reflect any time-localized characteristic of $f(t)$ into frequency domain. It only provides the frequency behavior of $f(t)$ in the interval $-\infty < t < \infty$. Gabor addressed this problem by introducing a window function to localize $f(t)$ and calculating the

49

Fourier transform of the windowed signal as[35]

$$F_{SF}(\Omega, \tau) = \int_{-\infty}^{\infty} w(t - \tau)e^{-j\Omega t}f(t)dt \qquad (3.2)$$

where $w(t - \tau)$ is the appropriate, time-frequency localized, window function. This transform is called the windowed or Short-Time Fourier Transform (STFT) (also referred to the Gabor transform when the window function used in the STFT is Gaussian).

The major advantage of Short-Time Fourier Transform is that if a signal has most of its energy in the given time interval $[-T, T]$ and in the frequency interval $[-\Omega, \Omega]$, then its STFT will be localized in the region $[-T, T] \times [-\Omega, \Omega]$ of the time-frequency plane. Of course, the uncertainty principle prevents the possibility of having arbitrarily high resolution in both time and frequency domains, since it lower bounds the time-bandwidth product of any basis function by $\Delta T \Delta \Omega \geq \frac{1}{4\pi}$ where $(\Delta T)^2$ and $(\Delta \Omega)^2$ are the variances of time function and its Fourier transform respectively[25][26].

An important parameter of a window function is its size (or scale). The selection of an appropriate window size poses a fundamental problem in signal analysis. Thus, by varying the window function used, one can trade the resolution in time for the resolution in frequency. An intuitive way to achieve this is to have short time duration high frequency basis functions, and long time duration low frequency ones. Fortunately, the wavelet transform provides for this desired feature and defined as,

$$W_f(a, b) = a^{-\frac{1}{2}} \int_{-\infty}^{\infty} \psi(\frac{t - b}{a})f(t)dt \qquad (3.3)$$

where $a \in R^+, b \in R$. Here a, and b are the scale and shift variables respectively, and they are continuous variables. Depending on the scaling parameter a, the wavelet function $\psi(t)$ dilates or contracts in time and causing the corresponding contraction or dilation in frequency domain respectively. Therefore a flexible time-frequency

resolution is achievable with the wavelet transforms. Another significant difference of these transforms, the STFT is never a real function on the time-frequency plane regardless of the choice of $w(t)$, but the wavelet transform is real if the basic wavelet $\psi(t)$ is chosen to be real.

3.3 Continuous Wavelet Transform

The continuous wavelet transform maps a function $f(t)$ onto time-scale space as

$$W_f(a,b) = \frac{1}{|a|^{1/2}} \int_{-\infty}^{\infty} \psi(\frac{t-b}{a}) f(t) dt \tag{3.4}$$

This operation can be expressed in a simpler inner product notation as

$$W_f(a,b) = <\psi_{ab}(t), f(t)> \tag{3.5}$$

$\psi_{ab}(t)$ represents a family of functions obtained from a single wavelet function $\psi(t)$ and the dilation and translation parameters a and b as

$$\psi_{a,b}(t) = \frac{1}{|a|^{1/2}} \psi(\frac{t-b}{a}) \tag{3.6}$$

where a and b continuous.

The wavelet function $\psi(t)$ is a band-pass function. It is desired that this function has a good time and frequency localization so that $f(t)$ is decomposed into elementary building blocks which are jointly well localized in time and frequency. The wavelet function has to satisfy the "*admissibility*" condition that makes it an isometry (up to a constant) of $L^2(R)$ onto $L^2(R \times R)$. This requirement limits the wavelet functions which must satisfy[40][41]

$$C_h = \int_{-\infty}^{\infty} \frac{|\Psi(\Omega)|^2}{|\Omega|} d\Omega < \infty \tag{3.7}$$

where $\Psi(\Omega)$ is the Fourier transform of the wavelet function $\psi(t)$. The admissibility condition is directly related to the decay of the wavelet function $\psi(t)$ which is

51

required to have a good localization. The admissibility condition for a continuous $\Psi(\Omega)$ is equivalent to a zero-mean wavelet function in time

$$\Psi(0) = \int_{-\infty}^{\infty} \psi(t)dt = 0 \qquad (3.8)$$

This condition forces that the wavelet function is a band pass function and decays at least as fast as $|t|^{1-\epsilon}$ in time (in practice we need to have much faster decay of $\psi(t)$, in order to have good time localization).

The admissibility condition assures that the "resolution of the identity" holds[40]. This guarantees that any function $f(t) \in L^2(R^n)$ can be reconstructed from the wavelet space as

$$f(t) = \frac{1}{C_h} \int_{-\infty}^{\infty} \frac{1}{a^2} da \int_{-\infty}^{\infty} W_f(a,b)\psi_{a,b} db \qquad (3.9)$$

where the wavelet coefficients were defined earlier in Eq.(3.4) Its mathematical proof will is given in[40][41]. Whenever $\psi(t)$ is a real function, the integral limits of C_h expression in Eq.(3.9) are changed from 0 to ∞.

Resolution of the identity ensures that the Continuous Wavelet Transform (CWT) is complete if $W_f(a,b)$ are known for all a and b. A continuous signal $f(t)$ is represented by a band pass function $\psi(t)$ and its dilated and translated versions. The dilation in time leads to different resolutions in frequency. Fig. 3.1 displays a wavelet function $\psi(t)$ and its dilations for different values of parameter "a" along with their Fourier transforms. This figure helps to visualize of the time-frequency plain and emphasizes the band pass nature of $\psi(t)$ and its dilations. Fig. 3.1 also displays the time-frequency resolution cells of wavelet transform compared with the $STFT$. This figure indicates the fixed time-frequency resolution of $STFT$ versus more flexible resolution of wavelet transforms.
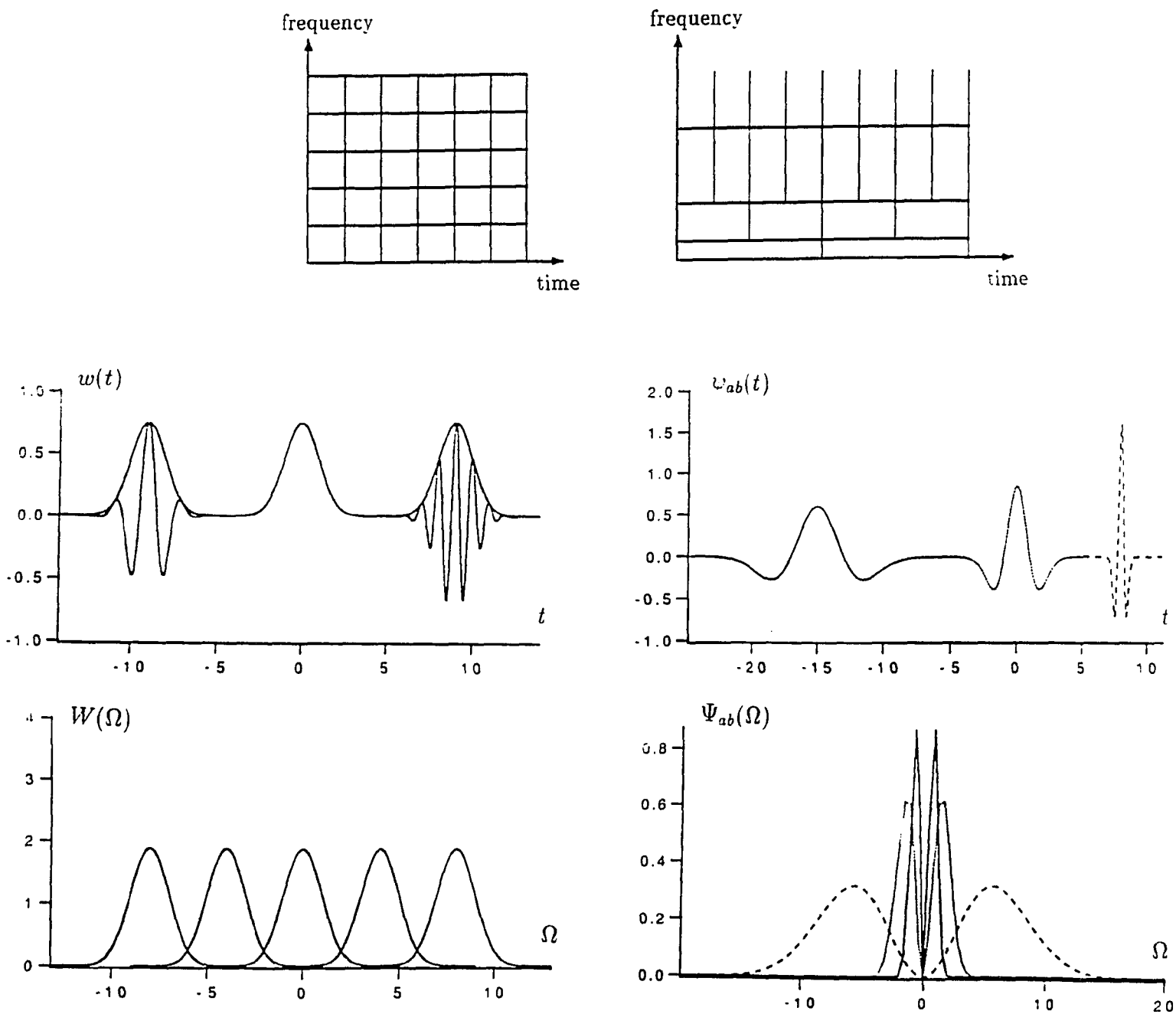
Fig. 3.1. The time-frequency plane resolution cells of the $STFT$ vs wavelet transform.

The STFT yields the decomposition of a signal into a set of equal bandwidth functions sweeping all the frequency spectrum. On the other hand the wavelet transform provides the decomposition of a signal by a set of constant Q (or equal bandwidth on a logarithmic scale) bandpass functions. The constant bandwidth condition on a logarithmic scale can be easily seen by the following relation,

$$\psi_{ab}(t) = \frac{1}{|a|^{1/2}}\psi(\frac{t-b}{a}) \Longleftrightarrow \Psi_{ab}(\Omega) = |a|^{1/2}\Psi(a\Omega)e^{-j\Omega b} \qquad (3.10)$$

The roles played by the transform parameters are different for *STFT* and wavelet transforms. The time parameter τ in STFT refers to actual time instant, while the parameter b in the continuous wavelet transform refers to the time instant $a^{-1}b$.

There is a time-frequency resolution trade-off in wavelet transform. To quantify how the continuous wavelet transform spans the time frequency-plane, the measures of time and frequency resolutions are defined. Let σ_t and σ_Ω be the standard deviations of the mother wavelet function $\psi(t)$ in time and frequency domains respectively and the corresponding variances are defined as[37]

$$\sigma_t^2 = \int (t - t_0)^2 |\psi(t)|^2 dt \qquad (3.11)$$

and

$$\sigma_\Omega^2 = \int (\Omega - \Omega_0)^2 |\Psi(\Omega)|^2 d\Omega \qquad (3.12)$$

Let the wavelet function $\psi(t)$ be centered at (t_0, Ω_0) in time-frequency plane. Hence $\psi(\frac{t-b}{a})$ is centered at $(t_0, \Omega_0/a)$ with the variances

$$\begin{aligned}
\sigma_{ab_t}^2 &= \int_{-\infty}^{\infty} (t - t_0)^2 |\psi_{ab}(t)|^2 dt \\
&= a^2\sigma_t^2
\end{aligned} \qquad (3.13)$$

and

$$\begin{aligned}
\sigma_{ab_\Omega}^2 &= \int_0^\infty (\Omega - \frac{\Omega_0}{a})^2 |\psi_{ab}(\Omega)|^2 d\Omega \\
&= \frac{1}{a^2}\sigma_{\Omega^2}
\end{aligned} \qquad (3.14)$$

54

These results explain the role of scaling parameter a in wavelet transform. Fig. 3.2 displays time-frequency resolutions of the wavelet and scaling functions for different values of a.

3.3.1 Parseval Relation of Wavelet Transforms (Energy Preservation Property)

We will now show that the Parseval relation in wavelet transform

$$E = \int_{-\infty}^{\infty} \int_{-\infty}^{\infty} |W_f(a,b)|^2 \frac{dadb}{a^2} = C_h \int_{-\infty}^{\infty} |f(t)|^2 dt \tag{3.15}$$

holds for any signal $f(t)$ which is square-integrable. Its proof requires the admissibility condition which was defined in Eq.(3.7). By using the dual relation of wavelet transform in time-frequency domain

$$W_f(a,b) = f(t) * \psi_{ab}(-t)|_{t=b} \iff F(\Omega)|a|^{1/2}\overline{\Psi(a\Omega)}e^{j\Omega b}$$

one can get

$$\int_{-\infty}^{\infty} \int_{-\infty}^{\infty} |W_f(a,b)|^2 \frac{dadb}{a^2} = \frac{1}{2\pi} \int_{-\infty}^{\infty} |F(\Omega)|^2 \underbrace{\int_{-\infty}^{\infty} \frac{|\Psi(a\Omega)|^2}{|a|}da}_{C_h} \, d\Omega$$

$$= C_h \int_{-\infty}^{\infty} |f(t)|^2 dt \tag{3.16}$$

It is worth nothing that the wavelet transform energy preserves also between the different scales such that

$$\int_{-\infty}^{\infty} |\psi(t)|^2 dt = \int_{-\infty}^{\infty} \frac{1}{|a|} |\psi_{ab}(t)|^2 dt \tag{3.17}$$

55

$$\frac{1}{a_3^2}\sigma_\Omega^2$$

$$\frac{1}{a_2^2}\sigma_\Omega^2 \qquad \sigma_\Omega^2$$

$$\sigma_t^2$$

$$\frac{1}{a_1^2}\sigma_\Omega^2$$

t_1 time

$\psi_{ab}(t)$

2

1

0

-1

-2

0   5   10   15   20   25

t

$\Psi_{ab}(\Omega)$

1.0

0.8

0.6

0.4

0.2

0.0

-60   -40   -20   0   20   40   60

Ω

56
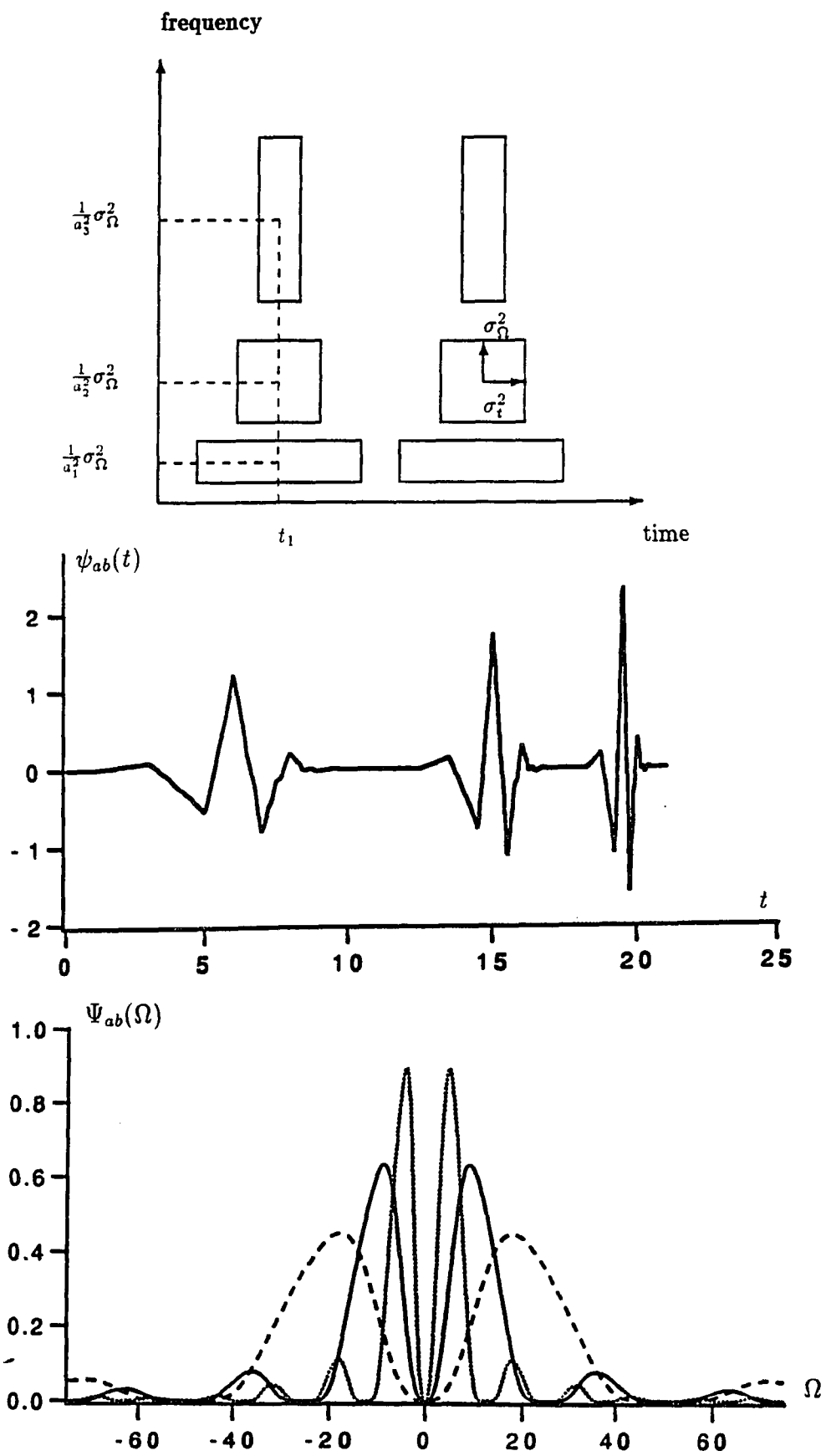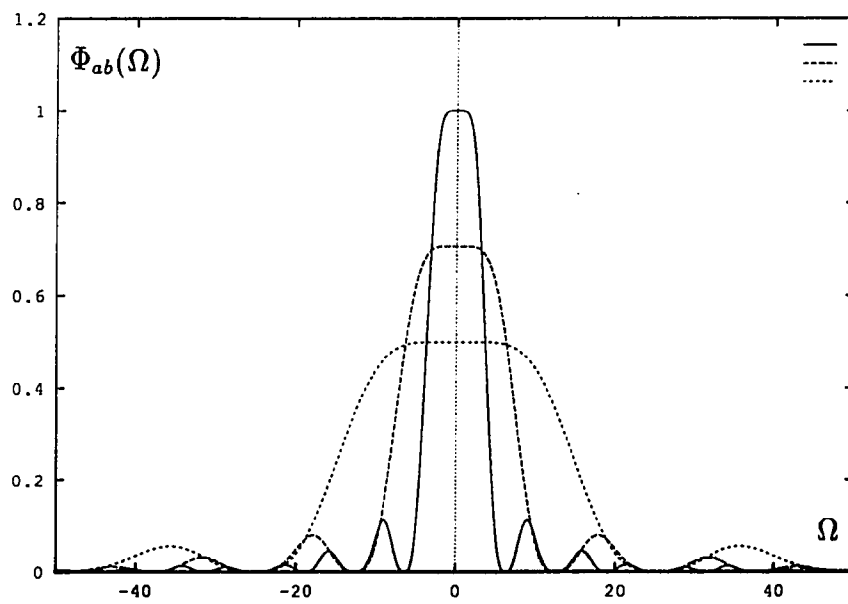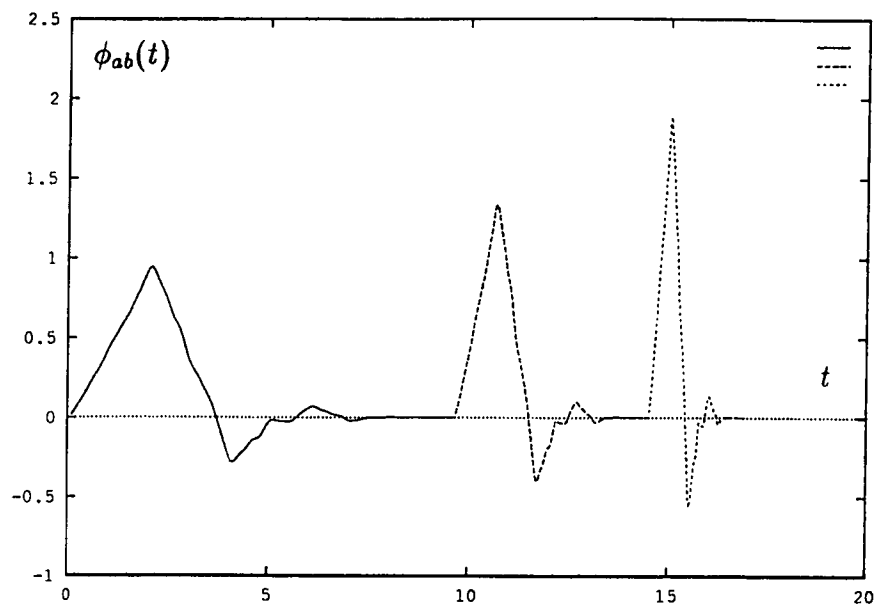
Fig. 3.2. The role of scaling parameter a in wavelet transform.

3.4 Discrete Wavelet Transform

Although the admissibility condition assures the complete representation of $f(t)$ with its wavelet transform coefficients $W_f(a, b)$, it requires the wavelet transform operation to be performed for all values of a and b which are continuous parameters. This transform representation is not practical. One would prefer to perform the wavelet transform operation as few times as possible. Therefore these scaling or dilation, and translation or shift parameters, a and b respectively, are discretized. This discretization provides a transform grid or frame on the time-scale plane for the representation of signal $f(t)$. It is intuitive that this grid or frame should be defined properly such that the complete representation of $f(t)$ is still possible. This is called the Discrete Wavelet Transformation(DWT). This version of the wavelet transform reduces the redundancies of the wavelet space $W_f(a, b)$ significantly. The mathematical reasonings on the choice of frames or grids are perfectly treated in the literature.

Now we can define the basis functions of a Discrete Wavelet Transform as the subset of continuous wavelet functions[37][38][40][41]

$$\psi_{ab}(t) = \frac{1}{|a|^{1/2}} \psi(\frac{t - b}{a}) \tag{3.18}$$

with the corresponding discrete transform lattices or grids

$$a = a_0^m \quad b = nb_0 a_0^m$$

Hence, the discrete wavelet transform basis functions can be expressed as

$$\psi_{mn}(t) = a_0^{-\frac{m}{2}} \psi(a_0^{-m}t - nb_0) \tag{3.19}$$

Here m and n are integers. It is intuitively seen that this discrete wavelet family approaches to a continuous wavelet family when $a_0 \to 1$ and $b_0 \to 0$.

58

It can be shown that the functions of a discrete wavelet transform basis $\psi_{mn}(t)$ can form a frame or the sets of m and n parameters are proper for the completeness if the wavelet function $\psi(t)$ satisfies the admissibility condition. Then the frame bounds are constrained by the inequalities[40] $0 < A < B < \infty$

$$A \le \frac{\pi}{b_0 log a_0} \int \frac{|\Psi(\Omega)|^2}{|\Omega|} d\Omega \le B \tag{3.20}$$

These inequalities hold for any choice of a_0 and b_0. These bounds diverge for non-admissible wavelet functions.

The discrete wavelet transform is defined on the grid points or in the frame of time-scale plane as

$$W_f(m,n) = <\psi_{mn}, f> = a_0^{-\frac{m}{2}} \int_{-\infty}^{\infty} \psi(a_0^{-m}t - nb_0) f(t) dt \tag{3.21}$$

and the wavelet transform representation of the signal

$$f(t) = \sum_m \sum_n W_f(m,n) \psi_{mn}(t) \tag{3.22}$$

There is a particular interest on binary or dyadic grid where $a_0=2$ and $b_0=1$, which leads to the conventional multiresolution concept and the orthonormal discrete wavelet transforms.

3.5 Compactly Supported Orthonormal Wavelet Bases and Their Linkages with Unitary FIR PR-QMFs

In general, the wavelet transform functions in a frame are not linearly independent therefore there is a redundancy within the frame. In many applications a minimum possible redundancy in the frame is desired. An orthonormal basis is a frame with $A = 1$ and $B = 1$ in Eq.(3.20). Orthonormal bases are of special interest to us.

The first orthonormal wavelet bases were studied by Stromberg[42], Meyer[43], Battle[44], and Lemarié[45]. In the Meyer basis, the wavelet function $\psi(t)$ has a

compact support and has infinitely many times differentiable Fourier transform. It follows that $\psi(t)$ itself is infinitely many times differentiable, and it decays faster than any inverse polynomial. For the support length of N, there exists a constant C_N so that[43]

$$|\psi(t)| \leq \frac{C_N}{(1 + |t|)^N}$$

For practical purposes, however, the constants C_N turn out to be so large and give rather bad numerical localization properties. The Stromberg and Battle - Lemarié bases[42][44] have less differentiability (typically they are k times differentiable), but they have exponential decay in time,

$$|\psi(t)| \leq ce^{-\alpha t}$$

The decay constant α tends to be zero as k (the degree of differentiability of $\psi(t)$) tends to go to infinity.

Mallat and Meyer, by using multiresolution analysis, developed an elegant framework for constructing orthonormal wavelet basis which includes all existing nice wavelet bases. The first constructed wavelet bases are the special case of this general technique[37][38].

These bases turn out to be related to a special type of quadrature mirror filters(QMF). As will be seen later, these wavelet bases lead to a multiresolution signal representation scheme and has very strong connections with the PR subband dyadic tree structures which were presented in Chapter 2. Interestingly enough, the compactly supported orthonormal wavelet transform algorithms are very closely related to the dyadic tree FIR PR-QMF algorithms. The whole wavelet transform operations can be confined to the transform domain for the different dilations and translations. It is shown that any unitary FIR PR-QMF bank which has some degree of regularity leads to a compactly supported orthonormal wavelet transform basis.

The multiresolution signal analysis concept provides the best framework to understand the compactly supported orthonormal wavelet bases and their design. The idea of multiresolution analysis is to write an L^2-function $f(t)$ as the limit of successive approximations, each of which is smoothed version of $f(t)$, with more and more concentrated smoothing functions. The successive approximations of a function thus correspond to different resolutions, therefore the name multiresolution analysis is used. This smoothing or approximation is accomplished with the use of a kernel low-pass approximation function called the scaling function $\phi(t)$.

A multiscale analysis of signals consists of a sequence $\{V_m | m \in Z\}$ of closed subspaces of $L^2(R)$ which satisfy the following conditions[40][41][49]

- Containment Property :

$$\ldots V_2 \subset V_1 \subset V_0 \subset V_{-1} \subset V_{-2} \ldots$$

- Completeness Property :

$$\bigcap_{m \in Z} V_m = \{0\} \qquad \bigcup_{m \in Z} V_m = L^2(R)$$

- Scaling Property :

$$f(.) \in V_m \iff f(2.) \in V_{m-1} \text{ for any function } f \in L^2(R)$$

- The Basis/Frame Property :

There exists a function $\phi(t) \in V_0$ such that $\forall m \in Z$, the set

$$\{\phi_{mn}(t) = 2^{-m/2}\phi(2^{-m}t - n)| \ \forall n \in Z; \ \text{spans } n \in Z\}$$

Let W_m denote the orthogonal complement of subspaces V_m and V_{m+1}. Let us also denote by P_m and Q_m, the projection operators from $L^2(R)$ onto V_m and W_m respectively. Clearly, the containment and completeness properties imply the

existence of subspaces W_m and projection operators are well defined. The completeness property also ensures that $\lim_{m \to -\infty} P_m f = f$ for any signal $f \in L^2(R)$, where the limit are taken in L^2 norm. The containment property implies that $P_m f$, for successively decreasing m, leads to successively better approximations of f. That is, for given $P_m f$, $P_{m+1} f$ is completely determined. The scaling property ensures that the approximations reside on different scales.

If the functions $\phi_{mn}(t)$, for a fixed m, form a basis for V_m, then by using Gram orthonormalization process in the Hilbert space $L^2(R)$, a function $\tilde{\phi}_{mn}(t)$ is constructed from $\phi_{mn}(t)$ such that $\tilde{\phi}_{mn}(t)$ forms an orthonormal basis for $L^2(R)$. Therefore, the function set $\{\phi_{mn}(t)\}$ is assumed to be an orthonormal set.

The Containment Property imposes a restriction on the scaling function $\phi(t)$ since

$$\phi(t) \in V_0 \subset V_{-1} = span\{\phi_{-1n}(t); n \in Z\}$$

Therefore, we have the fundamental scaling equation, which is stated as the two scaling functions of the adjacent resolutions, for example $m = 0$ and 1, must have the functional linear inter-scale relationship

$$\phi(t) = \sum_n h_0(n)\phi(2t - n) \tag{3.23}$$

The coefficient set $\{h_0(n)\}$ in Eq.(3.23) is called the *inter-scale basis coefficients*. If we take the Fourier transform of both sides in this equation

$$\Phi(\Omega) = \sum_n h_0(n)e^{-j\frac{\Omega}{2}nT_0}\Phi(\frac{\Omega}{2}) \tag{3.24}$$

Additionally, let us define the Fourier transform of the discrete time sequence, inter-scale coefficients $\{h_0(n)\}$ as

$$H_0(e^{j\omega}) = \sum_n h_0(n)e^{-j\omega n} \tag{3.25}$$

Therefore we can rewrite Eq.(3.24) with $\Omega = \frac{\omega}{T_0}$

$$\Phi(\Omega) = H_0(e^{j\frac{\omega}{2T_0}})\Phi(\frac{\Omega}{2}) \tag{3.26}$$

$H_0(e^{j\frac{\omega}{2T_0}})$ is a periodic function with the period of 4π.

Similarly for the next two adjacent resolutions we can write the relationship of their scaling functions as

$$\phi(2t) = \sum_n h_0(n)\phi(4t - n)$$

This implies the relationship in the frequency domain

$$\Phi(\frac{\Omega}{2}) = H_0(e^{j\frac{\omega}{4T_0}})\Phi(\frac{\Omega}{4})$$

Therefore we can rewrite $\Phi(\Omega)$ of Eq.(3.26) in the form

$$\Phi(\Omega) = H_0(e^{j\frac{\omega}{2T_0}})H_0(e^{j\frac{\omega}{4T_0}})\Phi(\frac{\Omega}{4})$$

Notice now that $H_0(e^{j\frac{\omega}{4}})$ has a period of 8π. If we repeat this procedure infinite times, using that $\frac{\Omega}{\infty} \to 0$,

$$\Phi(\Omega) = \Phi(0)\prod_{k=1}^{\infty} H_0(e^{j\frac{\omega}{2^k T_0}}) \tag{3.27}$$

One can show that the completeness property of a multiresolution approximation implies that any scaling function satisfies non-zero mean constraint[40]

$$\int_{-\infty}^{\infty} \phi(t)dt \neq 0$$

If one restricts the case where $\phi(t)$ is a real function, then $\phi(t)$ is determined uniquely, up to a sign, by the requirement that $\phi_{0n}(t)$ be orthonormal. Therefore,

$$\int_{-\infty}^{\infty} \phi(t)dt = \pm 1 \tag{3.28}$$

63

which is equivalent to

$$
\begin{aligned}
|\Phi(0)| &= |\int_{-\infty}^{\infty} \phi(t)dt| \\
&= |H_0(e^{j\frac{\omega}{T_0}})|_{\omega=0} = 1 \quad\quad\quad (3.29)
\end{aligned}
$$

It is interesting that the Fourier transform of the continuous scaling function is obtained by the infinite resolution product of the Fourier transform of the inter-scale coefficients $\{h_0(n)\}$. If the duration of the inter-scale coefficients $\{h_0(n)\}$ is finite, the scaling function $\phi(t)$ is called *compactly supported*. Furthermore, if $h_0(n)$ has the duration $0 \leq n \leq N - 1$, $\phi(t)$ is also supported within the interval $0 \leq t \leq N - 1$[40][49].

The orthogonal or complementary space W_m is given by the difference $V_{m-1} \ominus V_m$. Now consider that $\phi(t-n) \in V_0$ and $\phi(2t-n) \in V_1$. Since $V_0 = span\{\phi(t-n)\}$ and $V_1 = span\{\phi(2t-n)\}$, it is reasonable to expect the existence of a function $\psi(t)$, such that $W_0 = span\{\psi(t-n)\}$. This is indeed true and can be proven by the group representation arguments. This function $\psi(t)$ is the wavelet function, associated with the multiscale analysis. Clearly, by the scaling property, $W_m = span\{\psi(2^{-m}t-n)\}$. W_m are also (as V_m) generated by the translates and dilations, $\psi_{mn}(t)$, of a single wavelet or kernel function $\psi(t)$. The containment and completeness properties together with $W_m \perp V_m$, and $V_{m-1} = V_m \oplus W_m$ imply that the spaces W_m are all mutually orthogonal, and also their direct sum is equal to $L^2(R)$. Since for each m, the set $\{\psi_{mn}(t) ; n \in Z\}$ constitutes an orthonormal basis for W_m, it follows that the whole collection $\{\psi_{mn}(t) ; m, n \in Z\}$ is an orthonormal wavelet basis for $L^2(R)$. Now $L^2(R)$ can be decomposed as

$$
L^2(R) = ... \oplus W_j \oplus W_{j-1} ... \oplus W_0 ... \oplus W_{-j+1} \oplus W_{-j+2} ...
$$

which implies that $L^2(R) = span\{2^{-m/2}\psi(2^{-m}t-n)\}$. The set $\{\psi_{mn}(t) = 2^{-m/2}\psi(2^{-m}t - n)\}$ is the wavelet basis associated with the multiscale analysis.

For the multiresolution analysis described above, there exists the corresponding orthonormal wavelet function, similar to the scaling function. These band-pass nature wavelet functions are also linearly related to the next better resolution low-pass scaling functions as

$$\psi(t) = \sum_n h_1(n)\phi(2t - n) \tag{3.30}$$

This is the fundamental wavelet equation, and dual of the fundamental scaling equation.

Note that if the scaling function $\phi(t)$ is compactly supported in the interval $[0, N - 1]$, the corresponding wavelet function $\psi(t)$ is also compactly supported within the interval $[1 - \frac{N}{2}, \frac{N}{2}]$.

Now we take the Fourier transform of both sides in Eq.(3.30)

$$\Psi(\Omega) = \sum_k h_1(k)(e^{-j\frac{\Omega}{2}k})\Phi(\frac{\Omega}{2}) \tag{3.31}$$

If we define the Fourier Transform of the new inter-scale coefficient sequence $\{h_1(k)\}$ as

$$H_1(e^{j\omega}) = \sum_k h_1(k)e^{-j\omega k}$$

We can rewrite the wavelet function in Fourier domain with $\Omega = \frac{\omega}{T_0}$

$$\Psi(\Omega) = H_1(e^{j\frac{\omega}{2T_0}})\Phi(\frac{\Omega}{2}) \tag{3.32}$$

If we replace the second term in the right hand side of this equation with the infinite frequency product derived earlier in Eq.(3.27)

$$\Psi(\Omega) = H_1(e^{j\frac{\omega}{2T_0}}) \prod_{k=2}^{\infty} H_0(e^{j\frac{\omega}{2^k T_0}}) \tag{3.33}$$

The scaling function has to satisfy the conditions of an orthonormal set within a scale, for a fixed m as

$$< \phi_{mn}(t), \phi_{ml}(t) > = \delta_{nl} \tag{3.34}$$

65

Therefore the scaling function of a given resolution and its translates $\{\phi_{mn}(t)\}$ provide an orthonormal basis. Since the scaling functions $\{\phi(t-n)\}$ provide an orthonormal basis their Fourier transforms must satisfy the unitary condition

$$\sum_k |\phi(\Omega + 2\pi k)|^2 = 1 \qquad (3.35)$$

Its proof is given in Appendix A. If we employ the Fourier domain relationship of the adjacent resolution scaling functions of Eq.(3.26)

$$\Phi(2\Omega) = H_0(e^{j\frac{\omega}{T_0}})\Phi(\Omega) \qquad (3.36)$$

in the orthonormality condition of Eq.(3.35), we obtain the equation[39]

$$\sum_k |H_0(e^{j(\frac{\omega}{T_0}+k\pi)})|^2 |\phi(\Omega + k\pi)|^2 = 1 \qquad (3.37)$$

This equation can be rewritten as the sum

$$|H_0(e^{j(\frac{\omega}{T_0}+\pi)})|^2 \sum_{2k+1} |\phi(\Omega + (2k+1)\pi)|^2 + |H_0(e^{j\frac{\omega}{T_0}})|^2 |\sum_{2k} \phi(\Omega + 2k\pi)|^2 = 1 \quad (3.38)$$

This last equation yields the magnitude square condition of the inter-scale coefficient sequence $\{h_0(n)\}$

$$|H_0(e^{j\frac{\omega}{T_0}})|^2 + |H_0(e^{j(\frac{\omega}{T_0}+\pi)})|^2 = 1 \qquad (3.39)$$

The orthonormal wavelet bases are complementary to the scaling bases and satisfy the intra and inter-scale orthonormalities as

$$< \psi_{mn}(t), \psi_{kl}(t) > = \delta_{mk}\delta_{nl}$$

where m and k are the scale, and n and l are the translation parameters. Notice that the orthonormality conditions of wavelets hold for different scales, in addition to the same scale which is the only case for scaling functions. Since $\{\psi(t-n)\}$ forms

66

an orthonormal basis for W_0, their Fourier transforms must satisfy the unitary condition in frequency

$$\sum_k |\Psi(\Omega + 2\pi k)|^2 = 1 \tag{3.40}$$

As found earlier, the wavelet function in Fourier domain is expressed as

$$\Psi(2\Omega) = H_1(e^{j\frac{w}{T_0}})\Phi(\Omega) \tag{3.41}$$

Similarly, if we employ Eq.(3.40) into Eq.(3.41) the sequence $\{h_1(n)\}$ should satisfy

$$|H_1(e^{j\frac{w}{T_0}})|^2 + |H_1(e^{j(\frac{w}{T_0}+\pi)})|^2 = 1 \tag{3.42}$$

These scaling and wavelet functions also satisfy the orthonormality condition between themselves as

$$< \phi_{mn}(t), \psi_{kl}(t) >= 0$$

Note that the orthonormality condition of wavelet and scaling functions are satisfied for the different scales, in addition to the same scale. This time domain condition implies its counterpart in the frequency domain as

$$\sum_k \Phi(\Omega)\Psi(\Omega - 2\pi k) = 0 \tag{3.43}$$

Now, if we use Eqs.(3.43), (3.41), and (3.36) then we obtain the frequency domain condition

$$H_0(e^{j\frac{w}{T_0}})H_1(e^{-j\frac{w}{T_0}}) + H_0(e^{j(\frac{w}{T_0}+\pi)})H_1(e^{-j(\frac{w}{T_0}+\pi)}) = 0 \tag{3.44}$$

This condition is automatically satisfied by relating the two inter-scale sequences in frequency as

$$H_1(e^{j\omega}) = -e^{-j\omega}H_0(e^{-j(\omega+\pi)}) \tag{3.45}$$

or in time domain

$$h_1(n) = (-1)^n h_0(1 - n)$$

Three conditions required from the inter-scale coefficients, $\{h_0(n)\}$ and $\{h_1(n)\}$ in Eq.(3.39), Eq.(3.42) and Eq.(3.44), to design compactly supported orthonormal wavelet basis are then equivalent to the requirement that the matrix $\mathcal{H}(e^{j\omega})$ with normalized $T_0 = 1$

$$\mathcal{H}(e^{j\omega}) = \begin{bmatrix} H_0(e^{j\omega}) & H_1(e^{j\omega}) \\ H_0(e^{j(\omega+\pi)}) & H_1(e^{j(\omega+\pi)}) \end{bmatrix} \tag{3.46}$$

be unitary for all ω.

It is very interesting that these conditions of the inter-scale coefficient sequences $\{h_0(n)\}$ and $\{h_1(n)\}$ for the orthonormal wavelet basis design are nothing else but the perfect reconstruction conditions of 2-band unitary FIR PR-QMF banks.

It has been shown that, the requirements for the design of a compactly supported orthonormal wavelet bases, are identical to the requirements of 2-band unitary FIR PR-QMF bank design as discussed in Chapter 2.

3.5.1 Wavelet Representation of Signals in Finite Number of Resolutions

A given function $f(t)$ can be represented by the orthonormal scaling function $\phi(t)$ and its translates as

$$f(t) = \sum_{n=-\infty}^{\infty} s(0,n)\phi(t-n) \tag{3.47}$$

where the scaling coefficients are

$$s(0,n) = \int_{-\infty}^{\infty} f(t)\phi(t-n)dt \tag{3.48}$$

If one desires to approximate $f(t)$ in a lower resolution with the coarser version of orthonormal scaling function and its translates as

$$f_A^1(t) = \sum_{n=-\infty}^{\infty} s(1,n)\phi(\frac{t}{2}-n) \tag{3.49}$$

68

where the scaling coefficients

$$s(1,n) = \int_{-\infty}^{\infty} f_A^1(t)\phi(\frac{t}{2} - n)dt \tag{3.50}$$

This implies the approximation error

$$f_E^1(t) = f(t) - f_A^1(t)$$

Since the approximation or scaling functions are smooth or low-pass in nature, it is intuitively expected that the approximation error has a band pass characteristic. Therefore we may represent this $f_E^1(t)$ function by employing an orthonormal function set with the band-pass nature.

We can now express the approximation error by employing the wavelet basis as

$$f_E^1(t) = \sum_{n=-\infty}^{\infty} W_f(1,n)\psi(\frac{t}{2} - n) \tag{3.51}$$

where the wavelet coefficients are found as

$$W_f(1,n) = \int_{-\infty}^{\infty} f(t)\psi(\frac{t}{2} - n)dt \tag{3.52}$$

Therefore, $f(t)$ can now be completely represented as the summation of its approximation in the lower resolution and the approximation error

$$f(t) = \sum_{n=-\infty}^{\infty} s(1,n)\phi(\frac{t}{2} - n) + \sum_{n=-\infty}^{\infty} W_f(1,n)\psi(\frac{t}{2} - n) \tag{3.53}$$

Similarly, we can obtain an approximation of $f_A^1(t)$ by the use of its lower time resolution scaling function set as

$$f_A^2(t) = \sum_{n=-\infty}^{\infty} s(2,n)\phi(\frac{t}{4} - n)$$

and the new approximation error term can be expressed by the wavelet function of that lower resolution as

$$f_E^2(t) = \sum_{n=-\infty}^{\infty} W_f(2,n)\psi(\frac{t}{4} - n)$$

69

The signal $f(t)$ is now written as

$$f(t) = \sum_{n=-\infty}^{\infty} s(2,n)\phi(\frac{t}{4} - n) + \sum_{n=-\infty}^{\infty} W_f(2,n)\psi(\frac{t}{4} - n) + \sum_{n=-\infty}^{\infty} W_f(1,n)\psi(\frac{t}{2} - n)$$

$$(3.54)$$

If this process is repeated, $f(t)$ can be completely represented as

$$f(t) = \sum_{m=1}^{\infty} \sum_{n=-\infty}^{\infty} W_f(m,n)\psi(\frac{t}{2^m} - n) \qquad (3.55)$$

As seen from this function expansion formula, one needs infinite number of resolutions to completely represent $f(t)$. This is not a practically desired case. Therefore we would like to limit the coarsest desired resolution for the approximation of signal $f(t)$ as L and approximate the signal in that resolution with the corresponding scaling function set,

$$f_A^L(t) = \sum_{n=-\infty}^{\infty} s(L,n)\phi(\frac{t}{2^L} - n)$$

Using terms $m > L$ actually implies a band-limited low-pass approximation of $f(t)$. The wavelet functions for $m > L$ corresponds to lower end of the frequency spectrum. Since the number of resolutions used in the representation is limited, the corresponding approximation error now becomes

$$f_E^L(t) = \sum_{m=1}^{L} \sum_{n=-\infty}^{\infty} W_f(m,n)\psi(\frac{t}{2^m} - n)$$

Hence, the signal $f(t)$ can be represented in a finite resolution as

$$f(t) = \sum_{n=-\infty}^{\infty} s(L,n)\phi(\frac{t}{2^L} - n) + \sum_{m=1}^{L} \sum_{n=-\infty}^{\infty} W_f(m,n)\psi(\frac{t}{2^m} - n) \qquad (3.56)$$

Last equation shows that $f(t)$ can be represented as its low-pass approximation and sum of detail signals in different resolutions.

3.5.2 Dyadic Subband Filter Banks as Fast Wavelet Transform Algorithms

Multiresolution analysis of continuous signals presented in the previous sections can be performed within the discrete domain. This was first shown by S. Mallat[37].

Let us examine explicitly how this algorithm works.

If we start with the premise that only samples $f(n) = s(0, n)$ of the signal $f(t)$ available, we can form an interpolated signal $\hat{f}(t)$, $\hat{f}(t) \in V_0$ with the original sequence $\{s(0, n) ; n \in Z\}$, by defining[37][40][46]

$$\hat{f}(t) = \sum_n s(0, n)\phi(t - n)$$

Since $V_0 = V_1 \oplus W_1$, $\hat{f}(t)$ can be decomposed uniquely into an element of V_1 plus an element of W_1. These two components can be expanded into $\phi_{1n}(t)$ and $\psi_{1n}(t)$, respectively; since $\{\phi_{1n}(t) ; n \in Z\}$ is an orthonormal basis of V_1, and $\{\psi_{1n}(t) ; n \in Z\}$ an orthonormal basis of W_1. It is expressed as

$$
\begin{aligned}
\hat{f}(t) &= \hat{f}_A^1(t) + \hat{f}_E^1(t) \\
\hat{f}(t) &= \sum_n s(1, n)\phi(\frac{t}{2} - n) + \sum_n W_f(1, n)\psi(\frac{t}{2} - n)
\end{aligned}
\tag{3.57}
$$

The sequences $s(1, n)$ and $W_f(1, n)$ can be computed directly from $s(0, n)$ as

$$
\begin{aligned}
s(1, n) &= <\phi_{1n}(t), \hat{f}_A^1(t)> = <\phi_{1n}(t), \hat{f}(t)> \\
&= \sum_k s(0, k) <\phi_{1n}(t), \phi_{0k}(t)>
\end{aligned}
\tag{3.58}
$$

where

$$
\begin{aligned}
<\phi_{1n}(t), \phi_{0k}(t)> &= \frac{1}{2} \int \phi(\frac{t}{2} - n)\phi(t - k)dt \\
&= \frac{1}{2} \int \phi(\frac{t}{2})\phi(t - (n - 2k))dt
\end{aligned}
\tag{3.59}
$$

Then Eq.(3.58) can be rewritten as

$$s(1, n) = \sum_k h_0(k - 2n)s(0, k) \tag{3.60}$$

with

$$h_0(n) = \frac{1}{2} \int \phi(\frac{t}{2})\phi(t - n)dt \tag{3.61}$$

71

Note that $\{h_0(n)\}$ are nothing else but the inter-scale basis coefficients defined in Eq.(3.23). It can be similarly shown that the wavelet coefficients of the approximation error or high frequency component of the discrete time signal $s(0,n)$

$$W_f(1,n) = \sum_k h_1(k-2n)s(0,k) \qquad (3.62)$$

with the coefficient values

$$h_1(n) = \frac{1}{2}\int \psi(\frac{t}{2})\phi(t-n)dt \qquad (3.63)$$

Since $\int \phi(t)dt = 1$ the sequence $s(1,n)$ can be considered as an "averaged" version of the $s(0,n)$ on a scale twice as large, and therefore sampled by 2. This is expressed in Eq.(3.60) which is a discrete time convolution followed by a down sampler with factor of 2. The sequence $W_f(1,n)$ corresponds to the difference information between the original signal $s(0,n)$ and its low-pass version $s(1,n)$. $W_f(1,n)$ also downsampled by 2, as seen in Eq.(3.62). The original sequence $s(0,n)$ therefore can be reconstructed from $s(1,n)$ and $W_f(1,n)$ by using the inter-scale coefficients $\{h_0(n)\}$ and $\{h_1(n)\}$ as[41]

$$
\begin{aligned}
s(0,n) &= \;<\phi_{0n}(t),\hat{f}(t)>=<\phi_{0n}(t),\hat{f}_A^1(t)+\hat{f}_E^1(t)> \\
&= \sum_k s(1,k)<\phi_{0n}(t),\phi_{1k}(t)> + \sum_k W_f(1,k)<\phi_{0n}(t),\psi_{1k}(t)> \\
&= \sum_k s(1,k)h_0(2k-n) + \sum_k W_f(1,k)h_1(2k-n) \qquad (3.64)
\end{aligned}
$$

The decomposition of $s(0,n)$ into $s(1,n)$ and $W_f(1,n)$ is only the first step. In the next stage we similarly decompose $s(1,n)$ into an even coarser sequence $s(2,n)$ and a new difference sequence $W_f(2,n)$. To do this, we again use the multiresolution analysis as a tool

$$
\begin{aligned}
\hat{f}_A^1(t) \in V_1 &= V_2 \oplus W_2 \\
\hat{f}_A^1(t) &= \hat{f}_A^2(t) + \hat{f}_E^2(t) \\
&= \sum_n [s(2,n)\phi_{2n}(t) + W_f(2,n)\psi_{2n}(t)] \qquad (3.65)
\end{aligned}
$$

with

$$s(2, n) = \; < \phi_{2n}(t), \hat{f}_A^2(t) > = < \phi_{2n}(t), i\hat{f}_A^1(t) >$$

$$= \sum_k s(1, k) < \phi_{2n}(t), \phi_{1k}(t) > \tag{3.66}$$

One easily shows that

$$< \phi_{m+1,k}(t), \phi_{m,n}(t) > = h_0(n - 2k)$$

independent from m. It follows that

$$s(2, n) = \sum_k s(1, k) h_0(2k - n) \tag{3.67}$$

Similarly,

$$W_f(2, n) = \sum_k s(1, k) h_1(2k - n) \tag{3.68}$$

Hence, one obtains that

$$s(1, n) = \sum_k [s(2, k) h_0(2k - n) + W_f(2, k) h_1(2k - n)] \tag{3.69}$$

Note that, for a given resolution level m, $s(m, n)$ captures the information of the signal at resolution 2^m and the $W_f(m, n)$ captures the new information or detail in the signal going from the resolution 2^m to resolution 2^{m+1}. Therefore, it is possible to construct these multiresolution representations such that the transform coefficients are related through the discrete time decimation and interpolation relations as

$$s(m + 1, n) = \sum_k s(m, k) h_0(2k - n)$$

$$W_f(m + 1, n) = \sum_k s(m, k) h_1(2k - n)$$

$$s(m, n) = \sum_k [s(m + 1, k) h_0(2k - n) + W_f(m + 1, k) h_1(2k - n)]$$

$$\tag{3.70}$$

Then the whole wavelet decomposition + reconstruction transform operations can be represented as in Fig. 3.3. As seen for any resolution L, $s(0,n)$ is decomposed into $s(L,n)$, $W_f(1,n)$, $W_f(2,n)$, ..., $W_f(L,n)$.
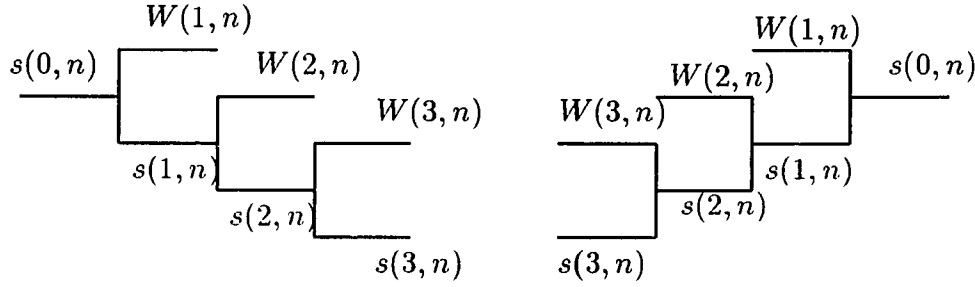
Fig. 3.3. Decomposition+Reconstruction operation in wavelet transform.

The dyadic subband tree-structure, together with easy convolution and decimation structure makes this algorithm work very fast. In fact, for the implementation of Mallat's algorithm[37], one only needs two filters $h_0(n), h_1(n)$; their multiresolution analysis origins are not used explicitly. One may therefore try to isolate the relevant properties of the filters, and design filters satisfying all these properties of unitary 2-band PR-QMF. Therefore, any PR-QMF solution can be used to construct orthonormal wavelet basis as long as they satisfy zero mean high-pass filter condition.

3.5.3   Wavelet Regularity and Daubechies Wavelet Bases

Daubechies constructed orthonormal wavelet bases which have good frequency localization as well as time localization. She developed compactly supported basis functions(time localization) such that they not only satisfy all the multiresolution analysis conditions but also have good frequency localization[40].

For typical engineering applications, the scaling function $\phi(t)$ must be reasonably smooth. This restriction can be reflected into the decay of Fourier transform of the scaling function. A decay in the Fourier domain can be achieved if the

Fourier transform of the sequence has a factor of the form $(1 + e^{-j\omega})^N$ for some integer N. This introduces an ω^{-N} factor in the Fourier transform of this sequence. This idea was used by Daubechies to prove the following sufficiency condition on the inter-scale sequence $\{h_0(n)\}$ for the smoothness of the scaling function.

Let the Fourier transform of the sequence $\{h_0(n)\}$ be in the form of

$$H_0(e^{j\omega}) = (1 + e^{-j\omega})^N P(e^{j\omega}) \tag{3.71}$$

for some trigonometric polynomial $P(e^{j\omega})$. Furthermore, Let $P(e^{j\omega})$ satisfy the following equation

$$\underset{\omega \in R}{\text{Max}} \; | \prod_{k=0}^{k=l} P(e^{j\frac{\omega}{2}k}) | \leq 2^{l(N-m-1)} \tag{3.72}$$

for some $l > 1$, then $h_0(n)$ leads to a scaling function that is m times continuously differentiable. Imposing these restrictions on $h_0(n)$ characterizes a multiscale analysis. Daubechies constructed a family of orthonormal scaling and wavelet functions that are compactly supported and have a degree of regularity which increases approximately linear with the support of $\phi(t)$.

As found in Eq.(3.39) the necessary condition on the inter-scale sequence $\{h_0(n)\}$

$$|H_0(e^{j\omega})|^2 + |H_0(e^{j(\omega+\pi)})|^2 = 1$$

On the other hand, by imposing the regularity condition, inter-scale coefficients should be in the form of

$$H_0(e^{j\omega}) = (1 + e^{-j\omega})^N P(e^{j\omega}) \tag{3.73}$$

for some integer $N \geq 2$. Then the trigonometric polynomial $P(e^{j\omega})$ has to satisfy the following equation[40]

$$|P(e^{j\omega})|^2 = \sum_{k=0}^{N-1} \binom{N-1+k}{k} sin^{2k}(\frac{\omega}{2}) + sin^{2N}(\frac{\omega}{2}) R(\frac{1}{2}cos\omega) \tag{3.74}$$

75

where $R(x)$ is an odd polynomial such that

$$R(x) = -R(1 - x)$$

By choosing $R(x) \equiv 0$ we obtain the compactly supported orthonormal wavelet bases which are called Daubechies wavelets in the literature. The support width of both the scaling function $\phi(t)$ and the wavelet function $\psi(t)$ is $2N$. Daubechies wavelet and scaling functions and their Fourier transforms are given in Fig. 3.4 for $N = 6$.

The regularity criterion used by Daubechies is defined as

$$|\Phi(\Omega)| \leq \frac{c}{(1 + |\Omega|)^{r+1}} \quad \text{for all real numbers } \Omega \tag{3.75}$$

where c is a constant. Then $\phi(t)$ will be m times continuously differentiable whenever $r > m$. The maximum value of r in Eq.(3.75) is therefore referred as the regularity of the scaling function. The linear inter-scale relationship of Daubechies scaling and wavelet functions are given in Fig. 3.5. Additionally, Fig. 3.6. shows that these bases satisfy the adjacent scale orthogonality of wavelet functions and orthogonality of scaling functions with integer dilations.

Note that, in the view of Eq.(3.32), $\Phi(\Omega)$ and $\Psi(\Omega)$ are defined as the infinite products of the Fourier transforms of inter-scale coefficient sequences as,

$$
\begin{aligned}
\Phi(\Omega) &= \prod_{k=1}^{\infty} H_0(e^{j\frac{\omega}{2^k T_0}}) \\
\Psi(\Omega) &= H_1(e^{j\frac{\omega}{2 T_0}}) \prod_{k=2}^{\infty} H_0(e^{j\frac{\omega}{2^k T_0}})
\end{aligned}
\tag{3.76}
$$

by letting $\omega = 0$ we find that $H_0(e^{j\omega})$ must have at least one zero at $\omega = \pi$ in order to satisfy the admissibility condition. We also have Fourier duality

$$\psi(t) = \sum_{n} h_1(n)\phi(2t - n)$$
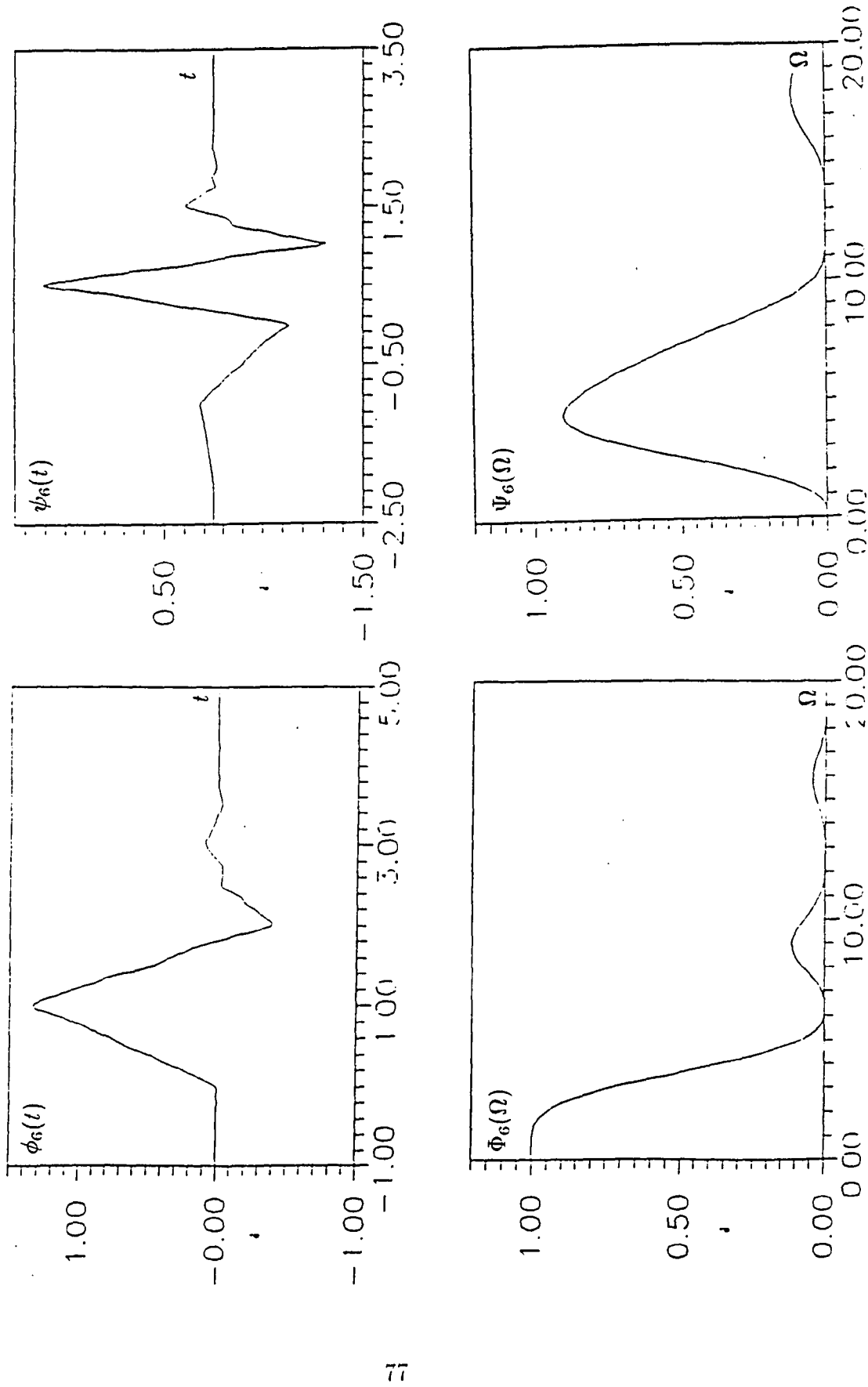
Fig. 3.4 Daubechies wavelet and scaling functions and their Fourier transforms for

$N = 6$

Therefore, all the regularity properties derived for $\phi(t)$ will be carried over $\psi(t)$ so that we can restrict ourselves to design of $\phi(t)$ only.

Daubechies derived a simple, useful estimate for the regularity[40]. Let $H_0(z)$ be an N-tap FIR filter. Assume $H_0(z)$ has K zeros at $z = -1$ then we have

$$H_0(z) = (1 + z^{-1})^K P(z)$$

and define

$$M_{K,L} = \underset{\omega \in R}{\text{Max}} \; |\prod_{k=0}^{L-1} P(e^{j\frac{\omega}{2^k}})|^{1/L} \tag{3.77}$$

then the following estimate for the regularity r of $H_0(z)$ holds in

$$r \geq -\frac{1}{2} - log_2 M_{K,L} \tag{3.78}$$

The number of zeros of $H_0(z)$ at $z = -1$, K, plays an important role for the estimation of the regularity in Eq.(3.78). Also, we have seen that $K \geq 1$ is necessary for the smoothness of $\phi(t)$.

Note that, imposing K zeros at $z = -1$ for $H_0(z)$ is equivalent to impose a "flatness" requirement on the frequency response of the inter-scale coefficient sequence $|H_0(z)|$ at $\omega = \pi$. This implies that its first $K-1$ derivatives should vanish at those points, along with $H_0(-1)$. The flatness requirement is also equivalent in time to

$$\sum_n (-1)^i n^i h_0(n) = 0 \quad \text{for i=0,1,...,K-1} \tag{3.79}$$

which in turn amounts to imposing $K - 1$ vanishing moments on the inter-scale sequence $h_1(n)$

$$\sum_n n^i h_1(n) = 0 \quad \text{for i=0,1,...,K-1} \tag{3.80}$$

This is equivalent to satisfy

$$\sum_i (2n)^i h_0(2n) = \sum_i (2n+1)^i h_0(2n+1) \quad \text{for } k \leq \frac{N}{2} - 1 \tag{3.81}$$

78
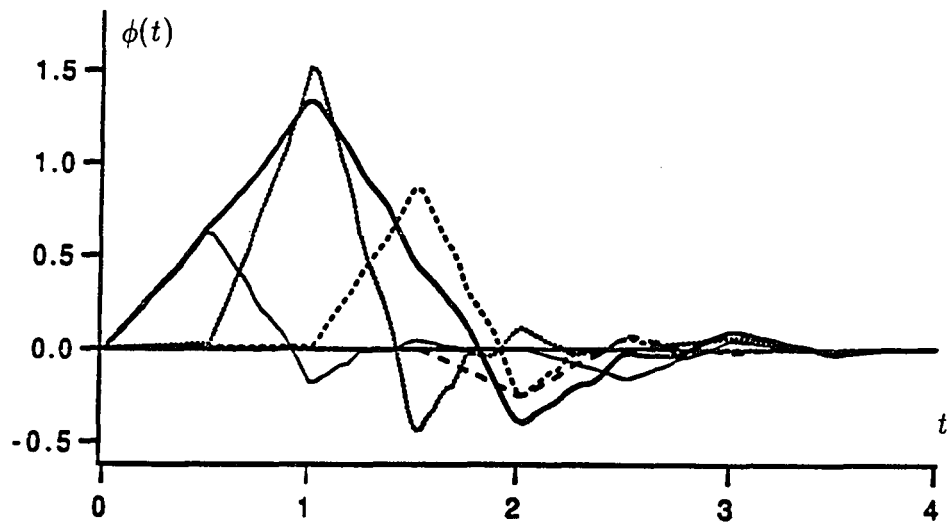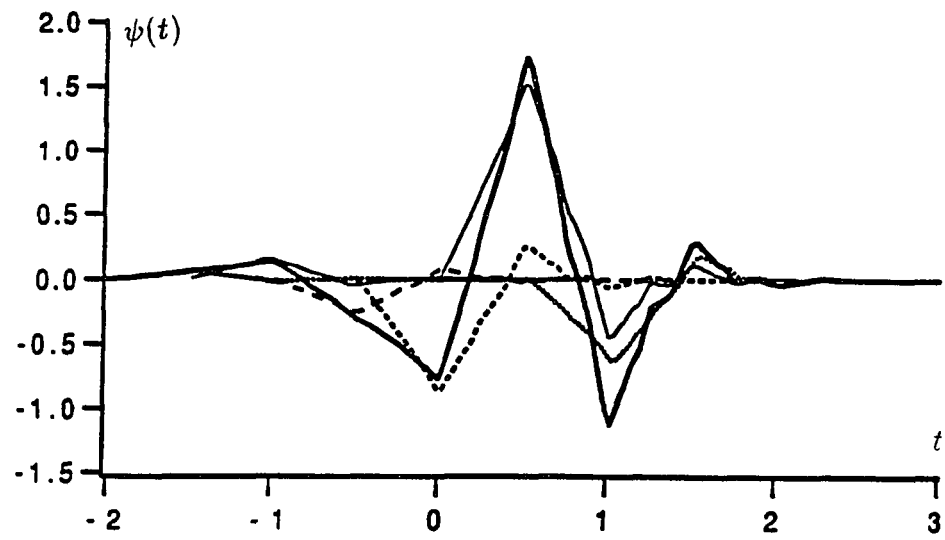
Fig. 3.5 Functional linear inter-scale relationship of Daubechies scaling and wavelet basis functions with N=6.
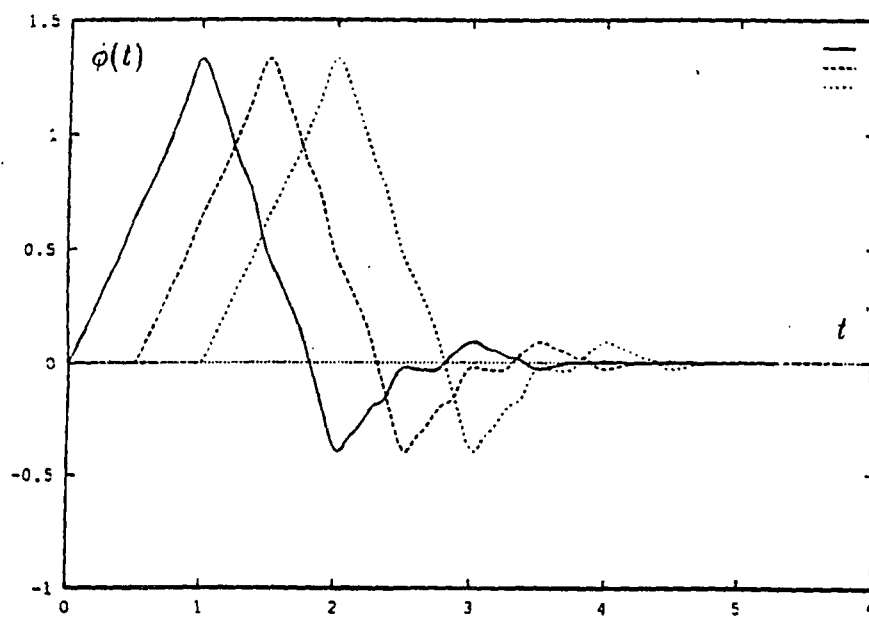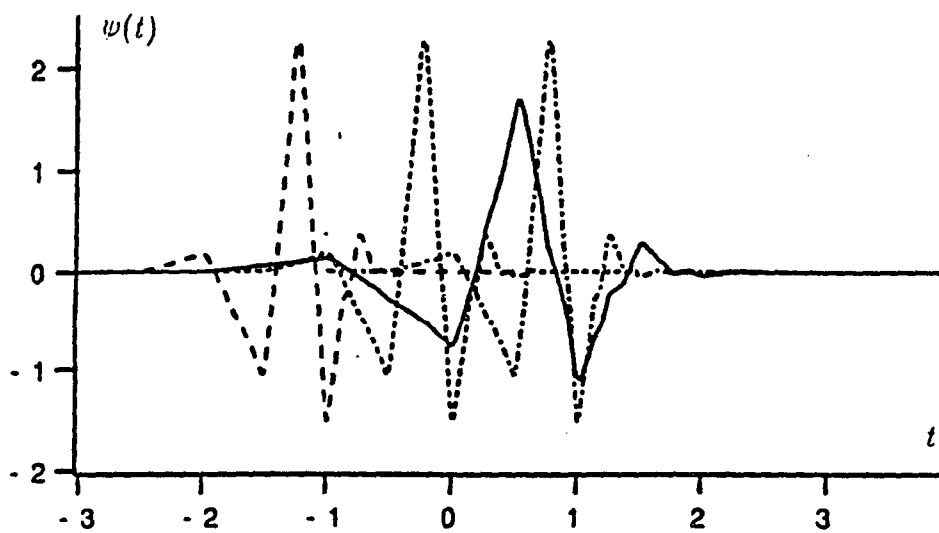
resolution and also their integer dilations. b) Orthogonality of Daubechies scaling

functions with integer dilations.

By choosing $R(x) \equiv 0$ in Eq.(3.74) K reaches its maximum value $N/2$ for an N tap filter. Imposing $R(x) \equiv 0$, i.e. $K = N/2$, corresponds to the unique "maximally flat" magnitude square response in which the number of vanishing derivatives of $|H_0(e^{j\omega})|^2$ at $\omega = 0$ and $\omega = \pi$ are equal. This inter-scale coefficient sequence $\{h_0(n)\}$ is identical to the unit sample response of Binomial-QMF derived in Chapter 4.

The regularity of the wavelet function $\psi(t)$ constructed by Daubechies increases linearly with its support width. Imposing higher order divisibility of $H_0(e^{j\omega})$ by $\frac{1}{2}(1 + e^{-j\omega})$ is used as a tool to obtain regularity. Daubechies and Lagarias have proven that maximally flat solution does not lead to the highest regularity on wavelet function. Defining a regularity estimate slightly different from Eq.(3.78) and using the two N-dimensional finite matrices and reducing the zeros of $H_0(z)$ at $z = -1$, they found higher regularity for the same support width. Unfortunately, this improved method requires considerable effort to compute $M_{K,L}$. Therefore, it is impractical even for the moderate values of N[46].

It is worth noting that if we restrict our attention to orthonormal bases of compactly supported wavelets only, then it is impossible to obtain $\psi(t)$ which is either symmetric or antisymmetric, except for the trivial Haar case. In order to obtain $h_0(n)$ as close to linear phase as possible we have to choose the zeros of its magnitude square function $|H_0(e^{j\omega})|^2$ alternatively from inside and outside the unit circle as frequency increases. This will lead the non-minimum phase FIR filter solutions. When N is sufficiently large, the impulse responses of $h_0(n)$ and $h_1(n)$ will have acceptable symmetry or antisymmetry. Obviously the larger support width will lead to more symmetrical filter solutions. In Daubechies wavelet bases there are $2^{[N/4]-1}$ different filter solutions. It is clear that for $N = 4$ and 6, there is effectively only one pairs of $\phi(t)$ and $\psi(t)$. For $N \geq 8$ we could choose the solution

which is closest to the linear phase. Even if minimum-phase solution has the worst phase response among the those solutions, it is still quite symmetrical for moderate values of N. The resulting $\{h_0(n)\}$ filter coefficients for minimum phase and the most symmetrical solutions are tabulated in Table 3.1 and Table 3.2 for different values of N[47][53].

3.5.4 Coiflet Bases :

For a fixed support width, Daubechies wavelet function $\psi(t)$ has the maximum number of vanishing moments. The scaling function $\phi(t)$ does not satisfy any moment condition, except $\int \phi(t)dt = 1$. For numerical analysis applications, it may be useful to give up some of the zero moments of wavelet function $\psi(t)$ in order to obtain some zero moments for the scaling function $\phi(t)$ as[47]

$$
\begin{aligned}
\int \phi(t)dt &= 1 \\
\int t^\nu \phi(t)dt &= 0 \quad \text{for} \quad \nu = 1, 2, ..., L-1 \\
\int t^\nu \psi(t)dt &= 0 \quad \text{for} \quad \nu = 0, 1, ..., L-1
\end{aligned}
\tag{3.82}
$$

Imposing such vanishing moments on scaling function $\phi(t)$ also increases its symmetry.

The conditions in Eq.(3.82) are equivalent in frequency to

$$
\begin{aligned}
\Phi(0) &= 1 \\
\frac{d^\nu}{d\Omega^\nu}\Phi(0) &= 0 \quad \text{for} \quad \nu = 1, 2, ...L-1 \\
\frac{d^\nu}{d\Omega^\nu}\Psi(0) &= 0 \quad \text{for} \quad \nu = 0, 1, ...L-1
\end{aligned}
$$

In terms of $H_0(e^{j\omega})$, these conditions imply

$$
\begin{aligned}
H_0(e^{j\omega})|_{\omega=0} &= 1 \\
\frac{d^\nu}{d\Omega^\nu}H_0(e^{j\omega})|_{\omega=0} &= 0 \quad \text{for} \quad \nu = 1, 2, ..., L-1
\end{aligned}
$$

$$\frac{d^\nu}{d\Omega^\nu}H_0(e^{j\omega})|_{\omega=\pi} = 0 \quad \text{for} \quad \nu = 0, 1, ..., L-1 \tag{3.83}$$

In order to satisfy those conditions, $H_0(e^{j\omega})$ has to be the in form of

$$H_0(e^{j\omega}) = 1 + (1 - e^{j\omega})^L S(e^{j\omega}) \tag{3.84}$$

From Eq.(3.83), $H_0(e^{j\omega})$ has the zero of order L at $\omega = \pi$. Consequently, $H_0(e^{j\omega})$ must satisfy,

$$H_0(e^{j\omega}) = \left[\frac{1}{2}(1 + e^{-j\omega})\right]^L P(e^{j\omega}) \tag{3.85}$$

where, $P(e^{j\omega})$ as found earlier

$$|P(e^{j\omega})|^2 = \sum_{k=0}^{L} \left(\begin{array}{c} L-1+k \\ k \end{array} \right) sin^{2k}(\frac{\omega}{2}) + sin^{2L}(\frac{\omega}{2})R(\frac{1}{2}cos\omega)$$

where $R(x)$ is an odd polynomial as given in Eq.(3.74). Together Eq.(3.84) and Eq.(3.85) lead to L independent linear constraints on the coefficients of $S(e^{j\omega})$.

For L even, $L = 2K$. A similar analysis could be carried out for L odd. Daubechies imposes $H_0(e^{j\omega})$ be the form

$$H_0(e^{j\omega}) = 1 + (sin^2(\frac{\omega}{2}))^K \left[-\sum_{k=0}^{K-1} \left(\begin{array}{c} K-1+k \\ k \end{array} \right) (cos^2(\frac{\omega}{2}))^k + (cos^2(\frac{\omega}{2}))^k f(\omega) \right] \tag{3.86}$$

in order to satisfy Eq.(3.84) and Eq.(3.85) simultaneously. Remaining $f(\omega)$ must be chosen such that PR conditions in Eq.(3.39) are satisfied. The inter-scale coefficients of Coiflet solutions are given in Table 3.3.

We will show later in Chapter 5 that these filters are obtained as the special cases of the generalized unitary 2-band PR-QMF design technique proposed in this dissertation.

3.6   Generalization of Orthonormal Wavelet Bases

The dilation factor 2 of in the definition of the orthonormal wavelet basis that forces $\psi(t)$ to have a bandwidth of at least one octave. In some applications it is

desirable to have better a frequency localization which can be achieved by choosing a dilation factor larger than 2. For general N, the step of one resolution space V_m to the coarser resolution space V_{m+1} corresponds to a jump of $\log_2 N$ octaves in frequency, since there is a dilation factor N between two resolutions, and every factor 2 corresponds to one octave[41][50].

The theory of orthonormal wavelet transforms can be generalized by choosing dilation factor N instead of 2 which is a special case. In general, a multiresolution scheme uses one scaling function $\phi(t)$, and $M-1$ different wavelets $\psi^i(t)$ $i = 1, 2, ..., N-1$

The families of the wavelet functions $\psi^i_{mn}(t)$ is of the form

$$\psi^i_{mn}(t) = N^{-m/2}\psi^i(N^{-m}t - n) \tag{3.87}$$

Similar to the case where the scaling factor is 2, there is also a sequence of embedded closed vector spaces $\{V_m\}$ here. Defining the low-pass scaling function as

$$\phi_{mn}(t) = N^{-m/2}\phi(N^{-m}t - n) \tag{3.88}$$

Then V_m is spanned by $\{\phi_{mn}(t)\}$ for fixed m. Then $N-1$ wavelets $\psi^i_{mn}(t)$ generate $N-1$ different families of spaces W^i_m, and for any m, the $N-1$ spaces W^i_{m+1} are orthogonal complement of V_{m+1} to constitute the space V_m as

$$V_m = V_{m+1} \oplus \left[\begin{array}{c} N-1 \\ \oplus \\ i = 1 \end{array} \; W^i_{m+1} \right] \tag{3.89}$$

The fundamental scaling equation, the linear relation of two scaling function of the adjacent resolutions, for the scaling factor N

$$\phi(t) = \sum_n h(n)\phi(Nt - n) \tag{3.90}$$

The frequency domain counterpart of this relation

$$\Phi(\Omega) = H_0(e^{j\omega/N})\Phi(\Omega/N) \tag{3.91}$$

84

Then $N-1$ different wavelet functions $\psi^i(t)$ can all be written as the linear combinations of the scaling function $\phi(Nt - n)$ as

$$\psi^i(t) = \sum_n h_i(n)\phi(Nt - n) \quad i = 1, 2, ..., N - 1 \tag{3.92}$$

Therefore There exists trigonometric polynomials $H_i(e^{j\omega})$ such that in Fourier domain

$$\Psi^i(\Omega) = H_i(e^{j\omega/N})\Phi(\Omega/N) \tag{3.93}$$

Since we are only interested in compact support bases, the scaling function $\phi(t)$ and wavelet functions $\psi^i(t)$, also $h_0(n)$ and $h_i(n)$ must have finite durations.

Orthonormality of different subspaces in the multiresolution analysis ensures that[41][52]

$$
\begin{aligned}
<\phi_{0n}(t), \phi_{0l}(t)> &= \delta_{n-l} \\
<\phi_{mn}(t), \psi^i_{kl}(t)> &= 0 \quad i = 1, 2, ...N - 1 \\
<\psi^i_{mn}(t), \psi^j_{kl}(t)> &= \delta_{i-j}\delta_{m-k}\delta_{n-l}
\end{aligned}
\tag{3.94}
$$

By forcing the orthonormality condition in Eq.(3.94) with the admissibility condition on the wavelet functions, one could get necessary conditions on the wavelet filters such that

- $\sum_n h_0(n) = 1$
- $\sum_n h_i(n) = 0 \quad i = 1, 2, ...N - 1$
- $\sum_n h_i(n)h_j(n + kN) = \delta_{i-j}\delta_k$

Note that, These above conditions implies all filters have unit energy and orthogonal with each other with decimation factor N. Using the z-domain expression for decimation by N,

$$\frac{1}{N} \sum_{n=0}^{N-1} H_i(zW^n)H_j(zW^n) = \delta_{i-j} \tag{3.95}$$

85

with $W = e^{-j2\pi/N}$. Therefore, These conditions can be transformed into the frequency domain such that the $N \times N$ matrix

$$\mathcal{H}(e^{j\omega}) = \begin{bmatrix} H_0(e^{j\omega}) & H_1(e^{j\omega}) & ... & H_{N-1}(e^{j\omega}) \\ H_0(e^{j(\omega+\frac{2\pi}{N})}) & H_1(e^{j(\omega+\frac{2\pi}{N})}) & ... & H_0(e^{j(\omega+\frac{2\pi}{N})}) \\ \vdots & \vdots & \vdots & \vdots \\ H_0(e^{j(\omega+(N-1)\frac{2\pi}{N})}) & H_1(e^{j(\omega+(N-1)\frac{2\pi}{N})}) & ... & H_{N-1}(e^{j(\omega+(N-1)\frac{2\pi}{N})}) \end{bmatrix}$$

(3.96)

be unitary. Thus we obtain the filters $h_0(n), h_1(n), ..., h_{N-1}(n)$. If the wavelet basis is orthonormal then the bank of filters $h_0(n)$ through $h_{N-1}(n)$ should form a N-channel maximally decimated PR filter bank. Note that PR filter bank design and wavelet basis construction are converged here, the same as 2-band case.

One way of getting N-band PR filter bank solution is to use two band PR filter bank in tree structure. Similar method is also available for orthonormal wavelet bases. Given an orthonormal wavelet basis with dilation factor 2, the following equivelency generates an orthonormal wavelet basis with dilation factor 2^N. Let us generate the wavelet basis with dilation factor 4[46]. We need to find $H_i(e^{j\omega})$ $i = 0, 1, 2, 3$ so that the corresponding 4×4 matrix is unitary. By defining

$$H_0^{(4)}(e^{j\omega}) = H_0(e^{j\omega})H_0(e^{j2\omega})$$

$$H_1^{(4)}(e^{j\omega}) = H_0(e^{j\omega})H_1(e^{j2\omega})$$

$$H_2^{(4)}(e^{j\omega}) = H_1(e^{j\omega})H_1(e^{j2\omega})$$

$$H_3^{(4)}(e^{j\omega}) = H_1(e^{j\omega})H_0(e^{j2\omega}) \tag{3.97}$$

where $H_1(e^{j\omega}) = -e^{-j\omega}H_0(e^{-j(\omega+\pi)})$ and $H_0(e^{j\omega})$ is the frequency response of low the pass filter associated with the given orthonormal wavelet basis $N = 2$. One can easily verify that, with the choice of Eq.(3.130), 4×4 matrix is indeed unitary for all ω so that It provides an orthonormal wavelet basis with the dilation factor 4. Note that this choice is equivalent to parallel realization of the cascaded tree structure which is covered in Chapter 2.

86

For the case, even better frequency localization is desired, this splitting approach can be repeated. One can replace the wavelet function $\psi(t)$ by 2^j new wavelet functions each corresponding to a 2^{-j}-octave bandwidth, and have to be translated by integer multiples of 2^j.

$$Span\{\psi(t-n)\} = Span\{\psi_l^{(2^j)}(t-2^j n) \; ; \; l = 1, 2, ..., 2^j \; n \in Z\}$$

The functions $\psi_l^{(2^j)}(t)$ are the special cases of the "wave packets" concept proposed by R. Coiffman and Y. Meyer. The concept of the best adapted wave packet bases is to introduce an algorithm for selecting the most efficient representation of a signal from a library of orthonormal basis functions. They also prove that its complexity is $O(N)$ for a sequence of length N. In one framework it includes many different choices of orthonormal bases of which the wavelet basis is one extreme example. Another extreme with the same framework is a basis closer in spirit to the windowed Fourier transforms, infinitely many intermediate choices are possible.

n	h(n)	h(n)	h(n)	h(n)	h(n)
0	0.05441584422	0.11154074335	0.230377813309	0.332670552950	0.482962913145
1	0.31287159091	0.49462389039	0.714846570553	0.806891509311	0.836516303738
2	0.67563073629	0.75113390802	0.630880767930	0.459877502118	0.224143868042
3	0.58535468365	0.31525035170	-0.027983769417	-0.135011020010	-0.129409522551
4	-0.01582910525	-0.22626469396	-0.187034811719	-0.085441273882	
5	-0.28401554296	-0.12976686756	0.030841381836	0.035226291882	
6	0.00047248457	0.09750160558	0.032883011667		
7	0.12874742662	0.02752286553	-0.010597401785		
8	-0.01736930100	-0.03158203931			
9	-0.04408825393	0.00553842201			
10	0.01398102791	0.00477725751			
11	0.00874609404	-0.00107730108			
12	-0.04870352993				
13	-0.00391740373				
14	0.00067544940				
15	-0.00011747678				

Table 3.1 Daubechies minimum phase wavelet filters.

n	h(n)	h(n)	h(n)
0	0.002672793393	0.021784700327	-0.107148901418
1	-0.000428394300	0.004936612372	-0.041910965125
2	-0.021145686528	-0.166863215412	0.703739068656
3	0.005386388754	-0.068323121587	1.136658243408
4	0.069490465911	0.694457972958	0.421234534204
5	-0.038493521263	1.113892783926	-0.140317624179
6	-0.073462508761	0.477904371333	-0.017824701442
7	0.515398670374	-0.102724969862	0.045570345896
8	1.099106630537	-0.029783751299	
9	0.680745347190	0.063250562660	
10	-0.086653615406	0.002499922093	
11	-0.202648655286	-0.011031867509	
12	0.010758611751		
13	0.044823623042		
14	-0.000766690896		
15	-0.004783458512		

Table 3.2 Daubechies non-minimum phase wavelet filters which are the best phase response among the solutions.

n	h(n)	h(n)	h(n)	h(n)
0	0.000630961046	-0.002682418671	0.011587596739	-0.051429728471
1	-0.001152224852	0.005503126709	-0.029320137980	0.238929728471
2	-0.005194524026	0.016583560479	-0.047639590310	0.602859456942
3	0.011362459244	-0.046507764479	0.273021046535	0.272140543058
4	0.018867235378	-0.043220763560	0.574682393857	-0.051429972847
5	-0.057464234429	0.286503335274	0.294867193696	-0.011070271529
6	-0.039652648517	0.561285256870	-0.054085607092	
7	0.293667390895	0.302983571773	-0.042026480461	
8	0.553126452562	-0.050770140755	0.016744410163	
9	0.307157326198	-0.058196250762	0.003967883613	
10	-0.047112738865	0.024434094321	-0.001289203356	
11	-0.068038127051	0.011229240962	-0.000509505539	
12	0.027813640153	-0.006369601011		
13	0.017735837438	-0.001820458916		
14	-0.010756318517	0.000790205101		
15	-0.004001012886	0.000329665174		
16	0.002652665946	-0.000050192775		
17	0.000895594529			
18	-0.000416500571			
19	-0.000183829769			
20	0.000044080354			
21	0.000022082857			
22	-0.000002304942			
23	-0.000001262175			

Table 3.3 The coefficients of coiflet filters.

Chapter 4

Binomial-QMF Wavelet Transform

4.1 Introduction

Subband signal decomposition has been introduced earlier in Chapter 2. In this chapter, we describe a class of orthogonal Binomial filters which provide basis functions for a perfect reconstruction bank of finite impulse response QMFs. The orthonormal wavelet filters derived by Daubechies from a discrete compactly supported wavelet transform approach which was given in section 3.5.3 are shown to be identical to the solutions inherent in the Binomial-based QMFs.

The compaction performance of the Binomial QMF based subband decomposition is computed and shown to be better than the DCT for Markov source models, as well as real world images. The proposed Binomial QMF structure is efficient, simple to implement on VLSI, and suitable for multiresolution signal decomposition and coding applications.

4.2 The Binomial- Hermite Family

The Binomial-Hermite sequences are a family of finite duration discrete polynomials weighted by a Gaussian-like Binomial envelope[54][55]. These sequences are

orthogonal on $[0, N]$ with respect to a weighting function. The Binomial sequence $\begin{pmatrix} N \\ k \end{pmatrix}$ is the generating function of this family; the other members are obtained by successive differencing of this kernel.

Filters based on this family have two characteristics which render them useful in signal processing applications. First, they are very efficient since they can be implemented with no multiply operations. Secondly, the spatial and frequency domain responses have Gaussian-like shapes which make them particularly attractive in image processing applications. References [55] and [58] describe applications to filtering seismic data, and in pyramid image coding.

In this section, we summarize key features of the Binomial-Hermite family, and develop new properties which are relevant to QMF structures.

The generating function of this family is

$$x_0(k) = \begin{cases} \begin{pmatrix} N \\ k \end{pmatrix} = \dfrac{N!}{(N-k)!k!} & 0 \leq k \leq N \\ 0 & \text{otherwise} \end{cases} \tag{4.1}$$

Successive differencing

$$x_r(k) = \nabla^r \begin{pmatrix} N-r \\ k \end{pmatrix} \qquad r = 0, 1, \ldots, N \tag{4.2}$$

leads to

$$\begin{aligned} x_r(k) &= \begin{pmatrix} N \\ k \end{pmatrix} \sum_{\nu=0}^{r} (-2)^\nu \begin{pmatrix} r \\ \nu \end{pmatrix} \frac{k^{(\nu)}}{N^{(\nu)}} \\ &= \begin{pmatrix} N \\ k \end{pmatrix} H_r(k) \qquad k = 0, 1, \ldots, N \end{aligned} \tag{4.3}$$

where $k^{(\nu)}$ is a polynomial in k of degree ν,

$$k^{(\nu)} = \begin{cases} k(k-1)\ldots(k-\nu+1) & \nu \geq 1 \\ 1 & \nu = 1 \end{cases} \tag{4.4}$$

This family of binomially-weighted polynomials has a number of elegant properties which are unveiled in the transform domain. Taking z transforms, we

92

obtain

$$X_0(z) = (1 + z^{-1})^N$$

$$X_r(z) = Z\left\{\nabla^r \left(\begin{array}{c} N - r \\ k \end{array} \right)\right\} = (1 - z^{-1})^r Z\left\{\left(\begin{array}{c} N - r \\ k \end{array} \right)\right\}$$

$$= (1 - z^{-1})^r (1 + z^{-1})^{N-r} \qquad (4.5)$$
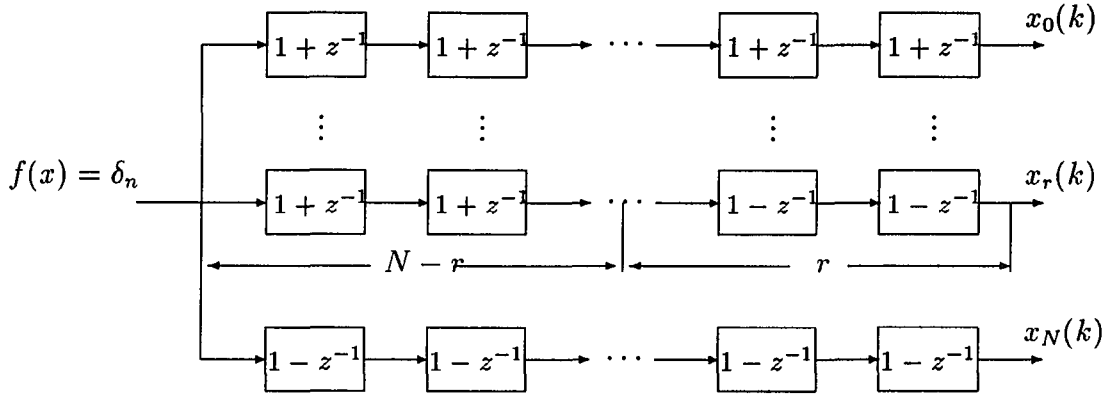
Fig. 4.1 Bank of Binomial-Hermite filters realized using N^2 delay elements

A network realization of this family of filters is shown in Fig. 4.1. This structure represents an interconnection of add and difference operators, in a purely non-recursive FIR form. Yet another configuration arises from the representation

$$X_r(z) = \left(\frac{1 - z^{-1}}{1 + z^{-1}}\right) X_{r-1}(z) = \left(\frac{1 - z^{-1}}{1 + z^{-1}}\right)^r X_0(z) = G_r(z)X_0(z) \qquad (4.6)$$

This form, Eq.(4.6) suggests the bank of filters shown in Fig. 4.2. The advantage of this structure is evident–the entire family is obtained by simply tapping off the appropriate point in Fig. 4.2. Since each $(1 - z^{-1})/(1 + z^{-1})$ block can be synthesized with one delay element, the pole-zero cancellation structure of Fig. 4.2 can be synthesized with $2N$ delay elements as compared with N^2 delays in Fig. 4.1. The pole-zero cancellation implicit in Eq.(4.6) can be achieved exactly since all coefficients are $\pm$ 1. However, care must be taken to clear all registers before data

is inputted to the front end of the filter. At any rate either realization is achieved without multiply operations.

$$\delta(k) \longrightarrow \boxed{(1+z^{-1})^N} \rightarrow \boxed{\frac{1-z^{-1}}{1+z^{-1}}} \rightarrow \boxed{\frac{1-z^{-1}}{1+z^{-1}}} \rightarrow \cdots \longrightarrow \boxed{\frac{1-z^{-1}}{1+z^{-1}}} \rightarrow$$

$$x_0(k) \qquad x_1(k) \qquad\qquad\qquad x_N(k)$$
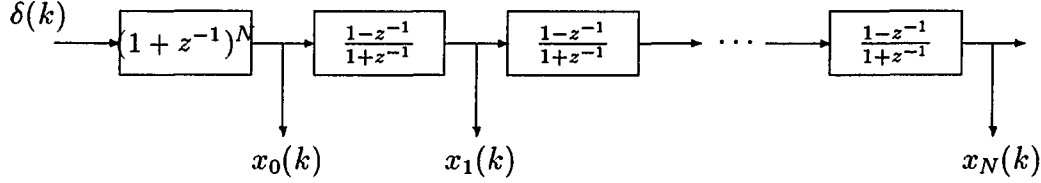
Fig. 4.2. Bank of Binomial-Hermite filters using pole-zero cancellation, and only $2N$ delay elements.

Further properties of the Binomial-Hermite sequences:

• *Orthogonality:* It was shown in that $\{H_r(k)\}$, $\{x_r(k)\}$ are orthogonal set on $[0, N]$ with respect to weighting function $\begin{pmatrix} N \\ k \end{pmatrix}$ and $\begin{pmatrix} N \\ k \end{pmatrix}^{-1}$ respectively[17][54],

$$\sum_{k=0}^{N} H_r(k)H_s(k) \begin{pmatrix} N \\ k \end{pmatrix} = \sum_{k=0}^{N} x_r(k)x_s(k) \begin{pmatrix} N \\ k \end{pmatrix}^{-1} = \begin{pmatrix} N \\ r \end{pmatrix}^{-1} (2)^N \delta_{r-s} \qquad (4.7)$$

Furthermore, the Hermite polynomials are symmetric with respect to index and argument,

$$H_r(k) = H_k(r)$$

The orthogonality property in Eq.(4.7) provided the underpinning for the modified Hermite Transform(MHT), an orthogonal transform used in signal coding.

• *Row-column orthogonality:* The Binomial matrix X is the $(N+1) \times (N+1)$ matrix whose r^{th} row is $x_r(k)$, $k = 0, 1, ..., N$. The salient property of this matrix is that the rows are orthogonal to the columns,

$$\sum_{k=0}^{N} x_r(k)x_k(s) = (2)^N \delta_{r-s} \qquad (4.8)$$

94

or

$$X^2 = (2)^N I \tag{4.9}$$

● *Mirror image filters:* The Binomial-Hermite filters are linear phase quadrature mirror filters. From Eq.(4.5), we see that

$$X_r(-z) = X_{N-r}(z)$$

which implies

$$(-1)^k x_r(k) = x_{N-r}(k) \quad r = 0, 1, ..., N \tag{4.10}$$

Also,

$$z^{-N} X_r(z^{-1}) = (-1)^r X_r(z)$$

implies

$$x_r(N - k) = (-1)^r x_r(k) \tag{4.11}$$

Eqs.(4.10) and (4.11) demonstrate the symmetry and asymmetry of the rows and columns of the Binomial matrix X. Eq.(4.10), for example, asserts that the filters represented by the bottom half of the Binomial matrix are mirror images of the filters in the top half. These last two equations can also be used to prove the orthogonality of rows and columns asserted by Eq.(4.8). Finally, from Eq.(4.10), we can infer that the complementary filters $X_r(z)$ and $X_{N-r}(z)$ have magnitude responses which are mirror images about $\omega = \pi/2$

$$\left| X_r(e^{j(\frac{\pi}{2}-\omega)}) \right| = \left| X_{N-r}(e^{j(\frac{\pi}{2}+\omega)}) \right| \tag{4.12}$$

Hence, the complementary rows and columns of X possess the mirror-filter property. The first half of the set $(r = 0, 1, \ldots, (N-1)/2)$ have significant energy in the half band $(0, \pi/2)$, while the second half, $(r = (N+1)/2, \ldots, N)$ span the upper

half band. The time and amplitude responses of the Binomial family for $N = 7$ are displayed in Fig. 4.3.
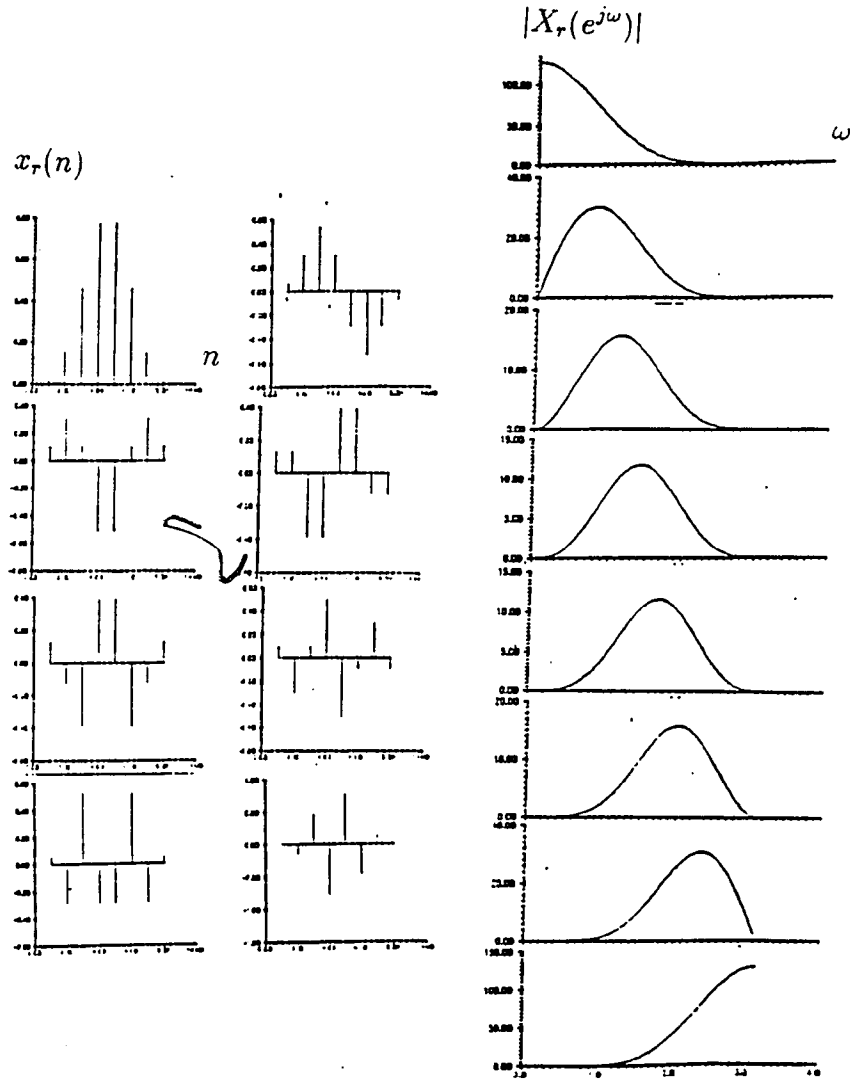
Fig. 4.3 The time and amplitude response functions of the Binomial family for

$$N = 7.$$

The Binomial family provides a set of basis sequences whose frequency responses are a family of linear phase, ripple free, low-pass, band-pass and high-pass filters which span the frequency axis, $0 \leq \omega \leq \pi$.

These considerations suggest that a low pass QMF can be obtained as linear combination of the lower half set of Binomial sequences. As we shall see, the coefficients of the expansion can be determined to satisfy perfect reconstruction requirements.

- *Convolutional properties:* Let $x_r^{(N)}(k) \leftrightarrow X_r^{(N)}(z)$ denote the Binomial-Hermite sequence on $[0, N]$ and its transform. We can show that[17]

$$X_r^{(N)}(z)X_s^{(M)}(z) = X_{r+s}^{(M+N)}(z) \qquad (4.13)$$

or

$$x_r^{(N)}(k) * x_s^{(M)}(k) = x_{r+s}^{(M+N)}(k) \qquad (4.14)$$

for $n = 0, 1, ..., (N-1)/2$ and $s = 0, 1, ..., (M-1)/2$.

There are various special cases of Eq.(4.14) which demonstrate recurrence relations among different sized Binomial families. The simplest permits us to generate higher order Binomial matrices from lower-order ones. Consider $M = 1, s = 0$. Then

$$X_r^{(N+1)}(z) = (1 + z^{-1})X_r^{(N)}$$

$$x_r^{(N+1)}(k) = x_r^{(N)}(k) * (\delta_k + \delta_{k-1}) \qquad (4.15)$$

This recurrence relation along with the mirror image property of Eq.(4.10) enable us to build up iteratively the Binomial-Hermite matrices. Let $X^{(N)}$ denote the $(N+1) \times (N+1)$ matrix. Then

$$X^{(1)} = \begin{bmatrix} 1 & 1 \\ 1 & -1 \end{bmatrix}$$

The first two rows of $X^{(2)}$ are obtained by convolving each row with $(\delta_k + \delta_{k-1})$, or more simply put, by shifting each row one position to the right and adding it to that original row. For example,

```
1  1              1  -1
   1  1              1  -1
_____       _____
1  2  1           1   0  -1
```

The third row is just the mirror of the first row. Hence,

$$X^{(2)} = \begin{bmatrix} 1 & 2 & 1 \\ 1 & 0 & -1 \\ 1 & -2 & 1 \end{bmatrix}$$

Continuing in this fashion, we obtain the higher order Binomial matrices.

- *Correlation properties:* For a given N, we define the cross-correlation of the sequences $x_r(n)$, and $x_s(n)$ by

$$\rho_{rs}(n) = x_r(n) * x_s(-n) = \sum_{k=0}^{N} x_r(k)x_s(n+k) \longleftrightarrow R_{rs}(z) \qquad (4.16)$$

and

$$R_{rs}(z) = X_r(z^{-1})X_s(z) \qquad (4.17)$$

Now for any real crosscorrelation,

$$\rho_{rs}(-n) = \rho_{sr}(n) \quad \forall\, s, r \qquad (4.18)$$

Furthermore, the quadrature mirror property of Eq.(4.10) implies that

$$\begin{aligned} \rho_{rs}(n) &= -\rho_{sr}(n) \quad (s-r) \text{ is odd} \\ \rho_{rs}(n) &= \rho_{sr}(n) \quad (s-r) \text{ is even} \end{aligned} \qquad (4.19)$$

We also have

$$\rho_{N-r,N-r}(n) = (-1)^n \rho_{r,r}(n)$$

$$\rho_{N-r,N-r}(2n) = \rho_{r,r}(2n)$$

These properties are subsequently used in arriving at the perfect reconstruction QMF equations in the next section.

We can build up higher order correlation matrices from lower order ones in a manner similar to that employed in constructing $X^{(N+1)}$ from $X^{(N)}$. Using superscript notation, we can easily show that

$$R_{rs}^{(N+1)}(z) = (z + 2 + z^{-1})R_{rs}^{(N)}(z)$$

or

$$\rho_{rs}^{(N+1)}(k) = (\delta_{k+1} + 2\delta_k + \delta_{k-1}) * \rho_{rs}^{(N)}(k) \qquad (4.20)$$

4.3   The Binomial-QMF

We have obtained in Chapter 2 that the PR requirement of 2-band orthogonal QMF filter bank is

$$\rho(2n) = \sum_{k=0}^{N} h(k)h(k + 2n) = \delta_n \qquad (4.21)$$

where the autocorrelation sequence $\rho(n)$ given by

$$\rho(n) = \sum_{k=0}^{N} h(k)h(k + n) = \rho(-n) \qquad (4.22)$$

It is now a straight forward matter to impose PR condition of Eq.(4.21) on the Binomial family. First, we take as the low-pass filter[17]

$$h(n) = \sum_{r=0}^{\frac{N-1}{2}} \theta_r x_r(n)$$

or

$$H(z) = \sum_{r=0}^{\frac{N-1}{2}} \theta_r (1 + z^{-1})^{N-r}(1 - z^{-1})^r = (1 + z^{-1})^{(N+1)/2}F(z) \qquad (4.23)$$

where $F(z)$ is FIR filter of order $(N - 1)/2$. For convenience, we take $\theta_0 = 1$. Substituting Eq.(3.23) into Eq.(3.22) gives

$$
\begin{aligned}
\rho(n) &= \left(\sum_{r=0}^{\frac{N-1}{2}} \theta_r x_r(n) \right) \odot \sum_{s=0}^{\frac{N-1}{2}} \theta_s x_s(n) \\
&= \sum_{r=0}^{\frac{N-1}{2}} \sum_{s=0}^{\frac{N-1}{2}} \theta_r \theta_s [x_r(n) \odot x_s(n)] \\
&= \sum_{r=0}^{\frac{N-1}{2}} \sum_{s=0}^{\frac{N-1}{2}} \theta_r \theta_s \rho_{rs}(n) \\
&= \sum_{r=0}^{\frac{N-1}{2}} \theta_r^2 \rho_{rr}(n) + \sum_{\substack{r=0 \\ r \neq s}}^{\frac{N-1}{2}} \sum_{s=0}^{\frac{N-1}{2}} \theta_r \theta_s \rho_{rs}(n)
\end{aligned}
\tag{4.24}
$$

Eq.(4.19) implies that the second summation in Eq.(4.24) has only terms where the indices differ by an even integer. Therefore the autocorrelation for the Binomial low-pass filter is

$$
\rho(n) = \sum_{n=0}^{\frac{N-1}{2}} \theta_r^2 \rho_{rr}(n) + 2 \sum_{l=1}^{\frac{N-3}{2}} \sum_{\nu=0}^{\frac{N-1}{2}-2l} \theta_\nu \theta_{\nu+2l} \rho_{\nu,\nu+2l}(n)
\tag{4.25}
$$

Finally, the PR requirement is

$$
\rho(n) = 0 \qquad n = 2, 4, \ldots, N - 1
\tag{4.26}
$$

This condition gives a set of $\frac{N-1}{2}$ nonlinear algebraic equations, in the $\frac{N-1}{2}$ unknowns $\theta_1, \theta_2 \ldots, \theta_{\frac{N-1}{2}}$. These equations were solved using software package Macsyma.

The implementation of these filters is trivially simple and efficient using either the purely FIR structure, or the pole-zero cancellation configuration. The latter is shown in Fig. 4.4 for $N = 5$. Wherein both low-pass and high-pass filters are simultaneously realized. Fig. 4.5 shows the QMF bank using the direct form. Coefficient θ_0 can be taken equal to unity, leaving only θ_1 and θ_2 as tap weights.

These are the only multiplications needed when using the Binomial network as the QMF rather than the six $h(n)$ weights in a transversal structure.
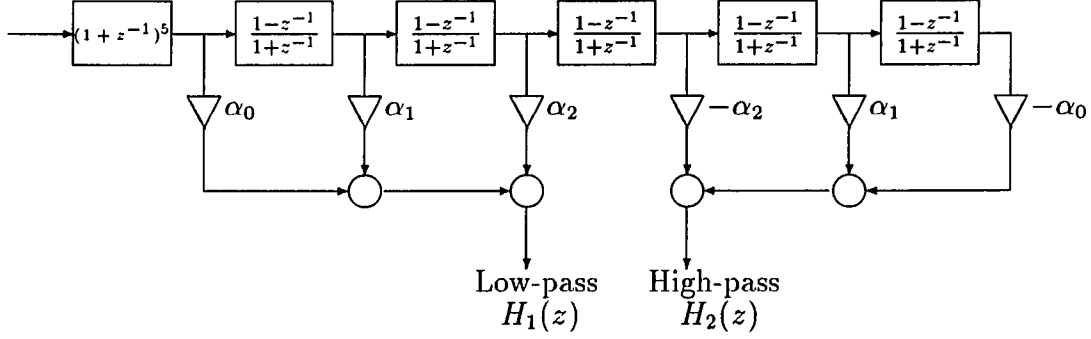
Fig. 4.4. Low-pass and high-pass QMF filters from Binomial Network.

The values of θ_r, for $N = 3, 5, 7$, (corresponding to 4,6,8 tap filters respectively) are given in Table 4.1 (where $\theta_0 = 1$). As seen, there are more than one filter solutions for a given N. For example, with $N = 3$, one obtains $\theta_1 = \sqrt{3}$, and also $\theta_1 = -\sqrt{3}$. The positive θ_1 corresponds to a minimum phase solution, while the negative θ_1 provides a non-minimum phase filter. The magnitude responses of both filters are identical. Although in our derivation, no linear phase constraint on $h(n)$ was imposed; it is noteworthy, that the phase responses are almost linear, the non-minimum phase filters even more so. The magnitude and phase responses of these minimum phase Binomial QMFs are given in Fig. 4.6 for the cases $N = 3, 5, 7$.

Table 4.2 provides the normalized 4,6,8 tap filter coefficients, $h(n)$ for both minimum and non-minimum phase cases. It is seen that these filters are Daubechies filters given in Table 3.1.

We may recognize that these filters are the unique maximally flat magnitude square PR-QMF solutions. In fact, it can be shown that the PR requirements of

of Eq.(4.21) are satisfied if we choose the θ_r coefficients to satisfy maximally flat requirements at $\omega = 0$, and $\omega = \pi$. Explicitly, with $R(\omega) = |H(e^{j\omega})|^2$, we can set θ_r to satisfy

$$R(0) = 1 \qquad R(\pi) = 0$$

$$\left. \frac{d^k R(\omega)}{d\omega^k} \right|_{\substack{\omega = 0 \\ \omega = \pi}} = 0, \quad k = 1, 2, \ldots .N$$

Herrmann[59] provides the unique maximally flat function on the interval [0,1].
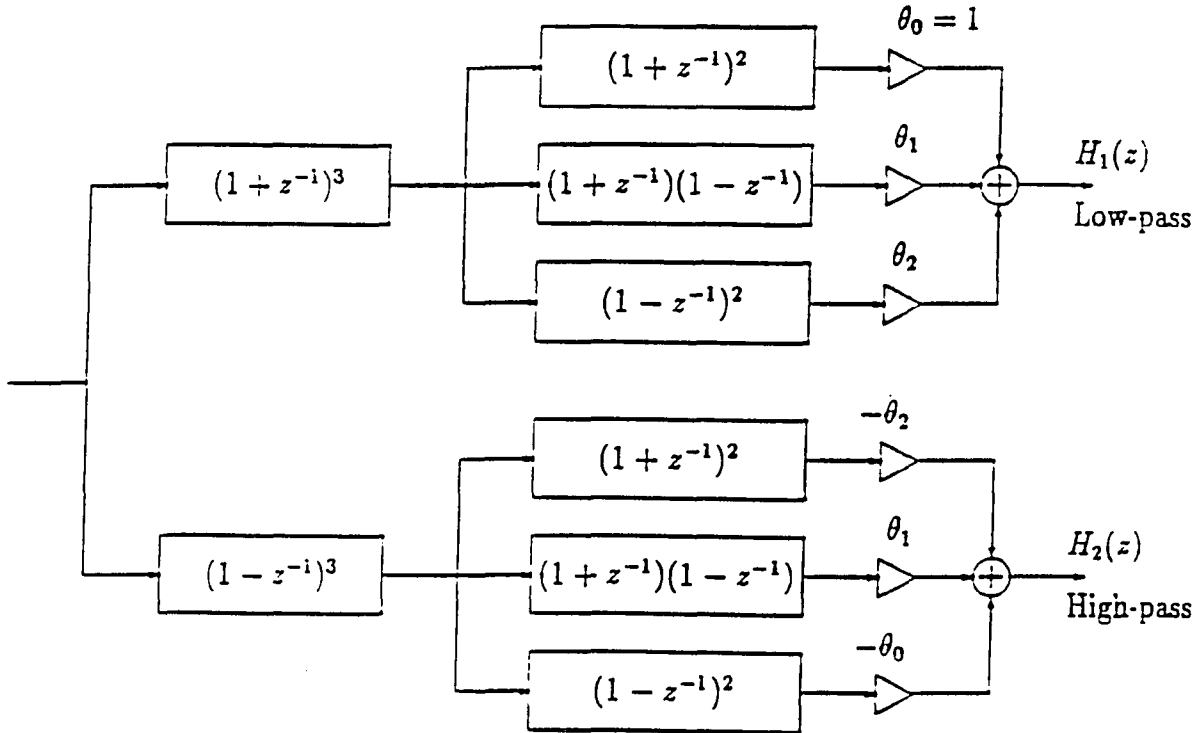
Fig. 4.5. Low-pass and high-pass QMFs using Direct Form Binomial structure

(Fig. 4.1.).

This function can be easily mapped onto z plane to obtain the maximally flat magnitude square function $R(z)$[61]. Now, one can obtain the corresponding $H(z)$

from $R(z)$ via factorization. This approach extends Herrmann's solution to the PR-QMF case. The explicit form of $R(z)$ is given in Eq.(4.29)
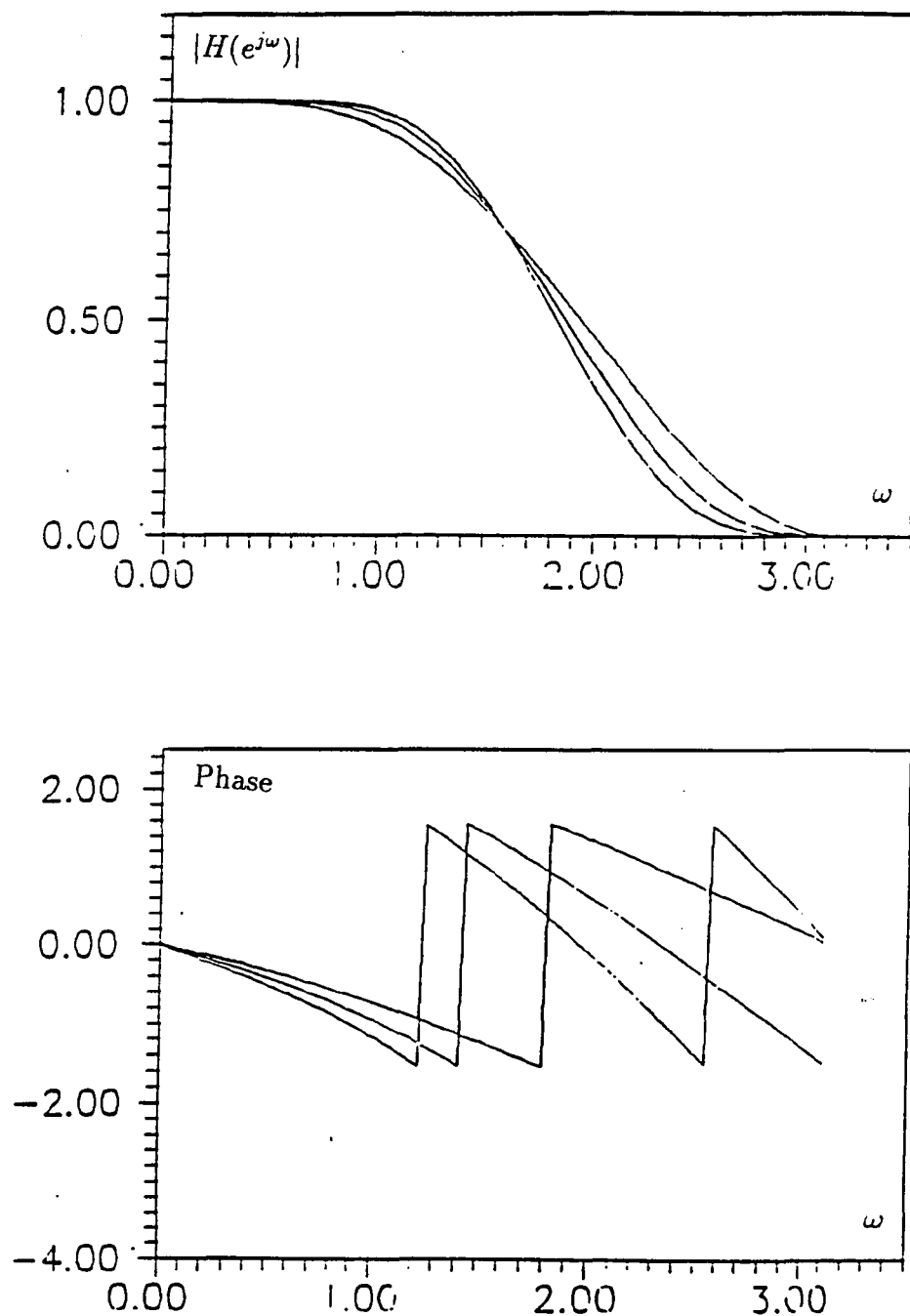
Fig. 4.6. Amplitude and phase responses of minimum phase Binomial QMFs for

$$N = 3, 5, 7$$

4.4 Orthonormal Wavelet Transforms and Binomial QMF

In this section, we emphasize and the linkages of Binomial QMF and the orthonormal wavelet filters derived by Daubechies[40].

The regularity concept is unique to wavelet filters. Conventional PR-QMF design does not invoke this requirement explicitly but some degree of regularity is imposed by forcing the high-pass filter to be zero mean. The Binomial QMF has this feature inherent. The regularity tool suggested in[40] assumes a low-pass scaling filter of length $N + 1$,

$$H(z) = (1 + z^{-1})^k F(z) \quad 1 \leq k \leq \frac{N+1}{2}$$

Here, $F(z)$ is a polynomial of degree $\frac{N+1}{2} \leq l \leq N$, such that $k + l = N$.

If $k = \frac{N+1}{2}$ the maximum number of zeros of $H(z)$ are located at $\omega = \pi$. Therefore $F(z)$ is of degree $\frac{N-1}{2}$. But the Binomial QMF, $H(z)$ in Eq.(4.23), now can be written

$$H(z) = (1 + z^{-1})^{\frac{N+1}{2}} \sum_{r=0}^{\frac{N-1}{2}} \theta_r (1 + z^{-1})^{\frac{N-1}{2}-r}(1 - z^{-1})^r \tag{4.27}$$

hence,

$$F(z) = \sum_{r=0}^{\frac{N-1}{2}} \theta_r (1 + z^{-1})^{\frac{N-1}{2}-r}(1 - z^{-1})^r \tag{4.28}$$

Combining this regular nature of $H(z)$ along with the PR requirement leads to the unique maximally flat magnitude square function[59],

$$R(z) = H(z)H(z^{-1}) = \frac{z^N(1 + z^{-1})^{N+1}}{4^{N+1}} \sum_{l=0}^{\frac{N-1}{2}} (-1)^l \binom{N}{l} (1 + z^{-1})^{N-1-2l}(1 - z^{-1})^{2l} \tag{4.29}$$

therefore

$$V(z) = F(z)F(z^{-1}) = z^{\frac{N-1}{2}} \sum_{l=0}^{\frac{N-1}{2}} (-1)^l \binom{N}{l} (1 + z^{-1})^{N-1-2l}(1 - z^{-1})^{2l} \tag{4.30}$$

$V(z)$ is identical to the polynomial used in[40]. This magnitude square function is a linear combination of the lower half, even-indexed Binomial sequences with length $2N + 1$. Here, the convolution decomposition feature of the Binomial sequences Eq.(4.15) are utilized to obtain $H(z)$ easily via factorization.

4.5   Performance of Binomial QMF-Wavelet Transform

The performance of the Binomial QMF signal decomposition scheme is compared with the industry standard, the Discrete Cosine Transform (DCT) in this section.

The energy compaction power of any unitary transform is a commonly used performance criterion. The gain of transform coding over PCM is defined as[7]

$$G_{TC} = \frac{\dfrac{1}{M} \displaystyle\sum_{k=0}^{M-1} \sigma_k^2}{\left[\displaystyle\prod_{k=0}^{M-1} \sigma_k^2 \right]^{1/M}} \tag{4.31}$$

where σ_k^2 are transform coefficient variances. This measure assumes that all coefficients as well as the original signal have the *same type* probability density function.

Similarly the gain of subband coding over PCM is defined as

$$G_{SBC} = \frac{\dfrac{1}{M} \displaystyle\sum_{l=0}^{M-1} \sigma_l^2}{\left[\displaystyle\prod_{l=0}^{M-1} \sigma_l^2 \right]^{1/M}} \tag{4.32}$$

Here σ_l^2 is the variance of the signal in the lth subband. This formula holds for a regular tree structure implying equal bandwidths.

We assume a Markov 1 source model with autocorrelation

$$R(k) = \rho^{|k|}, \qquad k = 0, \pm 1, \ldots \tag{4.33}$$

and G_{TC} and G_{SBC} are calculated for different cases. These results are displayed in Table 4.3. Eqs.(4.31) and (4.32) are easily extended to the 2-D case for separable transforms and separable QMFs.

The energy compaction performance of the two techniques were also tested for several standard images. These results are given in Table 4.4.

The results demonstrate that the 6-tap Binomial QMF outperforms the comparable sized DCT in both theoretical performance as well as for standard test images. We conclude therefore that the 6-tap Binomial QMF provides a better alternative to the DCT for image coding.

N=3		
θ_r	set 1	set 2
θ_0	1	1
θ_1	$\sqrt{3}$	$-\sqrt{3}$

N=5		
θ_r	set 1	set 2
θ_0	1	1
θ_1	$\sqrt{2\sqrt{10}+5}$	$-\sqrt{2\sqrt{10}+5}$
θ_2	$\sqrt{10}$	$\sqrt{10}$

N=7				
θ_r	set 1	set 2	set 3	set 4
θ_0	1	1	1	1
θ_1	4.9892	-4.9892	1.0290	-1.0290
θ_2	8.9461	8.9461	-2.9705	-2.9705
θ_3	5.9160	-5.9160	-5.9160	5.9160

Table 4.1 θ_r values for $N = 3, 5, 7$

n	h(n)			
	Mini Phase	Non-Minimum Phase		
	4 tap	4 tap		
0	0.48296291314453	-0.1294095225512		
1	0.83651630373780	0.2241438680420		
2	0.22414386804201	0.8365163037378		
3	-0.12940952255126	0.4829629131445		
	6 tap	6 tap		
0	0.33267055439701	0.0352262935542		
1	0.80689151040469	-0.0854412721235		
2	0.45987749838630	-0.1350110232992		
3	-0.13501102329922	0.4598774983863		
4	-0.08544127212359	0.8068915104046		
5	0.03522629355424	0.3326705543970		
	8 tap	8 tap	8 tap	8 tap
0	0.23037781098452	-0.0105973984294	-0.0757657137833	0.0322230981272
1	0.71484656725691	0.0328830189591	-0.0296355292117	-0.0126039690937
2	0.63088077185926	0.0308413834495	0.4976186593836	-0.0992195317257
3	-0.02798376387108	-0.1870348133969	0.8037387521124	0.2978578127957
4	-0.18703481339693	-0.0279837638710	0.2978578127957	0.8037387521124
5	0.03084138344957	0.6308807718592	-0.0992195317257	0.4976186593836
6	0.03288301895913	0.7148465672569	-0.0126039690937	-0.0296355292117
7	-0.01059739842942	0.2303778109845	0.0322230981272	-0.0757657137833

Table 4.2 Binomial QMF-Wavelet filters, $h(n)$, for $N = 3, 5, 7$

$$G_{sbc}$$

	ρ	$\underline{G_{TC}}$	4-tap	6-tap	8-tap	16-tap
4 × 4 Trans.	0.95	5.71	6.43	6.77	6.91	7.08
or	0.85	2.59	2.82	2.95	3.01	3.07
	0.75	1.84	1.95	2.02	2.05	2.09
4-band QMF	0.65	1.49	1.56	1.60	1.62	1.64
(2 levels)	0.5	1.23	1.26	1.28	1.29	1.30
8 × 8 Trans.	0.95	7.63	8.01	8.53	8.74	8.99
or	0.85	3.03	3.11	3.27	3.34	3.42
	0.75	2.03	2.06	2.14	2.17	2.22
8-band QMF	0.65	1.59	1.60	1.65	1.67	1.69
(3 level)	0.5	1.27	1.28	1.30	1.31	1.32

Table 4.3 Energy compaction comparison: DCT vs Binomial QMF for several AR(1) sources.

			G_{SBC}		
		G_{TC}	4-tap	6-tap	8-tap
4 × 4 2-D Trans.	LENA	16.002	16.70	18.99	20.37
or	BUILDING	14.107	15.37	16.94	18.17
16-Band Regular	CAMERAMAN	14.232	15.45	16.91	17.98
Tree	BRAIN	3.295	3.25	3.32	3.42
8 × 8 2-D Trans.	LENA	21.988	19.38	22.12	24.03
or	BUILDING	20.083	18.82	21.09	22.71
64-Band Regular	CAMERAMAN	19.099	18.43	20.34	21.45
Tree	BRAIN	3.788	3.73	3.82	3.93

Table 4.4 Energy compaction comparison: DCT vs Binomial QMF for several test images.

Chapter 5

A Parametric PR-QMF Design Technique Based on Bernstein Polynomial Approximation

5.1 Introduction

We introduce in this chapter a generalized, parametric PR-QMF design technique based on Bernstein polynomial approximation. This approach first tries to approximate to the given set of sample points of a desired magnitude square function by using Bernstein polynomials. This approximation is mapped onto z domain as $R(z)$. The corresponding filter function $H(z)$ is obtained from $R(z)$ via factorization.

5.2 Maximally Flat Magnitude Square Response

Let us assume that $h(n)$ is a length $2N$ low-pass filter with the system function

$$H(z) = \sum_{n=0}^{2N-1} h(n)z^{-n} \tag{5.1}$$

and its magnitude square function

$$
\begin{aligned}
|H(e^{j\omega})|^2 &= H(z)H(z^{-1}) \\
&= \rho(0) + 2\sum_{n=1}^{2N-1} \rho(n)cos(n\omega T)
\end{aligned}
\tag{5.2}
$$

with $T = 1$.

The sequence $\rho(n)$ satisfies the following conditions in frequency domain,

$$\left.\left|H(e^{j\omega})\right|^2\right|_{\omega=0} = 1 \tag{5.3}$$

$$\left.\frac{d^\nu}{d\omega^\nu}\left|H(e^{j\omega})\right|^2\right|_{\omega=0} = 0 \quad \nu = 1, 2, ..., 2(2N - 1 - k) + 1 \tag{5.4}$$

$$\left.\frac{d^\mu}{d\omega^\mu}\left|H(e^{j\omega})\right|^2\right|_{\omega=\pi} = 0 \quad \mu = 0, 1, ..., 2k - 1 \tag{5.5}$$

where k is an integer to be chosen arbitrarily within the limits $1 \leq k \leq 2N - 1$. The parameter k defines the degrees, ν, of flatness of the magnitude square function at $\omega = 0$ and μ, at $\omega = \pm\pi$.

If one defines the transform[59]

$$\cos\omega = 1 - 2x$$

$|H(e^{j\omega})|^2$ can be transformed into a simple polynomial of degree $2N - 1$ as

$$P_{2N-1,k}(x) = \sum_{\nu=0}^{2N-1} a_\nu x^\nu \tag{5.6}$$

with an approximation interval $0 \leq x \leq 1$ and the properties:

a.) $P_{2N-1,k}(x)$ has zeros of order k at $x = 1$

b.) $P_{2N-1,k}(x) - 1$ has zeros of order $2N - k$ at $x = 0$

This is a special case of Hermite interpolation problem and can be solved by using the Newton interpolation formula[60]. But there exists an explicit solution of this problem which is given by the expression

$$P_{2N-1,k}(x) = (1 - x)^k \frac{1}{(1-k)!}\frac{d^{k-1}}{dx^{k-1}}\sum_{\nu=0}^{2N-2} x^\nu \tag{5.7}$$

112

$$= (1-x)^k \sum_{\nu=0}^{2N-k-1} \binom{k+\nu-1}{\nu} x^\nu$$

The relation between the autocorrelation sequence of $h(n)$ and the polynomial coefficients a_ν is given by[59]

$$\rho(0) = \frac{1}{2} \sum_{k=0}^{\lceil \frac{2N-1}{2} \rceil} \left[2^{-2k} \binom{2k}{k} \sum_{i=2k}^{2N-1} 2^{-i} \binom{i}{2k} a_i \right] \tag{5.8}$$

and

$$\rho(l) = \sum_{k=0}^{\lceil \frac{2N-1-l}{2} \rceil} \left[2^{-(2k+l)} \binom{2k+l}{k} \sum_{i=2k+l}^{2N-1} 2^{-i} \binom{i}{2k+l} a_i \right] \quad l = 1,2,...,2N-1 \tag{5.9}$$

where $\lceil x \rceil$ means the integer part of x.

It is clear that this relation provides a simple filter design tool based on the desired degrees of flatness of magnitude square function at $\omega = 0$ and $\omega = \pm\pi$.

It has been stated that if one desires to design a half-band Quadrature Mirror Filter (QMF) bank, the perfect reconstruction of the signal after the synthesis stage requires that

$$H(z)H(z^{-1}) + H(-z)H(-z^{-1}) = 2$$

It is seen by inspection that a half-band maximally flat PR-QMF requires that its magnitude square function has maximum number of zeros at $\omega = 0$ and $\omega = \pm\pi$ equally, implying the symmetry around $\omega = \pi/2$. This is expressed as

$$\frac{d^\mu |H(e^{j\omega})|^2}{d\omega^\mu} \bigg|_{\omega=0} = 0 \tag{5.10}$$

$$\frac{d^\mu |H(e^{j\omega})|^2}{d\omega^\mu} \bigg|_{\omega=\pm\pi} = 0 \quad \mu = 1,2,..,2N-1$$

113

Therefore, $P_{2N-1,k}(x)$ becomes

$$P_{2N-1,k}(x) = (1-x)^N \sum_{\nu=0}^{N-1} \binom{N+\nu-1}{\nu} x^\nu \qquad (5.11)$$

Hence the magnitude square function can be expressed in[61]

$$H(z)H(z^{-1}) = z^{2N-1} \frac{(1+z^{-1})^{2N}}{4^{2N-1}} \sum_{l=0}^{N-1} \binom{2N-1}{l} (1+z^{-1})^{2(N-1-l)}(-1)^l(1-z^{-1})^{2l}$$

$$(5.12)$$

This indicates that the right hand side of the equation can also be expressed as the linear combination of even indexed, even symmetric, N binomial sequences of length $(4N-1)$[17]. This is shown in time as

$$\rho(n) = h(n) * h(-n) = \sum_{i=0}^{N-1} \frac{(-1)^i}{4^{2N-1}} \binom{2N-1}{i} x_{2i}(n) \quad n = 0,1,...,4N-2 \quad (5.13)$$

where

$$x_r(k) = \binom{4N-2}{k} \sum_{\nu=0}^{r} (-2)^\nu \binom{r}{\nu} \frac{k^{(\nu)}}{(4N-2)^{(\nu)}} \quad r,k = 0,1,...,4N-2 \quad (5.14)$$

5.3 A Generalized PR-QMF Design Technique Using Bernstein Polynomial Approximation

Two-band orthonormal PR-QMF requires the magnitude square condition,

$$\left|H(e^{j\omega})\right|^2 + \left|H(e^{j(\omega+\pi)})\right|^2 = 2$$

be satisfied. Where $|H(e^{j\omega})|^2$ is the magnitude square function of the low-pass filter to be designed with the length $2N$. Eq.(5.2) can be easily modified for an orthonormal PR-QMF case as

$$\left|H(e^{j\omega})\right|^2 = 1 + 2\sum_{k=1}^{N} \rho(2k-1)\cos(2k-1)\omega \qquad (5.15)$$

114

Let $f(x)$ be defined on the interval $[0,1]$, the Nth $(N \geq 1)$ order Bernstein polynomial to approximate to $f(x)$ is given as[60][62]

$$B_N(f;x) = \sum_{k=0}^{N} f(\frac{k}{N}) \left(\begin{array}{c} N \\ k \end{array} \right) x^k (1-x)^{N-k} \qquad (5.16)$$

Eq.(5.16) indicates that the interval $[0,1]$ is divided into N equal subintervals. Only the samples of $f(x)$ at those $(N+1)$ points are used to obtain the approximation $B_N(f;x)$. If $f(x)$ is differentiable, the approximation is also valid for its differentials. That implies

$$B_N(f;x) \rightarrow f(x)$$

$$B_N'(f;x) \rightarrow f'(x)$$

where prime means the derivative. This feature also holds for higher derivatives. Therefore the Bernstein polynomials provide simultaneous approximations of a function and its derivatives[60].

It is interesting that a monotonic and convex function is approximated by a monotonic and convex approximant if Bernstein polynomials are used. This tells us that the approximation follows the behavior of the approximated function up to a remarkable degree. The price paid for this beautiful feature is that these polynomials converge slowly to the function to be approximated.

Let's consider now a low pass function $f(x)$, $0 \leq x \leq 1$, with the sample values

$$f(\frac{i}{2N-1}) = \left\{ \begin{array}{ll} 1 & 0 \leq i \leq N-1 \\ 0 & N \leq i \leq 2N-1 \end{array} \right. \qquad (5.17)$$

which satisfies the PR-QMF magnitude square conditions in the interval [0,1]. The PR requirement can be mapped to x domain as,

$$f(x) + f(1-x) = 1$$

$$f(x) \geq 0 \qquad (5.18)$$

115

which is obtained by using Eq.(5.15) and the mapping $\cos\omega = 1 - 2x$. Substituting Eq.(5.17) into Eq.(5.16)[62],

$$
\begin{aligned}
B_{2N-1}(f;x) &= \sum_{i=0}^{N-1} \binom{2N-1}{i} x^i(1-x)^{2N-1-i} \\
&= (1-x)^N \sum_{i=0}^{N-1} \binom{N+i-1}{i} x^i
\end{aligned}
\tag{5.19}
$$

It is seen that Eq.(5.19) corresponds to a maximally flat symmetric function around $1/2$ within the interval $0 \le x \le 1$. This also corresponds to the magnitude square function of Binomial QMF-Wavelet Transform in x, Eq.(5.11).

If one maps x onto Ω, $\quad 0 \le \Omega \le \infty \quad$ as given in[62]

$$
x = \frac{\Omega^2}{1 + \Omega^2}
$$

the corresponding rational function in Ω,

$$
B_{2N-1}(f;\Omega) = \frac{\sum_{i=0}^{N-1} \binom{2N-1}{i} \Omega^{2i}}{(1 + \Omega^2)^{2N-1}}
\tag{5.20}
$$

Now let us define $q = j\Omega$ and employ the conformal mapping of

$$
z = \frac{1+q}{1-q}
$$

then the corresponding magnitude square function in z domain

$$
\begin{aligned}
R(z) &= z^{2N-1}\frac{(1+z^{-1})^{2N}}{4^{2N-1}} \sum_{i=0}^{N-1}(-1)^i \binom{2N-1}{i} (1+z^{-1})^{2(N-1-i)}(1-z^{-1})^{2i} \\
&= H(z)H(z^{-1})
\end{aligned}
\tag{5.21}
$$

is obtained. $R(z)$ is factorized to obtain $H(z)$.

Remark 1: $R(z)$ corresponds to a low pass function with $R(e^{j\frac{\pi}{2}}) = R(e^{j0})/2$. It is expressed as a combination of odd harmonics of the cosine functions. These

coefficients of the representation also correspond to the Fourier coefficients of the ideal low pass function.

Now, we extend the technique to obtain a broad family of smooth PR-QMFs defined by a set of approximation parameters. If one defines a set of non-increasing, positive function samples which will be the guide points of the approximation as

$$f\left(\frac{i}{2N-1}\right) = \begin{cases} 1 & i = 0 \\ 1 - \alpha_i & 1 \le i \le N-1 \\ \alpha_i & N \le i \le 2(N-1) \\ 0 & i = 2N-1 \end{cases} \tag{5.22}$$

where $\alpha_i = \alpha_{2N-1-i}$ and $0 \le \alpha_i < 0.5$ with $1 \le i \le N-1$ then the approximation to $f(x)$ with those constraints of Eq.(5.18) using the Bernstein polynomials is expressed as

$$B(f;x) = \sum_{i=0}^{N-1} \binom{2N-1}{i} x^i (1-x)^{2N-1-i} - \sum_{i=1}^{N-1} \alpha_i \binom{2N-1}{i} x^i (1-x)^{2N-1-i}$$

$$+ \sum_{i=N}^{2(N-1)} \alpha_i \binom{2N-1}{i} x^i (1-x)^{2N-1-i} \tag{5.23}$$

after applying similar mappings, the corresponding magnitude square function in z domain, $R(z)$, is obtained as[63]

$$R(z) = z^{2N-1} \frac{(1+z^{-1})^{2N}}{4^{2N-1}} \left\{ \sum_{i=0}^{N-1} (-1)^i \binom{2N-1}{i} (1+z^{-1})^{2(N-1-i)}(1-z^{-1})^{2i} \right.$$

$$- \sum_{i=1}^{N-1} (-1)^i \alpha_i \binom{2N-1}{i} (1+z^{-1})^{2(N-1-i)}(1-z^{-1})^{2i} \tag{5.24}$$

$$\left. + \sum_{i=N}^{2(N-1)} (-1)^i \alpha_i \binom{2N-1}{i} (1+z^{-1})^{2(N-1-i)}(1-z^{-1})^{2i} \right\}$$

Example: If one desires design a 6-tap smooth PR-QMF with the constraints

117

defined as

$$f\left(\frac{i}{2N-1}\right) = \begin{cases} 1 & 0 \le i \le 1 \\ 1-\alpha & i = 2 \\ \alpha & i = 3 \\ 0 & 4 \le i \le 5 \end{cases} \qquad (5.25)$$

where $0 \le \alpha < 0.5$ This set of constraints actually corresponds to a filter function $h(n)$ with two vanishing moments for $\alpha > 0$, and three vanishing moments for $\alpha = 0$[17][40]. The corresponding magnitude square function is similarly found as

$$R(z) = z^5 \frac{(1+z^{-1})^6}{4^5} \left\{ \sum_{i=0}^{2} (-1)^i \left(\begin{array}{c} 5 \\ i \end{array} \right) (1+z^{-1})^{2(2-i)}(1-z^{-1})^{2i} \right.$$

$$\left. -\alpha \left(\begin{array}{c} 5 \\ 2 \end{array} \right) (1-z^{-1})^4 - \alpha \left(\begin{array}{c} 5 \\ 3 \end{array} \right) (1+z^{-1})^{-2}(1-z^{-1})^6 \right\} \qquad (5.26)$$

From here via any factorization technique one may obtain the corresponding PR-QMF solution, $H(z)$. This design technique is exemplified in Fig. 5.1.

Remark 2: The vanishing moments of PR-QMF high pass filter $(-1)^n h(n)$ with length $2N$ is defined in time as

$$\sum_n (-1)^n n^i h(n) = 0 \quad i = 0, 1, ..., N$$

this is equivalent to the flatness requirement of the QMF filter response in frequency

$$\left. \frac{d^\nu H(e^{i(\omega+\pi)})}{d\omega^\nu} \right|_{\omega=0} = 0 \quad \nu = 0, 1, ..., N$$

It is seen that the maximally flat filters, Daubechies filters or Binomial-QMF, $i = N$, have the maximum number of vanishing moments on their high pass version. It is clear that all the possible moments are used only by the high-pass filter and low-pass filter does not have any vanishing moments.

Any $\alpha_i \ne 0$ of the proposed approach decreases the number of vanishing moments of the high-pass filter by one. The magnitude functions of several known smooth or regular $6 - tap$ QMFs and their α values are given in Fig. 5.2.[63]
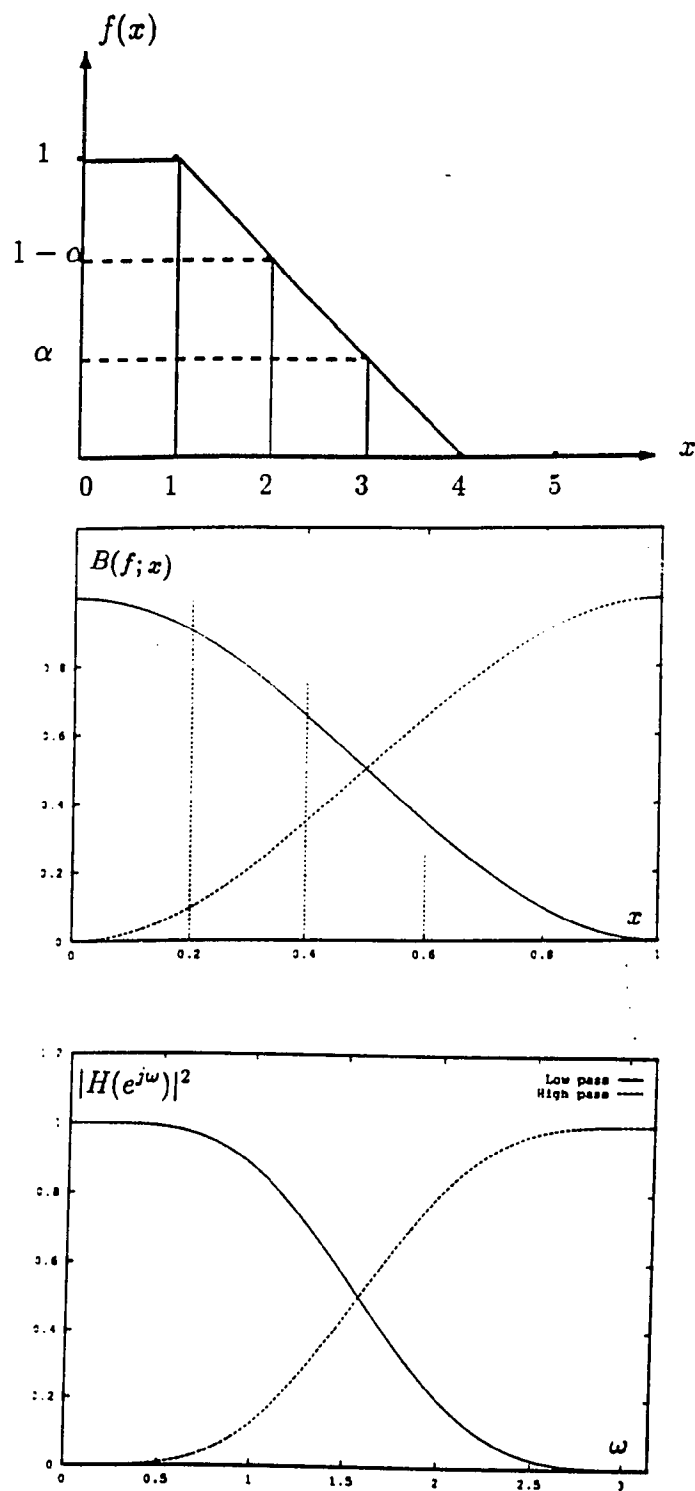
Fig. 5.1. a) $f(x)$ chosen such that Eq.(5.18) is satisfied and its sample values $f(\frac{i}{2N-1})$ are determined. b) Corresponding Bernstein polynomial approximation $B(f;x)$. c) Corresponding magnitude square function $|H(e^{j\omega})|^2$ in ω

119

Remark 3: It is found that $\alpha = 0.2708672$ corresponds to 6-tap Coiflet filter solution[46], as $\alpha = 0.0348642$ gives the 6-tap PR-QMF of the most regular orthonormal wavelet solution[48]. It is clear that $\alpha = 0$ gives the Binomial QMF-Wavelet Transform with three vanishing moments[17][40]. This parametric solution of the PR-QMF problem also leads to a useful tool for the design of orthonormal wavelet bases. The parameters of a known length PR-QMF solution are related to the regularity of the corresponding orthonormal wavelet functions.

5.4   Energy Compaction and Performance Results

Energy compaction gains G, of several decomposition techniques; DCT, KLT, Binomial-QMF, ideal subband filter banks, for different N and correlation $r = 0.95$ cases are given in Table 5.1. It is seen that the ideal subband structure reaches to the global performance upper bound, at infinite number of bands, faster than the optimum block transform KLT. It is also observed that the performance of 6-tap Binomial-QMF is better than the KLT for all the cases considered here.

Fig. 5.3. provides the 2-band energy compaction performance of $4 - tap$ and $6 - tap$ filters as a function of α for the input sources AR(0.75), AR(0.85), and AR(0.95). It is seen that $\alpha = 0$, the Binomial QMF, compacts better than all the other smooth QMF solutions. This is expected for this source model since $\alpha = 0$ corresponds to the maximally flat magnitude square function around $\omega = 0$. Fig. 5.4. displays the variations of the filter coefficients of all the possible smooth PR-QMFs as a function of α for $2N = 4$. Haar basis corresponds to $\alpha = 1/3$ in this figure. The phase responses of the filters in this α range is linear-like. Similarly, Fig. 5.5. gives the coefficients of all possible 6-tap smooth PR-QMFs as a function of parameter α. Here the high-pass filters have two vanishing moments except for

$\alpha = 0.$

5.4.1   Discussions and Conclusions

A parametric PR-QMF design technique based on Bernstein polynomial approximation is developed in this chapter. Any orthonormal PR-QMF can be designed with this technique. The filter examples we considered are smooth, ripple-free. This approach can also be easily applied for rippled QMF design problems. All PR-QMF filter solutions of a given length can be obtained as a function of the design parameters in this approach.

Since the wavelet functions are evaluated with their regularity, this approach provides a tool to design orthonormal wavelet bases with the desired degree of regularity. For this purpose, the parameters of the design technique are linked to the regularity of the corresponding wavelet function. This provides the pattern of the relations between the frequency behavior of PR-QMFs and the degree of regularity or differentiability of the corresponding orthonormal wavelet functions. This is a topic of future research.

From signal coding point of view the energy compaction is an important performance measure. It is observed that the QMF filters of the most regular wavelet solution[48] does not provide the best energy compaction for the signal sources considered here. It is also shown that the max-flat solutions, Binomial QMF-Wavelet filters[17][40], for the sources considered here have the best energy compaction over the smooth QMF solutions.

The energy compaction results also unify the evaluation of all popular signal decomposition techniques[64]. They scale their compaction performance comparatively. They can provide a vehicle for the trade-offs, performance versus computational complexity. It is clear that the filter banks considered here outperform the block transforms as expected.

We can conclude this chapter that any practically useful PR-QMF solution should consider the degrees of energy compaction, smoothness or regularity, phase response, and the computational complexity issues simultaneously. This intuition is extended in optimal PR-QMF design approach which will be presented in Chapter 7.

2N	DCT	KLT	6-tap B-QMF	Ideal
2	3.20	3.20	3.76	3.94
4	5.71	5.73	6.77	7.23
8	7.63	7.66	8.52	9.16
16	8.82	8.86	9.25	9.95
..	..	..	..	..
∞	10.25	10.25	10.25	10.25

Fig. 5.1 Energy compaction gains G. of several decomposition techniques; DCT. KLT. Binomial-QMF. ideal subband filter banks, for different N and correlation

$$\rho = 0.95 \text{ cases}$$
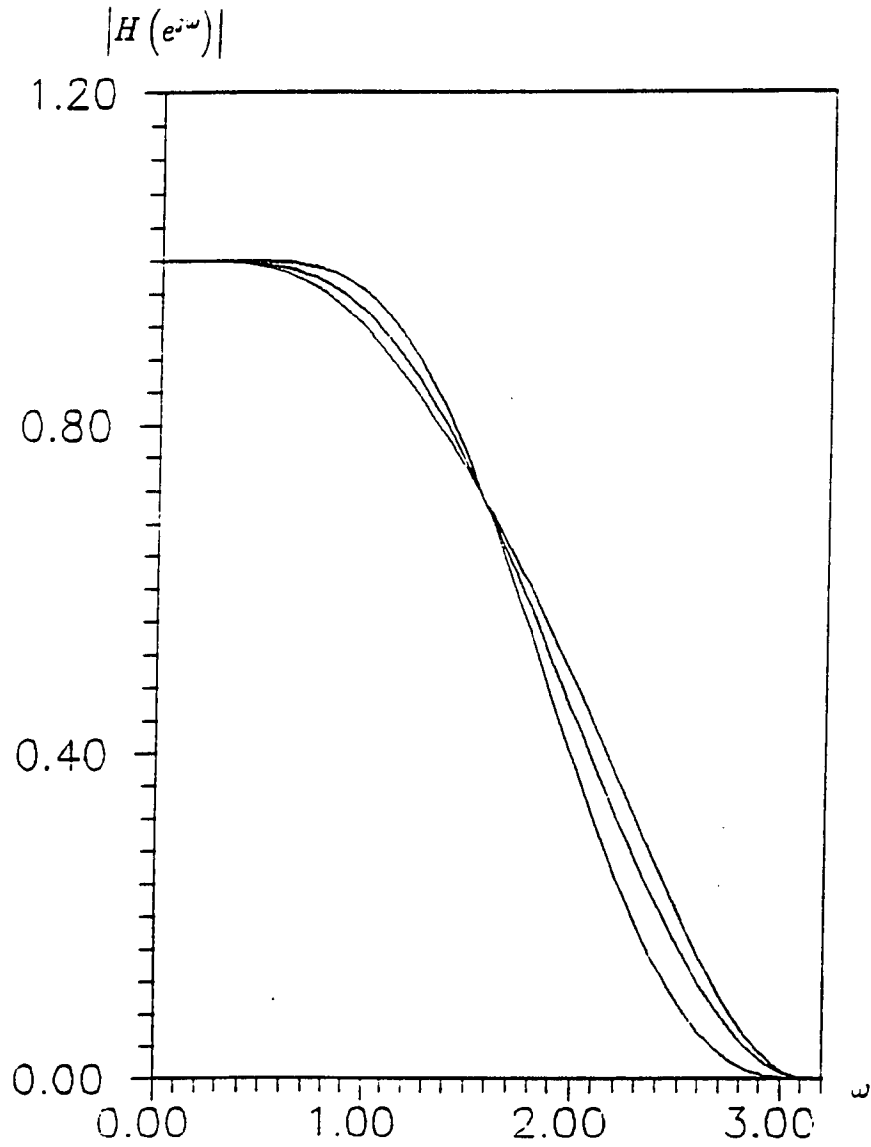
Fig. 5.2. Magnitude functions of three different 6-tap PR-QMFs: max-flat ($\alpha = 0$), coiflet, and for ($\alpha = 0.480$).
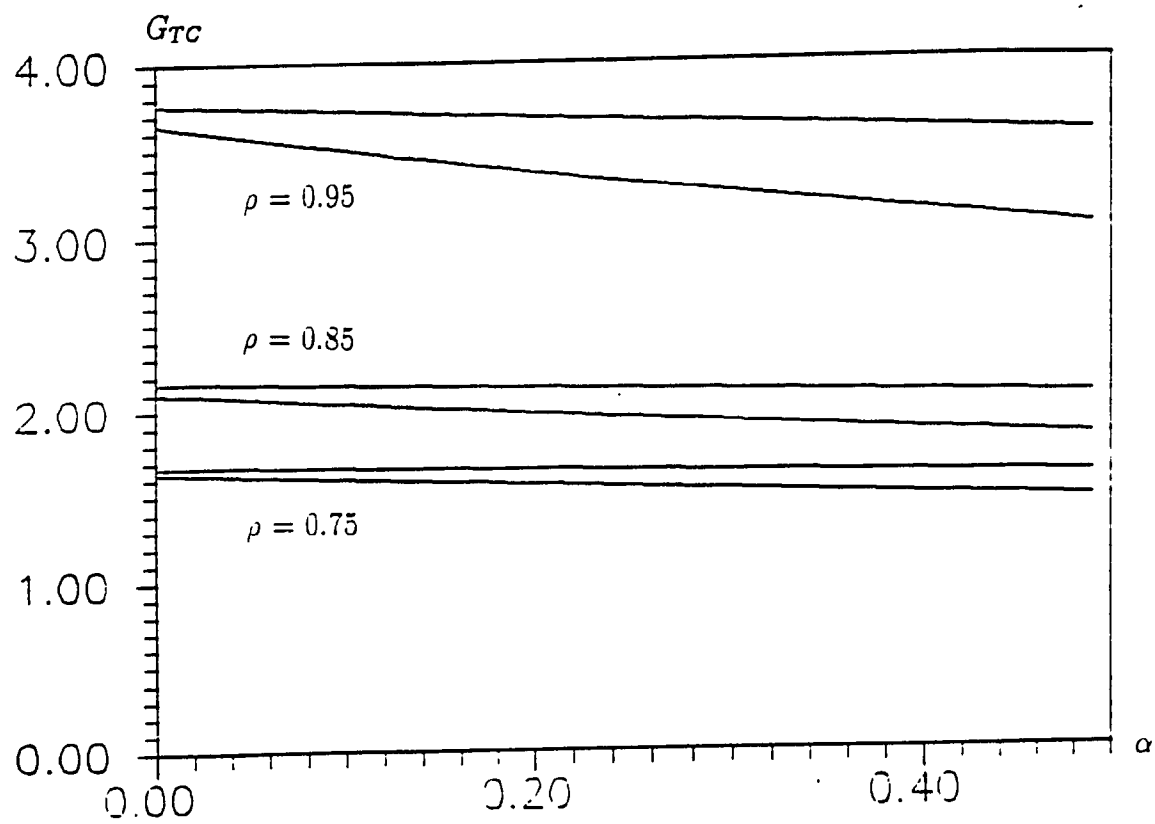
Fig. 5.3. 2 Band energy compaction of 4 and 6-tap PR-QMFs as a function of α

for AR(0.75), AR(0.85), AR(0.95).
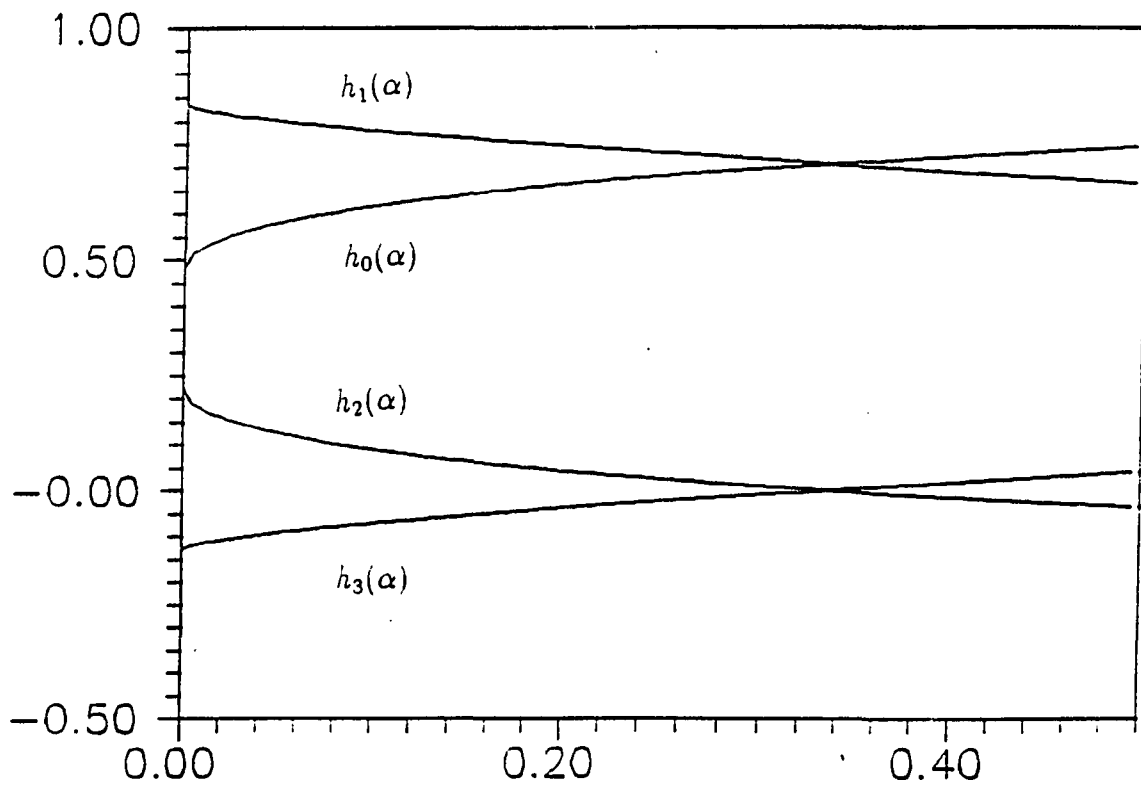
Fig. 5.4. All the possible smooth 4-tap PR-QMF coefficients as a function of α.
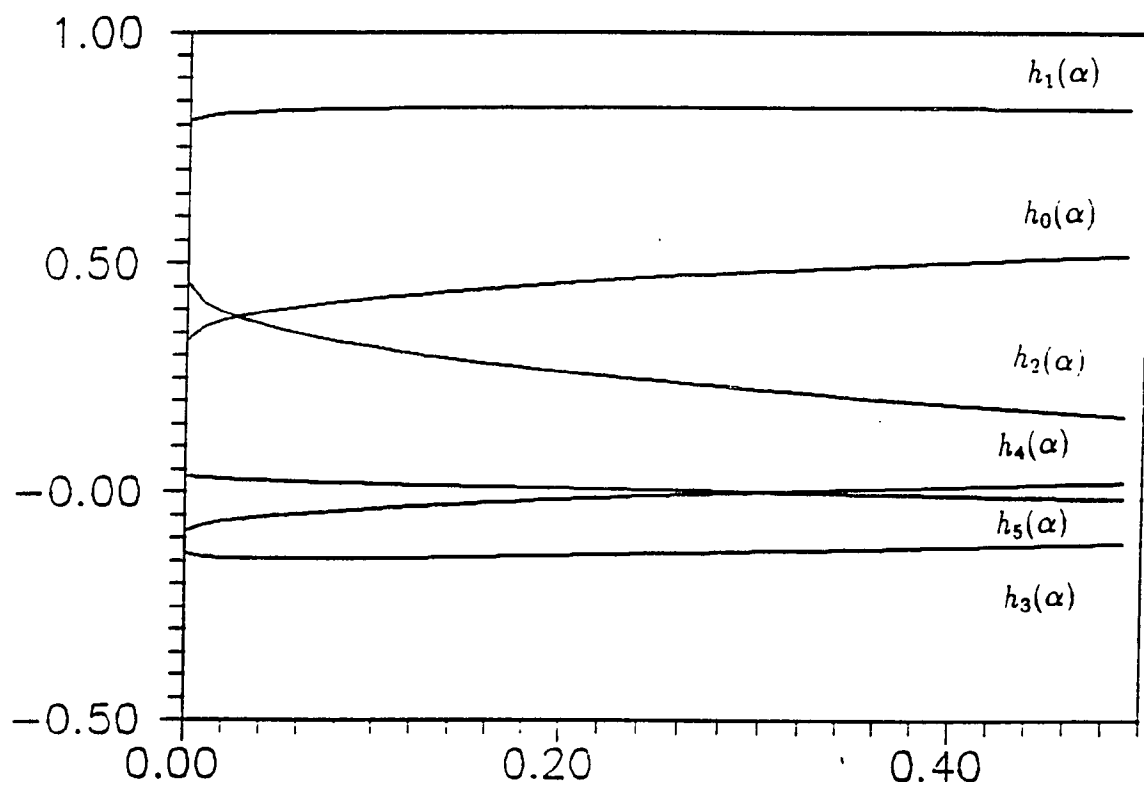
Fig. 5.5 All the possible smooth 6-tap PR-QMF coefficients as a function of α.

Chapter 6

An Objective Performance Measure in Multiresolution Signal Decomposition

6.1   Introduction

Since finite length functions are employed in practical signal decompositions, the imperfect frequency behavior is inevitable. This fact is clearly observed as aliasing or inter band energy leakage in signal coding applications[65][66]. Although this concept is inherent in any decomposition technique its effects are more clearly followed in multi-rate signal processing or filter bank environment.

This chapter attempts to analysis the aliasing energy in a filter bank structure and defines a new performance measure called Non-Aliasing Energy Ratio (NER)[65] for the evaluation of orthonormal signal decomposition techniques. The significance of the new measure is emphasized with the comparative performance results of the popular orthonormal decomposition techniques. It is shown that the new performance measure, Non-Aliasing Energy Ratio, complements the widely used energy compaction measure and is consistent with the experimental performance results.

6.2 Aliasing Effects of Decimation-Interpolation Operators

We are going to examine the effects of decimation/interpolation operators in a multirate branch which is depicted in Fig. 6.1 for the given input spectral density function $S_x(e^{j\omega})$. $H_i(e^{j\omega})$ is a band pass anti-aliasing filter with the bandwidth π/M and $G_i(e^{j\omega})$ is the interpolation filter for the ith branch or subband. The spectrum of the interpolated signal, or branch output $V_i(e^{j\omega})$ will be connected to the input spectral density. Its energy components, namely aliasing and non-aliasing, will be derived here. This analysis can be easily extended for M-band perfect reconstruction filter banks.
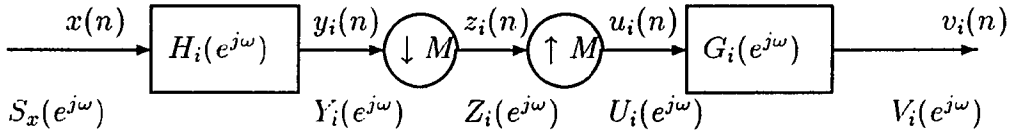
Fig. 6.1 A decimation/interpolation branch.

The output spectrum of $H_i(e^{j\omega})$ can be related to the input signal as

$$S_{y_i}(e^{j\omega}) = |H_i(e^{j\omega})|^2 S_x(e^{j\omega}) \tag{6.1}$$

The spectral density function of the M-fold down-sampled version of this output signal is expressed as

$$S_{z_i}(e^{j\omega M}) = \frac{1}{M} \sum_{n=0}^{M-1} S_{y_i}(e^{j(\omega+\frac{2\pi}{M}n)}) \tag{6.2}$$

substituting Eq.(6.1) into Eq.(6.2) yields

$$S_{z_i}(e^{j\omega M}) = \frac{1}{M} \sum_{n=0}^{M-1} |H_i(e^{j(\omega+\frac{2\pi}{M}n)})|^2 S_x(e^{j(\omega+\frac{2\pi}{M}n)}) \tag{6.3}$$

Following Fig. 6.1 for the interpolation operation indicates the branch output spectral density function[67]

$$S_{v_i}(e^{j\omega}) = \frac{1}{M} |G_i(e^{j\omega})|^2 S_{z_i}(e^{j\omega M}) \tag{6.4}$$

Now substituting Eq.(6.3) into the last equation

$$S_{v_i}(e^{j\omega}) = \frac{1}{M^2}|G_i(e^{j\omega})|^2 \sum_{n=0}^{M-1} |H_i(e^{j(\omega+\frac{2\pi}{M}n)})|^2 S_x(e^{j(\omega+\frac{2\pi}{M}n)}) \qquad (6.5)$$

which can also be rewritten as

$$S_{v_i}(e^{j\omega}) = S_i^N(e^{j\omega}) + S_i^A(e^{j\omega}) \qquad (6.6)$$

where

$$S_i^N(e^{j\omega}) = \frac{1}{M^2}|G_i(e^{j\omega})|^2|H_i(e^{j\omega})|^2 S_x(e^{j\omega}) \qquad (6.7)$$

and

$$S_i^A(e^{j\omega}) = \frac{1}{M^2}|G_i(e^{j\omega})|^2 \sum_{n=1}^{M-1} |H_i(e^{j(\omega+\frac{2\pi}{M}n)})|S_x(e^{j(\omega+\frac{2\pi}{M}n)}) \qquad (6.8)$$

It is seen that $S_i^N(e^{j\omega})$ consists of non-aliasing component of the output spectral density while $S_i^A(e^{j\omega})$ corresponds to the aliasing term which is caused by down and upsampling by the rate M. $S_i^A(e^{j\omega})$ consists of (M-1) aliasing terms which are somewhat misplaced in frequency.

If one goes one step further to calculate the branch output energy or variance for a zero mean input

$$\begin{aligned} \sigma_i^2 &= \frac{1}{2\pi} \int_{-\pi}^{\pi} S_{V_i}(e^{j\omega})d\omega \\ &= \sigma_{i_N}^2 + \sigma_{i_A}^2 \end{aligned} \qquad (6.9)$$

where

$$\begin{aligned} \sigma_{i_N}^2 &= \frac{1}{2\pi} \int_{-\pi}^{\pi} S_i^N(e^{j\omega})d\omega \\ \sigma_{i_A}^2 &= \frac{1}{2\pi} \int_{-\pi}^{\pi} S_i^A(e^{j\omega})d\omega \end{aligned} \qquad (6.10)$$

Hence we separate the branch output energy into its non-aliasing and aliasing components. The latter is caused by down and upsampling as mentioned earlier.

Fig. 6.2 displays the spectra of different points in the decimation/interpolation branch of Fig. 6.1 for the given input and filters. This figure assumes an AR(1) input source with $\rho = 0.5$ and employs 4-tap Binomial QMF[17].

The advantage of this analysis in a lossless M-band filter bank structure is its ability to decompose the signal energy into a kind of time-frequency plane. In this analysis we can express the decomposed signal energy of branches or subbands in the form of an energy matrix which is defined as

$$[E(i,k)] = \sigma^2_{(i,mod(k+i)_{M-1})} \qquad i,k = 0,1,...,M-1 \qquad (6.11)$$

Each row of the matrix E corresponds to one of the bands or channels in the filter bank. The columns of this matrix correspond to the distributions of subband energies in frequency. The energy matrices of 8 band DCT, 8 band hierarchical filter banks with 6-tap Binomial QMF(BQMF)[17], and the Most Regular Wavelet Filter(MRWF)[48] for an $AR(1)$ source with $\rho = 0.95$ are calculated as[65]

$$E_{DCT} = \begin{bmatrix} 6.6824 & 0.1211 & 0.0280 & 0.0157 & 0.0132 & 0.0157 & 0.0280 & 0.1211 \\ 0.1511 & 0.1881 & 0.1511 & 0.0265 & 0.0113 & 0.0091 & 0.0113 & 0.0265 \\ 0.0345 & 0.0136 & 0.0569 & 0.0136 & 0.0345 & 0.0078 & 0.0046 & 0.0078 \\ 0.0158 & 0.0032 & 0.0050 & 0.0279 & 0.0051 & 0.0032 & 0.0158 & 0.0061 \\ 0.0176 & 0.0032 & 0.0016 & 0.0032 & 0.0176 & 0.0032 & 0.0016 & 0.0032 \\ 0.0065 & 0.0012 & 0.0065 & 0.0022 & 0.0026 & 0.0132 & 0.0026 & 0.0022 \\ 0.0053 & 0.0004 & 0.0001 & 0.0004 & 0.0053 & 0.0033 & 0.0118 & 0.0033 \\ 0.0053 & 0.0002 & 0.0000 & 0.0000 & 0.0000 & 0.0002 & 0.0053 & 0.0155 \end{bmatrix}$$

$$E_{BQMF} = \begin{bmatrix} 7.1720 & 0.0567 & 0.0014 & 0.0005 & 0.0001 & 0.0005 & 0.0014 & 0.0567 \\ 0.0567 & 0.1987 & 0.0567 & 0.0258 & 0.0005 & 0.0014 & 0.0005 & 0.0258 \\ 0.0258 & 0.0025 & 0.0640 & 0.0025 & 0.0258 & 0.0042 & 0.0061 & 0.0042 \\ 0.0042 & 0.0014 & 0.0025 & 0.0295 & 0.0025 & 0.0014 & 0.0042 & 0.0196 \\ 0.0196 & 0.0019 & 0.0001 & 0.0013 & 0.0223 & 0.0013 & 0.0001 & 0.0019 \\ 0.0019 & 0.0061 & 0.0019 & 0.0046 & 0.0013 & 0.0167 & 0.0013 & 0.0045 \\ 0.0045 & 0.0001 & 0.0014 & 0.0001 & 0.0045 & 0.0020 & 0.0162 & 0.0020 \\ 0.0020 & 0.0001 & 0.0001 & 0.0001 & 0.0001 & 0.0001 & 0.0020 & 0.0220 \end{bmatrix}$$

$$E_{MRWF} = \begin{bmatrix} 7.1611 & 0.0589 & 0.0018 & 0.0006 & 0.0001 & 0.0006 & 0.0018 & 0.0589 \\ 0.0589 & 0.1956 & 0.0589 & 0.0262 & 0.0006 & 0.0017 & 0.0006 & 0.0262 \\ 0.0262 & 0.0028 & 0.0628 & 0.0028 & 0.0262 & 0.0043 & 0.0064 & 0.0043 \\ 0.0043 & 0.0018 & 0.0028 & 0.0291 & 0.0028 & 0.0018 & 0.0043 & 0.0196 \\ 0.0196 & 0.0020 & 0.0001 & 0.0014 & 0.0221 & 0.0014 & 0.0001 & 0.0020 \\ 0.0020 & 0.0064 & 0.0020 & 0.0047 & 0.0014 & 0.0164 & 0.0014 & 0.0047 \\ 0.0047 & 0.0001 & 0.0017 & 0.0001 & 0.0047 & 0.0020 & 0.0160 & 0.0020 \\ 0.0020 & 0.0001 & 0.0001 & 0.0001 & 0.0001 & 0.0001 & 0.0020 & 0.0218 \end{bmatrix}$$

$$(6.12)$$

If we sum the components of the energy matrix in a unitary M-band filter bank, the variance of the input is obtained as

$$\sigma_x^2 = \frac{1}{M} \sum_{i=0}^{M-1} \sum_{k=0}^{M-1} E(i,k) \qquad (6.13)$$

Additionally, the band variances are equal to the sum of rows in matrix E as

$$\sigma_i^2 = \sum_{k=0}^{M-1} E(i,k) \qquad (6.14)$$

6.3 Hierarchical Decimation Interpolation

Let us now consider the hierarchical decimation/interpolation multirate branch given in Fig. 6.3a. The input signal $x(n)$ is first decimated by the rate M_1 and then again by the rate M_2. The overall decimation rate is $M = M_1 M_2$. The interpolation part of the branch consists of the corresponding upsamplers and interpolation filters. Since the hierarchical branch is a typical module of the multiresolution signal decomposition theory it is worth to derive all the steps of the operations and to interpret the branch output accordingly.

131
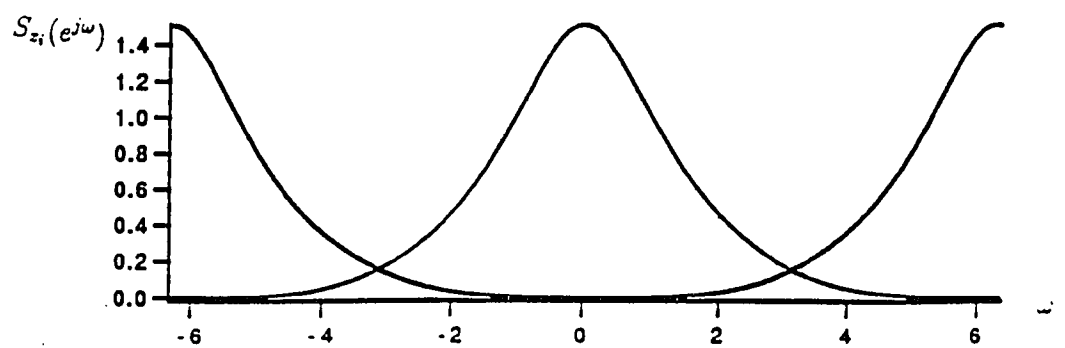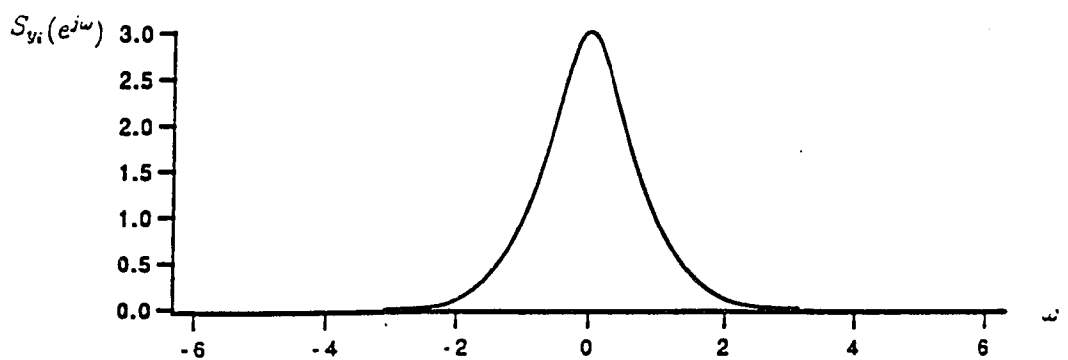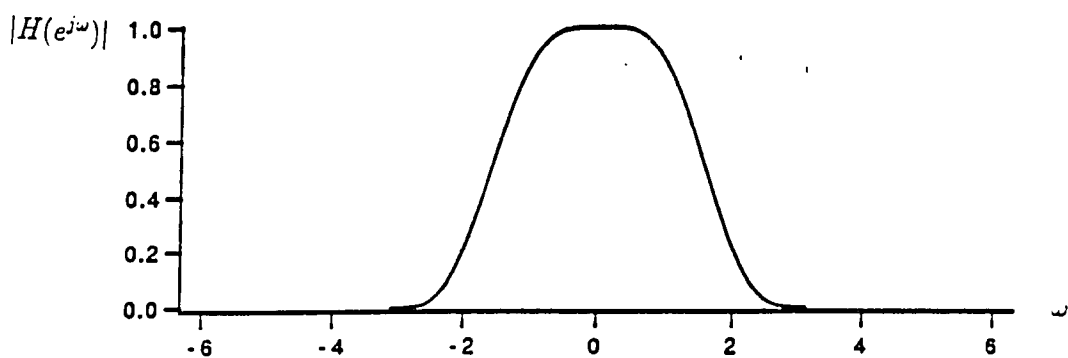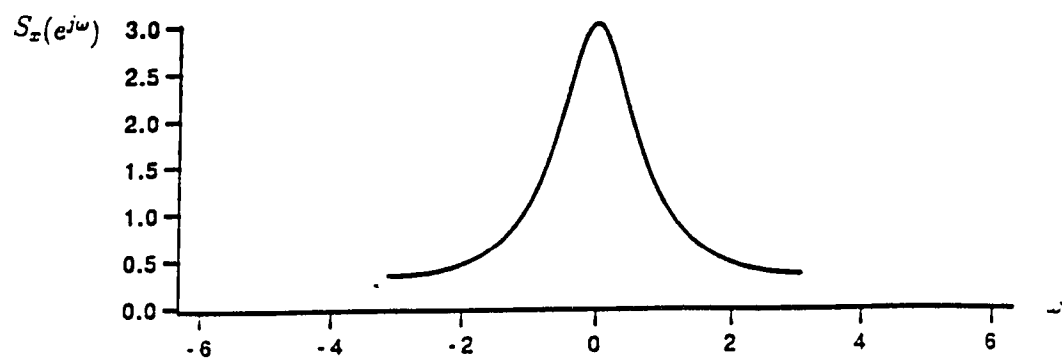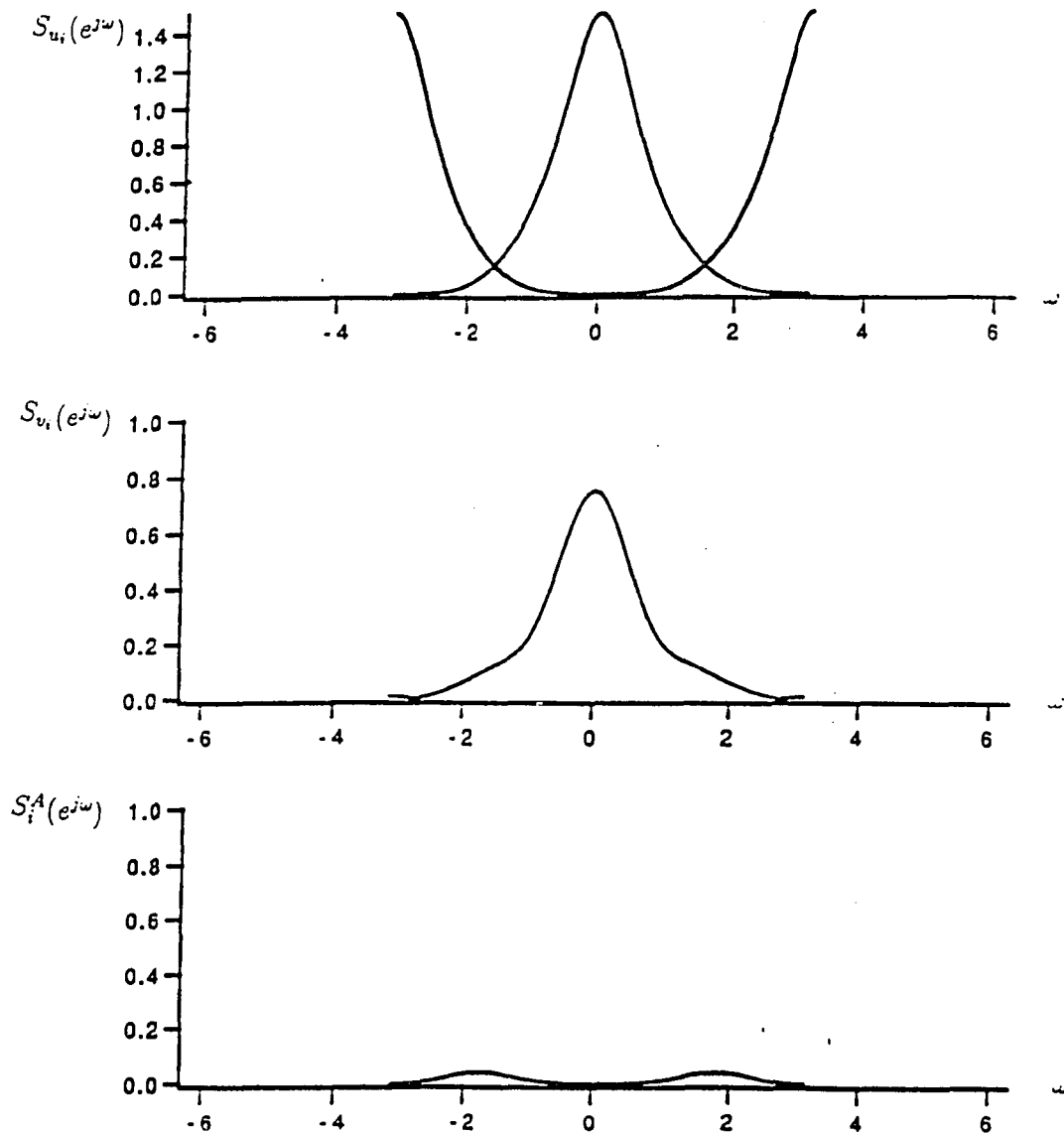
Fig. 6.2. The signal spectra of different points in the decimation/interpolation

branch of Fig. 6.1.
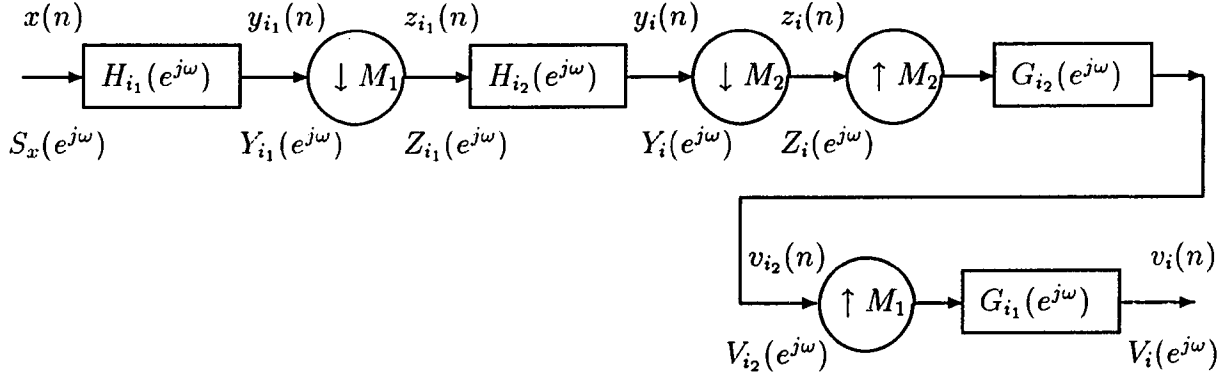
Fig. 6.3.a. Hierarchical decimation/interpolation branch.

We can easily modify Fig. 6.3a. by combining the two decimation steps into one decimation step with the rate $M = M_1 M_2$ as shown in Fig. 6.3b. Now the structure becomes like the previous case considered. Similarly we follow those steps to relate the output and input spectral densities of the multirate branch.
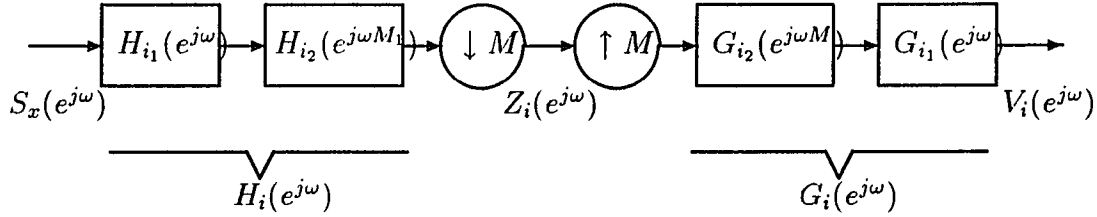
Fig. 6.3.b. Equivalent of hierarchical decimation/interpolation branch in Fig. 6.3.a.

The spectral density after the decimation by M can be similarly expressed as

$$S_{z_i}(e^{j\omega}) = \frac{1}{M} \sum_{n=0}^{M-1} |H_i(e^{j(\omega + \frac{2\pi}{M}n)})|^2 S_x(e^{j(\omega + \frac{2\pi}{M}n)}) \qquad (6.15)$$

where

$$|H_i(e^{j\omega})| = |H_{i_1}(e^{j\omega})||H_{i_2}(e^{j\omega M_1})| \qquad (6.16)$$

and the spectral density function of the branch output after the interpolation is

134

written as

$$S_{v_i}(e^{j\omega}) = \frac{1}{M^2}|G_i(e^{j\omega})|^2 \sum_{n=0}^{M-1} |H_i(e^{j(\omega+\frac{2\pi}{M}n)})|^2 S_x(e^{j(\omega+\frac{2\pi}{M}n)}) \qquad (6.17)$$

where

$$|G_i(e^{j\omega})| = |G_{i_1}(e^{j\omega})||G_{i_2}(e^{j\omega M_1})| \qquad (6.18)$$

Therefore we can similarly express the output energy of the branch with the two components. The first one corresponds to the non-aliasing term where the remaining part consists of (M-1) aliasing energy terms misplaced in frequency as defined earlier.

6.4   Hierarchical Perfect Reconstruction Filter Banks

Since the multi-resolution has become a desirable feature from the signal decomposition techniques 2-band PR-QMFs have been widely employed as the basic filter module. Most of the filter banks considered in the field are based on this simple 2-band structure. Additionally, their strong links with the Orthonormal Wavelet transforms made them very popular in signal processing field lately. We will now analysis the band energies of a hierarchical PR filter bank for the four band case and lay down the foundation of a new performance criterion for orthonormal signal decomposition techniques which will be explained in the following section.

The analysis filter bank of the case considered is given in Fig. 6.4a. After combining the decimation operations and also considering the synthesis stage the whole filter bank structure can be visualized as in Fig. 6.4b.

135
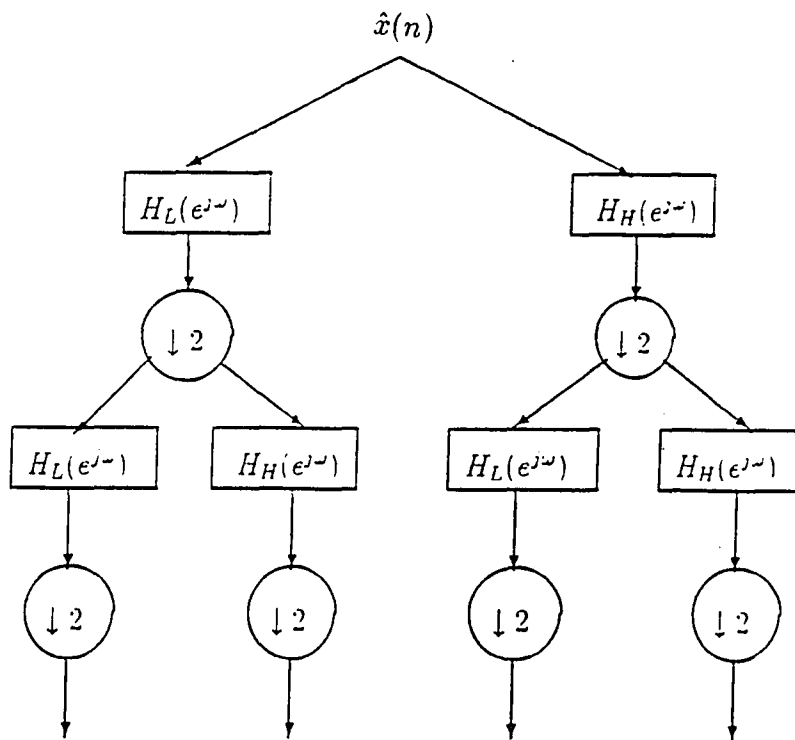
Fig 6.4.a. The two-level hierarchical analysis filter bank structure.
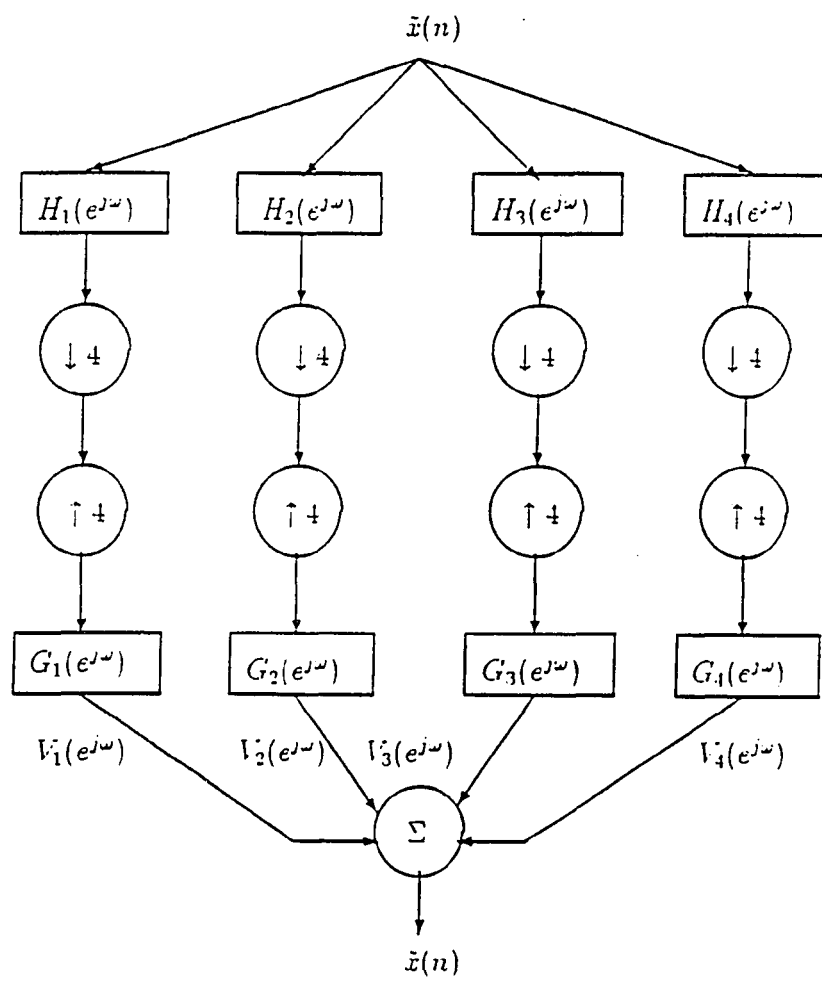
Fig. 6:4.b. Equivalent structure of the two-level, four band hierarchical filter bank.

The combined anti-aliasing and interpolation filters of Fig. 6.4.b can be expressed as

$$|H_1(e^{j\omega})| = |H_L(e^{j\omega})||H_L(e^{j\omega 2})|$$

$$|H_2(e^{j\omega})| = |H_L(e^{j\omega})||H_H(e^{j\omega 2})|$$

$$|H_3(e^{j\omega})| = |H_H(e^{j\omega})||H_L(e^{j\omega 2})|$$

$$|H_4(e^{j\omega})| = |H_H(e^{j\omega})||H_H(e^{j\omega 2})| \qquad (6.19)$$

and

$$|G_1(e^{j\omega})| = |H_L(e^{j\omega 2})||H_L(e^{j\omega})|$$

$$|G_2(e^{j\omega})| = |H_L(e^{j\omega 2})||H_H(e^{j\omega})|$$

$$|G_3(e^{j\omega})| = |H_H(e^{j\omega 2})||H_L(e^{j\omega})|$$

$$|G_4(e^{j\omega})| = |H_H(e^{j\omega 2})||H_H(e^{j\omega})| \qquad (6.20)$$

This set of filters is created properly so that the aliasing terms caused by the down and upsampling operations are cancelled and all the conditions of perfect reconstruction are satisfied.

These product anti-aliasing and interpolation filters should also have good band-pass characteristics additional to PR requirements. Fig. 6.5 displays the frequency selectivity of 8-tap 2-band Binomial-QMF[17] and its product filters in a hierarchical subband tree for the levels 2 and 3 implying 2, 4 and 8 band filter banks. It is clear that the nice frequency behavior of 2-band Binomial-QMF diminishes when we move in the tree. The effects of aliasing become severe for the increased levels of the subband tree. This is a very significant point to be considered when one employs a 2-band PR-QMF in a hierarchical subband tree. Although it is easier to implement 2-band PR-QMF the frequency behavior of the product filters should also be carefully monitored in applications for a good performance.

$|H^{(1)}(e^{j\omega})|$

$|H^{(2)}(e^{j\omega})|$

$|H^{(3)}(e^{j\omega})|$
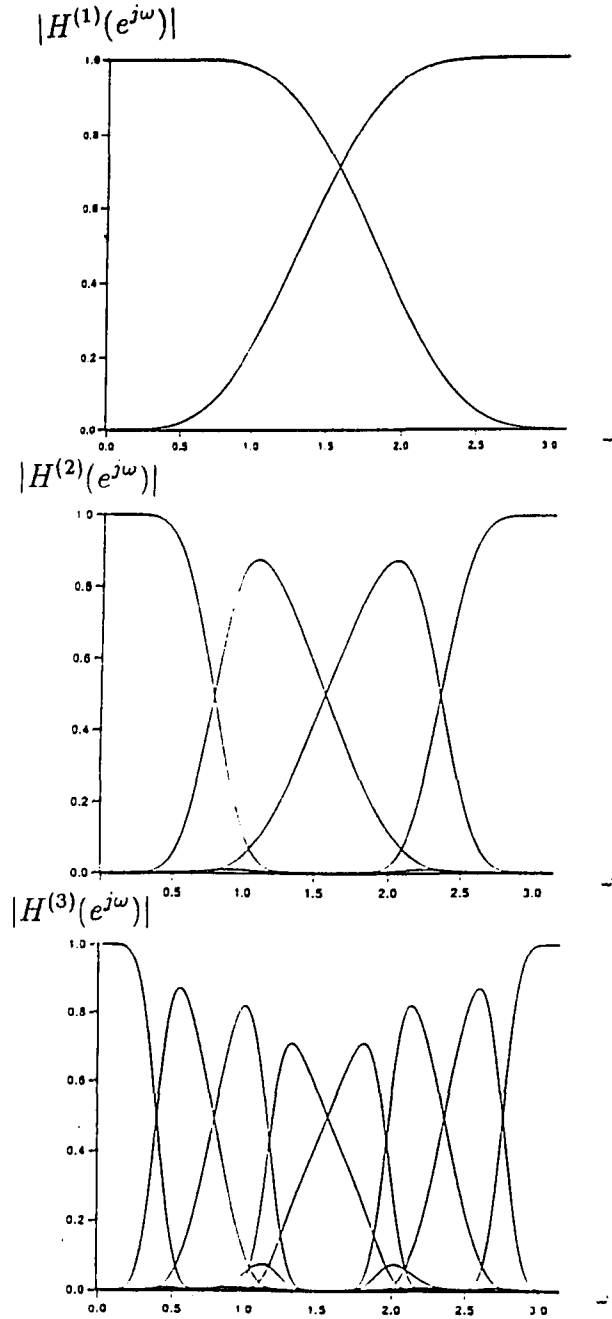
Fig. 6.5. The frequency characteristics of 2-band 8-tap BQMF and its product filters in the hierarchical subband filter bank structure.

We can consider each decimation/interpolation branch of this PR filter bank as the one discussed earlier in Section 6.2. Therefore the band energies of this 4-

139

band PR filter bank for the given input are also grouped into the parts which consist of non-aliasing and aliasing energy components as

$$\sigma_{i_N}^2 = \frac{1}{2\pi} \int_{-\pi}^{\pi} S_i^N(e^{j\omega})d\omega$$

$$\sigma_{i_A}^2 = \frac{1}{2\pi} \int_{-\pi}^{\pi} S_i^A(e^{j\omega})d\omega \qquad (6.21)$$

with

$$\sigma_i^2 = \sigma_{i_N}^2 + \sigma_{i_A}^2 \qquad (6.22)$$

where $S_i^N(e^{j\omega})$ and $S_i^A(e^{j\omega})$ are defined in Eqs.(6.7) and (6.8) respectively. The energy matrices of BQMF and MRWF given in Eq.(6.12) were calculated for the 8 band case using these analysis steps.

6.5 Non-Aliasing Energy Ratio (NER): A New Statistical Performance Measure for Orthonormal Signal Decomposition

Gain of transform coding over PCM, G_{TC}, has been a widely used performance measure particularly for the block transforms[7]. This measure is defined for a size N unitary transform as

$$G_{TC} = \frac{\sigma_x^2}{\left[\prod_{i=1}^{N} \sigma_i^2\right]^{1/N}} \qquad (6.23)$$

where σ_x^2 is the input variance, and $\{\sigma_i^2\}$ are band or coefficient variances and they satisfy the variance preserving condition

$$\sigma_x^2 = \frac{1}{N} \sum_{i=1}^{N} \sigma_i^2 \qquad (6.24)$$

This measure does not consider the distribution of the band energies in frequency. Therefore the aliasing portion of the band energy is not treated differently than the non-aliasing band energy. This fact becomes very important particularly when all the analysis subband signals are not used for the reconstruction. The

140

aliasing components of band energies at the outputs of decimation-interpolation branch represent a kind of misplaced energy contents. Whenever the aliasing cancellation in the reconstructed signal is not perfectly performed due to the available bits for coding the effects of aliasing energy become quite significant especially in image and video applications[66].

Because of the reasons explained we will decompose the band energies of the popular orthonormal signal decomposition techniques into their aliasing and non-aliasing energy components for a given input source.

We now define the energy components of the branch or subband i in a general 1D M-band orthonormal decomposition scheme as

$$\sigma_i^2 = \sum_{k=0}^{M-1} \sigma_{ik}^2 \quad i = 0, 1, ..., M-1 \tag{6.25}$$

where

$$\sigma_{ik}^2 = \frac{1}{2\pi M^2} \int_{-\pi}^{\pi} |G_i(e^{j\omega})|^2 |H_i(e^{j(\omega + \frac{2\pi}{M}k)})|^2 S_x(e^{j(\omega + \frac{2\pi}{M}k)}) d\omega \quad i, k = 0, 1, ..., M-1 \tag{6.26}$$

As seen from Eq.(6.26) the term corresponding to $k = 0$ is the non-aliasing band energy as given in Eq.(6.7)

$$\sigma_{i_N}^2 = \sigma_{i_0}^2 \tag{6.27}$$

on the other hand the total aliasing energy component of band i is expressed as

$$\sigma_{i_A}^2 = \sum_{k=1}^{M-1} \sigma_{ik}^2 \tag{6.28}$$

We now define the non-aliasing energy ratio of an M-band orthonormal decomposition technique as

$$NER = \frac{\sum_{i=0}^{M-1} \sigma_{i_0}^2}{\sum_{i=0}^{M-1} \sigma_i^2} \tag{6.29}$$

where the numerator term is the sum of the non-aliasing band energies. It is clear that the ideal filter bank yields $NER = 1$ for any M as the upper bound of this measure for an arbitrary input signal.

6.6 Simulations and Discussions

In the simulation studies we considered 4-6-8 tap Binomial-QMF(BQMF)[17] in a hierarchical subband filter bank structure as well as 8-tap Smith-Barnwell[13], and 6-tap most regular orthonormal wavelet filters[48], 4-6-8 tap Optimal QMF[68] along with the ideal filter banks. Additionally 2×2, 4×4, and 8×8 Discrete Cosine(DCT), Discrete Sine(DST), Walsh-Hadamard(WHT)[7], and Modified Hermite(MHT)[56] transforms are considered for comparison purposes. The simulations are carried out for the G_{TC} and NER performance calculations for those signal decomposition tools.

These simulations employed $AR(1)$ and *Generalized Correlation* source models. Table 6.1. displays G_{TC} and NER performance of the orthonormal signal decomposition techniques considered with $M = 2, 4, 8$ for $AR(1)$, $\rho = 0.95$ source which has the correlation function defined as

$$R_x(m) = \rho^{|m|} \quad m = 0, \pm1, \pm2, \ldots \ldots \tag{6.30}$$

Table 6.2. provides similar performance results for the generalized correlation source model which has the correlation function as

$$R_x(m) = e^{-\alpha|m|^\gamma} \quad m = 0, \pm1, \pm2, \ldots \ldots \tag{6.31}$$

where $\alpha = -\ln \rho$, $\rho = 0.95$, $\gamma = 1.137$ parameter values are used.

As discussed earlier, this approach provides the analytical tools to consider the non-aliasing and aliasing components of band energies. From practical point of view this is an important feature. It is well known in the field that the aliasing energies become annoying particularly at low bit rate image coding applications. The theoretical analysis provided here explains objectively some of the reasons behind this fact. Although the ratio of the aliasing energies over the whole signal

142

energy may look negligible, the misplaced aliasing energy components of bands may be well localized in frequency and cause the undesired subjective performance degradations.

It is also noteworthy that the larger M indicates better coding performance in G_{TC} measure. But it is a well known fact that the larger size transforms do not provide better subjective image coding performance[66]. This has been explained as the cause of undesired inter-coefficient or inter-band energy leakages in the literature. In other words it is the result of the aliasing problems in signal decomposition step. $M = 8$ or 16 are practically agreed transform sizes in image coding. The new measure indicates that the larger M values yield worse performance for the finite duration transform bases and the source models considered. This trend is consistent with the experimental results reported in the literature. The new objective performance measure, NER, indicates the importance of the aliasing energy in orthonormal signal decomposition which was not considered by the commonly used energy compaction measure, G_{TC}, in the literature.

Table 6.1. Performance of several orthonormal signal decomposition techniques

for AR(1), $\rho = 0.95$ source.

	M=2 G_{TC} (NER)	M=4 G_{TC} (NER)	M=8 G_{TC} (NER)
DCT	3.2026 (0.9756)	5.7151 (0.9372)	7.6316 (0.8767)
DST	3.2026 (0.9756)	3.9106 (0.8532)	4.8774 (0.7298)
MHT	3.2026 (0.9756)	3.7577 (0.8311)	4.4121 (0.5953)
WHT	3.2026 (0.9756)	5.2173 (0.9356)	6.2319 (0.8687)
Binomial-QMF(4tap)	3.6426 (0.9880)	6.4322 (0.9663)	8.0149 (0.9260)
Binomial-QMF(6tap)	3.7588 (0.9911)	6.7665 (0.9744)	8.5293 (0.9427)
Binomial-QMF(8tap)	3.8109 (0.9927)	6.9076 (0.9784)	8.7431 (0.9513)
Smith-Barnwell(8tap)	3.8391 (0.9937)	6.9786 (0.9813)	8.8489 (0.9577)
Most Regular(6tap)	3.7447 (0.9908)	6.7255 (0.9734)	8.4652 (0.9406)
Optimal QMF (8tap) *	3.8566 (0.9943)	7.0111 (0.9831)	8.8863 (0.9615)
Optimal QMF (8tap) **	3.8530 (0.9944)	6.9899 (0.9834)	8.8454 (0.9623)
Optimal QMF (6tap) *	3.7962 (0.9923)	6.8624 (0.9776)	8.6721 (0.9497)
Optimal QMF (6tap) **	3.7936 (0.9924)	6.8471 (0.9777)	8.6438 (0.9503)
Optimal QMF (4tap) *	3.6527 (0.9883)	6.4659 (0.9671)	8.0693 (0.9278)
Optimal QMF (4tap) **	3.6525 (0.9883)	6.4662 (0.9672)	8.0700 (0.9280)
Ideal Filter Bank	3.9458 (1.0000)	7.2379 (1.0000)	9.1587 (1.0000)

* Optimal QMF based on energy compaction (given in Chapter 7).

** Optimal QMF based on minimized aliasing energy (given in Chapter 7).

Table 6.2. Performance of several orthonormal signal decomposition techniques for Generalized Correlation source model given in Eq.(6.31).

	M=2 G_{TC} (NER)	M=4 G_{TC} (NER)	M=8 G_{TC} (NER)
DCT	3.2027 (0.9733)	5.7332 (0.9273)	7.6714 (0.8503)
DST	3.2027 (0.9733)	3.8836 (0.8458)	4.8638 (0.7138)
MHT	3.2027 (0.9733)	3.7401 (0.8241)	4.4011 (0.5843)
WHT	3.2027 (0.9733)	5.0582 (0.9253)	5.8865 (0.8405)
Binomial-QMF(4tap)	3.7724 (0.9879)	6.5636 (0.9633)	8.0087 (0.9123)
Binomial-QMF(6tap)	3.9241 (0.9913)	7.0011 (0.9728)	8.6688 (0.9332)
Binomial-QMF(8tap)	3.9915 (0.9929)	7.1851 (0.9773)	8.9449 (0.9439)
Smith-Barnwell(8tap)	4.0297 (0.9939)	7.2831 (0.9805)	9.0903 (0.9517)
Most Regular(6tap)	3.9055 (0.9909)	6.9465 (0.9716)	8.5847 (0.9306)
Optimal QMF (8tap) *	4.0489 (0.9945)	7.3171 (0.9822)	9.1279 (0.9558)
Optimal QMF (8tap) **	4.0455 (0.9945)	7.2954 (0.9825)	9.0869 (0.9567)
Optimal QMF (6tap) *	3.9699 (0.9924)	7.1231 (0.9762)	8.8521 (0.9418)
Optimal QMF (6tap) **	3.9680 (0.9925)	7.1113 (0.9764)	8.8318 (0.9425)
Optimal QMF (4tap) *	3.7895 (0.9883)	6.6200 (0.9646)	8.0960 (0.9152)
Optimal QMF (4tap) **	3.7894 (0.9883)	6.6205 (0.9647)	8.0970 (0.9154)
Ideal Filter Bank	4.1643 (1.0000)	7.5980 (1.0000)	9.4757 (1.0000)

Chapter 7

Optimal PR-QMF Design for Subband Image Coding

7.1 Introduction

2-band Perfect Reconstruction Quadrature Mirror Filters(PR-QMF) have been discussed in the previous chapters. Their modular nature leads to the hierarchical subband trees which have been widely used in the field. Additionally, it is shown that the 2-band PR-QMFs are the crucial components of the orthonormal wavelet basis design procedure.

This chapter deals with the optimal 2-band PR-QMF design problem. The approach taken here considers a set of design variables which are of great practical interest in image coding. Some of these variables have been considered earlier in the filter design field but this study uses them all simultaneously to obtain the optimal solutions.

Section 7.2. introduces the variables of optimization problem and their practical significance in image coding. It also discusses their mathematical definitions and lays the ground for the objective function of the optimization. Sections 7.3. and 7.4 look into two different sets of optimal PR-QMF design. Section 7.5 presents the optimal PR-QMF solutions for different scenarios considered and their comparative performance. The following section discusses the possible extensions of this

research and concludes the chapter.

7.2 Variables of Optimization and Their Significance in Image Processing

The proposed optimal PR-QMF design technique considers several parameters of practical significance in the filter design. These parameters, namely the energy compaction, aliasing energy, unit step response, zero mean high-pass filter, uncorrelated subband signals, constrained non-linear phase response, and input statistics are combined to define the objective function of the optimization problem. Some of these features have been well known in the filter design field and used by several researchers in the literature[66][67][68][69]. This study intuitively benefited from the earlier work in the field but also has significant novelty in the solution of PR-QMF problems particularly for image coding applications. We include the following variables in the design of optimal PR-QMFs:

● *Orthonormalty Requirement:* This set of requirements is included in the design to obtain the unitary perfect reconstruction condition which is of interest here. The orthonormal PR condition is important particularly in signal coding applications.

The high-pass filter is assumed to be the mirror of the low-pass filter $\{h(n)\}$ of length $2N$ which is also expressed in the vector form $\underline{h}$. Hence the unitary condition of the filter can easily be written in vector product form as

$$\underline{h}^T \underline{h} = 1 \qquad (7.1)$$

The perfect reconstruction condition of orthonormal 2-band PR-QMF is easily derived as

$$\sum_n h(n)h(n + 2k) = \delta(k) \qquad (7.2)$$

147

Eqs.(7.1) and (7.2) can be combined in the matrix form

$$\underline{h}^T C_i \underline{h} = 0 \qquad i = 1, 2, ..., N - 1 \tag{7.3}$$

where C_i are the proper *filter coefficient shuffling matrices* as

$$C_1 = \begin{bmatrix} 0 & 0 & 1 & 0 & ... & 0 \\ 0 & 0 & 0 & 1 & ... & 0 \\ 1 & 0 & 0 & 0 & ... & 0 \\ \cdot & \cdot & & & & \cdot \\ \cdot & \cdot & & & & \cdot \\ 0 & 0 & 1 & 0 & ... & 1 \\ 0 & 0 & 0 & 1 & ... & 0 \\ 0 & 0 & 0 & 0 & ... & 0 \end{bmatrix} , ..., \quad C_{N-1} = \begin{bmatrix} 0 & 0 & 0 & ... & 1 & 0 \\ 0 & 0 & 0 & ... & 0 & 1 \\ 0 & 0 & 0 & ... & 0 & 0 \\ 0 & 0 & 0 & ... & 0 & 0 \\ \cdot & \cdot & & & \cdot & \cdot \\ \cdot & \cdot & & & \cdot & \cdot \\ 1 & 0 & 0 & ... & 0 & 0 \\ 0 & 1 & 0 & ... & 0 & 0 \end{bmatrix} \tag{7.4}$$

Eq.(7.3) is satisfied as a part of the optimal filter solutions introduced later.

● *Energy Compaction:* This is a desired feature for any orthonormal signal decomposition technique. Energy compaction measure is derived with the help of the rate-distortion theory. The significance and the derivation of this measure can be found in reference[7]. This performance measure has been widely used in the literature for the comparison of different signal decomposition techniques[4].

The output energy of the low pass filter $h(n)$ for the given covariance matrix R_{xx} of a zero-mean input can be expressed as

$$\sigma_L^2 = \underline{h}^T R_{xx} \underline{h} \tag{7.5}$$

We are now looking for the optimal PR-QMF solution which maximizes Eq.(7.5). It is clear that this will be the sufficient condition to maximize the energy compaction measure, gain of transform coding over PCM(G_{TC}), which is given for the two-band case as

$$G_{TC} = \frac{\sigma_x^2}{(\sigma_L^2 \sigma_H^2)^{1/2}} = \frac{\sigma_x^2}{\sigma_L \sigma_H} \tag{7.6}$$

where the input signal variance is related to the band variances, σ_L^2 and σ_H^2, in the unitary case as

$$\sigma_x^2 = \frac{1}{2}(\sigma_L^2 + \sigma_H^2)$$

148

• *Aliasing Energy:* All of the orthonormal signal decomposition techniques satisfy the conditions of alias cancellation. In practice, since all the decomposition bands or coefficients are not used for the synthesis , or the different levels of quantization noise in subbands cause the non-cancelled aliasing energy components in the reconstructed signal. Its significance has been noticed particularly in image coding applications. It is known that the aliasing causes annoying patterns in encoded images at low bit-rates.

The aliasing energy component for the low-pass filter output in 2-band PR-QMF bank can be written for the given input spectral density function $S_{xx}(e^{j\omega})$[65]

$$\sigma_A^2 = \frac{1}{2\pi} \int_{-\pi}^{\pi} |H(e^{-j\omega})|^2 S_{xx}(e^{j(\omega+\pi)})|H(e^{j(\omega+\pi)})|^2 d\omega \qquad (7.7)$$

The time-domain counterpart of this relation is easily found as

$$\sigma_A^2 = \sum_k [\rho(n) * (-1)^n \rho(n)] R_{xx}(k) \qquad (7.8)$$

where $\rho(n)$ is the autocorrelation sequence of the filter coefficients $h(n)$ and defined as

$$\rho(n) = h(n) * h(-n)$$

$R_{xx}(k)$ is the autocorrelation sequence of the input. The optimal solution searched should minimize the aliasing energy component of the low-pass filter output as given in Eq.(7.8) in 2-band PR-QMF case.

Differently from the earlier design procedures in the literature, the aliasing energy is related to the spectral density function of the input rather than considering the deviations of the designed filter's frequency characteristics from the ideal filter.

• *Step Response:* The representation of edges in images is a crucial problem in image processing and coding. The edge structures are localized in time therefore they should be represented by the time-localized basis functions. Otherwise the ringing artifacts occur in encoded images. An edge can be considered as a step.

149

Therefore the step responses of the filters in the filter banks should be considered during the design procedure[66].

It is a well known phenomenon called the uncertainty principle which states that a signal can not be localized perfectly in one domain without the worst concentration in the other[35]. The human visual system is able to resolve the time-frequency plane therefore a joint time-frequency localization should be considered in a practically meritful filter bank design[69]. The trade-off between the time and frequency resolutions is also reflected in the aliasing and step response characteristics of the designed filters.

The unit step response of the filter $h(n)$ can be written as

$$a(n) = h(n) * u(n)$$

where $u(n)$ is the unit step sequence. The difference energy between the unit step response $a(n)$ of the filter and the unit step sequence $u(n)$ is expressed as

$$E_s = \sum_{k=0}^{2N-1} [\sum_{n=0}^{k} h(n) - 1]^2 \tag{7.9}$$

E_s is minimized for the optimal filter solution. The optimization variable E_s does not consider the symmetry of the unit step response around the step point. This point is addressed later since it is directly related to the linear phase condition of the desired filter.

• *Zero Mean High-Pass Filter:* Most of the practical signal sources have their significant energy located around the DC frequency. Therefore useful signal decomposition techniques should be able to represent the DC frequency component only within one basis function. Following this argument one should constrain the high-pass QMF function to have zero mean as

$$\sum_n (-1)^n h(n) = 0 \tag{7.10}$$

150

This requirement implies that there should be at least one zero of the low pass filter $h(n)$ at $\omega = \pi$.

• *Uncorrelated Subband Signals:* It is a well-known fact in signal coding field that any good signal representation technique should be able to provide uncorrelated transform coefficients or subband signals. The Karhunen-Loeve Transform(KLT)[7] is a typical example of this characteristic in the block transforms. Similarly the filter bank solutions under the constraints of this desired feature are sought in this study.

It is noteworthy to mention that the uncorrelatedness and the maximum energy compaction requirements merge in the KLT solutions of block transforms. But this is not true in filter banks.

The cross-correlation of the two subband signals for the given input is defined as

$$E\{y_L(m)y_H(m)\} = R_{LH}(0) = \sum_n [\sum_l h(l)(-1)^l h(n-l)]R_{xx}(n) \qquad \text{for all } m \quad (7.11)$$

There are more than one filter solutions which satisfy the condition $R_{LH}(0) = 0$. Obviously the one which maximizes the objective function is the meaningful solution.

• *Constrained Non-linearity in Phase Response:* Since there can not be any linear-phase orthonormal PR-QMF solution, the linearity condition on the phase responses of the filter functions is relaxed. Linear phase and PR are two conflicting conditions in orthonormal 2-band QMF design. But it is also known that the severe phase nonlinearities create undesired degradations in image and video applications. Therefore a measure which indicates the level of nonlinearity of the filter phase response is included as a parameter in the optimal filter design. Nonlinearity measure of the phase response is related to the non-symmetry of the

unit sample response and defined as

$$E_p = \sum_n [h(n) - h(2N - 1 - n)]^2 \qquad (7.12)$$

E_p is minimized in optimal filter solutions.

• *Given Input Statistics:* The characteristics of the input spectral density function are very important for the optimal filter design variables discussed earlier. Therefore the whole optimization procedure is related to the given input statistics. This will also lead to the input adaptive filter bank solutions which may be useful in some of the applications of the non-stationary sources. This study assumes an autoregressive, order 1, $AR(1)$ source model with the correlation coefficient $\rho = 0.95$ which is a crude approximation to the real world still frame images.

These variables of the optimization are included in the objective function and the set of constraints are considered. There are many filter bank solutions available based on different objective functions and parameter sets. We present the examples of objective functions to be optimized in the following two sections.

7.3   Optimal PR-QMFs

7.3.1   Optimal PR-QMF Design Based on Energy Compaction

This optimization problem consists of the PR and energy compaction conditions as defined in Eqs.(7.3) and (7.5), for an $AR(1)$ source with $\rho = 0.95$.

We now set the objective function J which is to be maximized as

$$J = \underline{h}^T R_{xx} \underline{h} + \lambda_0 [1 - \underline{h}^T \underline{h}] + \lambda_1 [\underline{h}^T C_1 \underline{h}] + \dots + \lambda_i [\underline{h}^T C_i \underline{h}] \qquad (7.13)$$

Hence,

$$\frac{\partial J}{\partial \underline{h}} = 0$$

therefore

$$R_{xx}\underline{h} + \lambda_1 C_1 \underline{h} + ... + \lambda_i C_i \underline{h} = \lambda_0 \underline{h} \tag{7.14}$$

If the terms in the left side of the equation are combined as

$$R\underline{h} = \lambda_0 \underline{h} \tag{7.15}$$

where

$$R = R_{xx} + \lambda_1 C_1 + ... + \lambda_i C_i$$

The vector $\underline{h}$ which satisfies Eq.(7.15) is the optimal PR-QMF low-pass filter.

7.3.2 Optimal PR-QMF Design Based on Extended Set of Variables

The aliasing energy, unit step response, constrained non-linear phase characteristics, zero-mean high-pass filter, uncorrelated subband considerations additional to Eq.(7.13) are included in the objective function. The optimization problem is now easily set as

$$\begin{aligned} J &= \underline{h}^T R_{xx} \underline{h} - \alpha \sum_k [\rho(n) * (-1)^n \rho(n)] R_{xx}(k) - \beta \sum_{k=0}^{2N-1} [\sum_{n=0}^{k} h(n) - 1]^2 \\ &\quad -\gamma \sum_n [h(n) - h(2N - 1 - n)]^2 \end{aligned} \tag{7.16}$$

with the set of unitary, PR, zero-mean high-pass filter, and uncorrelated subband signals constraints as

$$\sum_n h(n)h(n + 2k) = \delta(k)$$

153

$$\sum_n (-1)^n h(n) = 0$$

$$R_{LH}(0) = 0 \qquad\qquad (7.17)$$

This is a very general optimization problem. There are a set of parameters in the objective function which should be fine tuned for the application considered. Therefore the proposed optimal filter design approach should be supported with the experimental studies. The significance of the optimization variables in the objective function should be quantified for the human visual system. The following section presents examples of the optimal filters and their problem definitions.

7.4 Optimal PR-QMF Solutions and Their Performance

Since there is a set of parameters in the optimization problems defined earlier the possible filter solutions are many. Therefore we studied the interrelations of the optimization variables. In this framework we first attempt to relate the energy compaction and aliasing energy of the 2-band PR-QMF as defined in Eqs.(7.6) and (7.8) respectively. Fig. 7.1a displays this relation for 8-tap filer solutions and $AR(1)$ source with $\rho = 0.95$. As seen from the figure, this relation is linear-like and the energy compaction increases as the aliasing energy decreases. This trend is easily justified. The optimal PR-QMF solutions obtained are also consistent with this figure. Fig. 7.1b displays the relation of energy compaction and interband correlations again for the same source model. Although in block transforms these two variables merge in the unique optimal solutions, KLT, this is not true for the filter banks. In other words, there are more than one possible solutions. One should pick the solution which maximizes the objective function. Therefore the relations of uncorrelated interband and the energy compaction in filter banks are not as clear as in the block transforms. This point deserves further studies.

154

Fig. 7.1c shows the relations of 2-band energy compaction and the degree of nonlinearities in the phase responses of 8-tap filters.

Fig. 7.1d provides the relations of 2-band energy compaction and the imperfectness of filter unit-step responses. This plot indicates that whenever the unit-step response gets closer to the unit step function the energy compaction decreases. This relation clearly questions the practical merit of the energy compaction measure. Although the energy compaction may be optimal the subjective coding performance of the corresponding filter may not be necessarily optimal since its tracking of edges is not the best for image sources.

Table 7.1. provides the coefficients of 4, 6, 8, 12, and 16 tap optimal PR-QMFs based on energy compaction constraint. Similarly, Table 7.2. gives the optimal PR-QMF coefficients based on minimized aliasing energy . Table 7.3. and Table 7.4. has the zero-mean high pass constraint additional to the Table 7.1 and Table 7.2 respectively. Table 7.5. has the optimal PR-QMFs similar to Table 7.3. but additionally providing uncorrelated subbands or $R_{LH}(0) = 0$ for $AR(1)$ source with $\rho = 0.95$. Table 7.6. also adds this constraint to the conditions of Table 7.4.

Tables 7.7.a, b, c gives the optimal filters based on extended objective function of Eq.(7.16) with the weight variations of only the phase responses. Similarly, Tables 7.8.a, b, c provides the optimal filter coefficients with the weight variations only in the unit step response of Eq.(7.16). At last, Table 7.9. supply a set of PR-QMF filter coefficients based on energy compaction with different correlation functions. These solutions are obtained by using the software packages Mathematica and IMSL.

All of these Tables assume $AR(1)$ source of $\rho = 0.95$ and also include the performance of the filters presented for comparison.

155

7.5 Discussions

We have developed a framework in this chapter to design statistically optimized 2-band PR-QMFs suitable for subband image coding. This procedure considers the effects of the uncertainty principle of the time-frequency signal analysis. This is implicitly succeeded by considering the effects of the aliasing energy and the unit step response of the designed PR-QMFs for the given statistics.

The proposed PR-QMF solutions consider several practical parameters of image coding in the optimization problem. Therefore there are quite a few different filter solutions available with this approach. Therefore the parameters of the optimization should be tuned to the human visual system with the experimental studies for subjectively optimal PR-QMF solutions.

This approach somehow leads to the solutions of the input driven adaptive filter banks to overcome the difficulties of varying source characteristics in the non-stationary cases. It is seen that the statistically optimized PR-QMFs introduced in this chapter objectively perform better than the well-known PR-QMFs in the literature[17][18]. These filters should be incorporated in image, video processing and coding applications to prove their practical merits.

It should also be emphasized that some of the characteristics considered in the proposed optimized PR-QMF design procedure may not be significant in the 2-band case. But if a hierarchical subband tree structure based on 2-band PR-QMFs are created it is clearly observed that all of these characteristics become important. Therefore they all should be considered simultaneously in the design.

This approach can be extended to the $M-$band PR filter bank problem but as expected the procedure in that case is computationally quite complex for the larger values of M. This approach can also serve for the purpose of designing optimal compactly supported orthonormal wavelet transform bases which were dis-

cussed in Chapter 3.

n	h(n)	h(n)	h(n)	h(n)	h(n)
0	0.204212351	0.248070879	0.322844620	0.385659360	0.488485060
1	0.602581536	0.666509813	0.749222992	0.796281183	0.832218822
2	0.663204398	0.626640313	0.531149563	0.428145985	0.226198886
3	0.194273985	0.085288028	-0.061267577	-0.140851256	-0.132771300
4	-0.235011082	-0.251746902	-0.205510132	-0.106698546	
5	-0.151528819	-0.070668742	0.042673129	0.051676837	
6	0.120055833	0.134606123	0.061655714		
7	0.100225222	0.031174564	-0.026567812		
8	-0.075695486	-0.076826546			
9	-0.060939689	0.003537022			
10	0.053731391	0.028073733			
11	0.029632417	-0.010448872			
12	-0.038213006				
13	-0.002862284				
14	0.015950575				
15	-0.005405583				
G_{TC}	3.9222	3.9043	3.8565	3.7962	3.6526
σ_A^2	0.0056	0.0075	0.0113	0.0153	0.0234
$R_{LH}(0)$	0.0063	-0.1575	-0.0069	-0.0160	-0.0215
mean	0.0022	0.0034	0.0060	0.0000	0.0152
E_p	1.0616	1.0111	0.8542	1.2507	0.7532
E_s	3.3553	2.5679	1.7441	1.3059	0.8351

Table 7.1. A set of optimal PR-QMF filter coefficients and their performance.

The optimality is based on energy compaction.

n	h(n)	h(n)	h(n)	h(n)	h(n)
0	0.243659618	0.281523633	0.345040138	0.398655783	0.489209500
1	0.644059913	0.690896465	0.753694623	0.792728776	0.831649080
2	0.626170931	0.588844405	0.506545103	0.420459421	0.226466667
3	0.131446737	0.049708030	-0.065567763	-0.141949940	-0.133216819
4	-0.242318622	-0.247385008	-0.209739280	-0.112008481	
5	-0.120846194	-0.057696965	0.046502363	0.056328003	
6	0.130077143	0.138854841	0.069553743		
7	0.087002300	0.030435241	-0.031841857		
8	-0.084297240	-0.088626178			
9	-0.058280509	0.005881762			
10	0.062266297	0.036734185			
11	0.032963835	-0.014968294			
12	-0.050162203				
13	-0.002346194				
14	0.023824751				
15	-0.009013338				
G_{TC}	3.9191	3.9007	3.8530	3.7935	3.6425
σ_A^2	0.0054	0.0073	0.0112	0.0152	0.0234
$R_{LH}(0)$	0.0044	-0.1717	-0.0067	-0.0138	-0.0188
mean	0.0042	0.0057	0.0086	0.0000	0.0172
E_p	1.0506	0.9906	0.8425	1.2520	0.7536
E_s	3.2771	2.5138	1.7175	1.2930	0.8349

Table 7.2. A set of optimal PR-QMF filter coefficients and their performance.

The optimality is based on minimized aliasing energy.

n	h(n)	h(n)	h(n)	h(n)	h(n)
0	0.201087342	0.244206457	0.317976535	0.385659639	0.482962940
1	0.600007520	0.664513457	0.748898833	0.796281177	0.836516297
2	0.665259025	0.629717438	0.534939876	0.428145720	0.224143841
3	0.198773686	0.089423027	-0.058836349	-0.140851286	-0.129409515
4	-0.233790239	-0.251577216	-0.205817322	-0.106698578	
5	-0.153612998	-0.072467574	0.042523091	0.051676890	
6	0.118834741	0.134086583	0.060007692		
7	0.101350938	0.031916868	-0.025478793		
8	-0.074934374	-0.076499461			
9	-0.061434875	0.003706982			
10	0.053218300	0.027172980			
11	0.029837627	-0.009985979			
12	-0.037981695				
13	-0.002649357				
14	0.015413680				
15	-0.005165762				
G_{TC}	3.9220	3.9038	3.8548	3.7961	3.6426
σ_A^2	0.0056	0.0075	0.0115	0.0153	0.0239
$R_{LH}(0)$	0.0040	-0.1601	-0.0140	-0.0160	-0.0422
mean	0.0000	0.0000	0.0000	0.0000	0.0000
E_p	1.0622	1.0320	0.8566	1.2506	0.7500
E_s	3.3613	2.5730	1.7493	1.3059	0.8365

Table 7.3. A set of optimal PR-QMF filter coefficients and their performance.

The optimality is based on energy compaction with zero mean high-pass filter.

n	h(n)	h(n)	h(n)	h(n)	h(n)
0	0.239674169	0.276769143	0.339291195	0.398655794	0.482962940
1	0.641863878	0.689345705	0.753812779	0.792728512	0.836516297
2	0.628941341	0.592445147	0.510688095	0.420459801	0.224143841
3	0.136154317	0.054082233	-0.062731472	-0.141949922	-0.129409515
4	-0.241530316	-0.247471430	-0.210405609	-0.112008814	
5	-0.123175317	-0.059746881	0.046422128	0.056328191	
6	0.128959373	0.138373438	0.067533100		
7	0.088433853	0.031525301	-0.030396654		
8	-0.083586814	-0.088498729			
9	-0.058991180	0.006149179			
10	0.061697343	0.035489212			
11	0.033431236	-0.014248756			
12	-0.050042508				
13	-0.002023897				
14	0.022994193				
15	-0.008586110				
G_{TC}	3.9189	3.9002	3.8513	3.7935	3.6426
σ_A^2	0.0054	0.0073	0.0113	0.0152	0.02397
$R_{LH}(0)$	0.0001	-0.1849	-0.0170	-0.0138	-0.0422
mean	0.0000	0.0000	0.0000	0.0000	0.0000
E_p	1.0521	0.9933	0.8450	1.2520	0.7500
E_s	3.2836	2.5202	1.7232	1.2930	0.8365

Table 7.4. A set of optimal PR-QMF filter coefficients and their performance. The optimality is based on minimized aliasing energy with zero mean high-pass filter.

160

n	h(n)	h(n)	h(n)	h(n)	h(n)
0	0.224159871	-0.106117265	0.240118698	0.312656005	0.000000000
1	0.629151335	-0.041624773	0.688564034	0.754045521	0.707106781
2	0.642510825	0.444275957	0.638286732	0.543768338	0.707106781
3	0.158071546	0.761031030	0.017567002	-0.108851490	0.000000000
4	-0.240893371	0.427762258	-0.235301591	-0.149317562	
5	-0.133127916	-0.066013158	0.023295098	0.061912751	
6	0.128098122	-0.107784207	0.064002943		
7	0.090074845	0.085537312	- 0.022319352		
8	-0.081998711	0.051558425			
9	-0.055306473	-0.038422405			
10	0.058081519	-0.002588387			
11	0.026452620	0.006598776			
12	-0.040400680				
13	-0.001956582				
14	0.017549205				
15	-0.006252594				
G_{TC}	3.9207	3.8935	3.8408	3.7661	3.2025
σ_A^2	0.0055	0.0083	0.0126	0.0167	0.0487
$R_{LH}(0)$	0.0000	0.0000	0.0000	0.0000	0.0000
mean	0.0000	0.0000	0.0000	0.0000	0.0000
E_p	1.0531	0.8694	0.9011	1.3048	0.0000
E_s	3.3117	4.4123	1.8685	1.3968	1.4289

Table 7.5. A set of optimal PR-QMF filter coefficients and their performance. The optimality is based on energy compaction with zero mean high-pass and uncorrelated subband signals.

n	h(n)	h(n)	h(n)	h(n)	h(n)
0	0.240173769	-0.121396419	0.249509936	0.348319026	0.000000000
1	0.642454295	-0.035246082	0.688584306	0.758774508	0.707106781
2	0.628348271	0.467924401	0.632097530	0.510327483	0.707106781
3	0.135389521	0.751312762	0.015778256	-0.121232755	0.000000000
4	-0.241606760	0.412397276	-0.240993887	-0.151539728	
5	-0.122763195	-0.062892458	0.026838168	0.069565029	
6	0.129125126	-0.109012591	0.066493202		
7	0.088184458	0.093200632	- 0.024093948		
8	-0.083719165	0.059816603			
9	-0.058849491	-0.048300585			
10	0.061801498	-0.002622488			
11	0.033339516	0.009032511			
12	-0.050088120				
13	-0.002023074				
14	0.023072163				
15	-0.008625249				
G_{TC}	3.9188	3.8897	3.8399	3.7611	3.2025
σ_A^2	0.0054	0.0083	0.0126	0.0165	0.0487
$R_{LH}(0)$	0.0000	0.0000	0.0000	0.0000	0.0000
mean	0.0000	0.0000	0.0000	0.0000	0.0000
E_p	1.0518	0.8667	0.8941	1.3052	0.0000
E_s	3.2826	4.4280	1.8564	1.3539	1.4289

Table 7.6. A set of optimal PR-QMF filter coefficients and their performance.

The optimality is based on minimized aliasing energy with zero mean high-pass

and uncorrelated subband signals.

$\alpha = 0.5,\ \beta = 0.01,\ \gamma = 0.01$				
n	h(n)	h(n)	h(n)	h(n)	h(n)
0	0.349996497	0.360838504	0.377995233	0.442766931	0.466675669
1	0.731063819	0.744306049	0.768367237	0.805049213	0.840588657
2	0.505852096	0.490757098	0.462086554	0.352529377	0.240431112
3	-0.010803415	-0.036047928	-0.86013220	-0.146445561	-0.133481875
4	-0.229358399	-0.222383198	-0.194919256	-0.088189527	
5	-0.029975411	-0.005408341	0.055225994	0.048503129	
6	0.134362313	0.128127832	0.061944250		
7	0.026991307	0.000007678	- 0.030473229		
8	-0.089102151	-0.079675397			
9	-0.017502278	0.018522733			
10	0.062860841	0.029441941			
11	0.006564367	-0.014273411			
12	-0.045242724				
13	0.009260600				
14	0.017738308				
15	-0.008492207				
G_{TC}	3.8950	3.8809	3.8432	3.7829	3.6407
σ_A^2	0.0065	0.0080	0.0115	0.0158	0.0240
$R_{LH(0)}$	-0.0084	-0.2052	-0.0196	-0.01970	-0.0437
mean	0.0000	0.0000	0.0000	0.0000	0.0000
E_p	0.9859	0.9439	0.8432	1.2022	0.7303
E_s	3.1015	2.395	1.6745	1.2436	0.8503

Tables 7.7.a, b, c. Optimal PR-QMF filter solutions and their performance. The optimality is based on Eq.(7.16) and only the weight of the phase response variable is changed.

163

n	h(n)	h(n)	h(n)	h(n)	h(n)
		$\alpha = 0.5, \beta = 0.01, \gamma = 0.1$			
0	0.570782868	0.569472913	0.568917465	0.592766220	0.587090288
1	0.773403148	0.775299669	0.779977112	0.780949238	0.795662560
2	0.207871420	0.208282686	0.205671595	0.156911420	0.120016493
3	-0.101404580	-0.103659132	-0.112813827	-0.106155142	-0.088555779
4	-0.101233393	-0.101645713	-0.092613815	-0.042570859	
5	0.040562313	0.044417637	0.058274508	0.032312685	
6	0.064121473	0.064537457	0.025131536		
7	-0.022088292	-0.029119506	- 0.018331012		
8	-0.048700901	-0.045720022			
9	0.017118797	0.029114167			
10	0.039132815	0.012179460			
11	-0.015973034	-0.008946054			
12	-0.032702905				
13	0.021271073				
14	0.007835404				
15	-0.005782643				
G_{TC}	3.6246	3.6274	3.6272	3.5769	3.5554
σ_A^2	0.0216	0.0217	0.0224	0.0262	0.0283
$R_{LH}(0)$	-0.0083	-0.2195	-0.0171	-0.0149	-0.0274
mean	0.0000	0.0000	0.0000	0.0000	0.0000
E_p	0.9682	0.9580	0.9367	1.0614	0.9129
E_s	2.8281	2.1435	1.4567	1.0846	0.7413

$\alpha = 0.5$, $\beta = 0.01$, $\gamma = 0.5$				
n	h(n)	h(n)	h(n)	h(n)	h(n)
0	0.436459489	0.468918374	0.893161751	0.883792413	0.851141192
1	0.770165754	0.754465714	0.196575502	0.226143909	0.304498519
2	-0.210563240	-0.223237677	-0.055961409	-0.080641139	-0.144034410
3	0.076322596	-0.091820497	0.061848233	0.105611642	0.402608262
4	-0.015358635	-0.010004074	-0.047017781	-0.096044493	
5	-0.001475061	0.003575508	0.071219382	0.375351230	
6	0.007791289	0.042639010	-0.083075780		
7	-0.006978594	0.007741037	- 0.377463664		
8	0.013431262	0.116547022			
9	-0.002821529	0.043571171			
10	0.032517339	0.312244125			
11	0.011528011	-0.194067146			
12	0.105043470				
13	0.051791696				
14	0.337785806				
15	-0.191426092				
G_{TC}	1.3138	1.5253	1.5600	1.7714	2.1612
σ_A^2	0.3707	0.2724	0.2590	0.1979	0.1280
$R_{LH}(0)$	-0.2241	-0.3795	0.1232	0.0877	0.0478
mean	0.0000	0.0000	0.0000	0.0000	0.0000
E_p	0.6532	0.7087	0.3721	0.3970	0.4023
E_s	1.0674	1.0822	0.2193	0.2177	0.2180

165

n	$\alpha = 0.5,\ \beta = 0.01,\ \gamma = 0.00$				
	h(n)	h(n)	h(n)	h(n)	h(n)
0	-0.072118727	-0.140400385	0.338751710	0.414924083	0.450726782
1	0.032229491	-0.150338392	0.753050835	0.802108334	0.844019834
2	0.472159777	0.297817459	0.512178433	0.389177069	0.256379999
3	0.728661982	0.716925775	-0.062729040	-0.145175948	-0.136913053
4	0.412106727	0.562813589	-0.210590019	-0.096994371	
5	-0.089723281	0.074485419	0.046819239	0.050174395	
6	-0.180228443	-0.101597229	0.066766657		
7	0.058425583	0.069475983	- 0.030034253		
8	0.122112963	0.120498364			
9	-0.041446572	-0.033350030			
10	-0.076759955	-0.032025017			
11	0.044183696	0.029908027			
12	0.028424519				
13	-0.028379044				
14	0.001409920				
15	0.003154926				
G_{TC}	3.9135	3.8988	3.8516	3.7928	3.6357
σ_A^2	0.0060	0.0073	0.0113	0.0154	0.0243
$R_{LH}(0)$	-0.0049	0.0412	-0.0165	-0.0183	-0.0450
mean	0.0000	0.0000	0.0000	0.0000	0.0000
E_p	0.9063	0.7827	0.8454	1.2269	0.6906
E_s	4.7944	5.1120	1.7241	1.2735	0.8638

Tables 7.8.a, b, c. Optimal PR-QMF filter solutions and their performance. The optimality is based on Eq.(7.16) and only the weight of the step response variable is changed.

	$\alpha = 0.5$, $\beta = 0.1$, $\gamma = 0.00$				
n	h(n)	h(n)	h(n)	h(n)	h(n)
0	0.051858566	-0.055559533	0.377668686	0.531436244	0.000000000
1	0.380482562	0.289422202	0.749142516	0.825711921	0.707106760
2	0.712802256	0.758607778	0.474281619	0.155148903	0.707106760
3	0.420775226	0.396381623	-0.055253895	-0.105397216	0.000000000
4	-0.081862324	-0.027600992	-0.234063349	0.020521635	
5	-0.052470327	0.175485587	0.058196964	-0.013207924	
6	0.067027296	0.059980247	0.089219826		
7	-0.0159621296	-0.326344975	- 0.044978804		
8	-0.071890824	0.033259598			
9	0.240675222	0.183983737			
10	0.024453215	-0.061580317			
11	0.0220059481	-0.011821393			
12	0.059265979				
13	0.085890240				
14	-0.054547383				
15	0.007434635				
G_{TC}	3.5895	3.3675	3.8112	3.5753	3.2025
σ_A^2	0.0174	0.0255	0.0124	0.0275	0.0487
$R_{LH}(0)$	0.0120	-0.0422	-0.0199	-0.0414	0.0000
mean	0.0000	0.0000	0.0000	0.0000	0.0000
E_p	0.7792	0.6897	0.8192	1.0128	0.0000
E_s	3.7582	3.3832	1.6791	1.1293	1.4289

n	h(n)	h(n)	h(n)	h(n)	h(n)
			$\alpha = 0.5$, $\beta = 0.5$, $\gamma = 0.00$		
0	-0.036394166	0.009777307	0.000000000	0.000000000	0.000000000
1	-0.010653820	0.009950661	0.707106760	0.707106760	0.707106760
2	0.120319736	0.009163096	0.000000000	0.000000000	0.707106760
3	0.018782806	-0.100904704	0.000000000	0.000000000	0.000000000
4	-0.284341438	0.114277633	0.000000000	0.707106760	
5	0.071695457	0.689177732	0.000000000	0.000000000	
6	0.546197426	0.687908298	0.707106760		
7	0.315291373	0.111809215	0.000000000		
8	0.326491983	-0.124581108			
9	0.530216883	0.007451436			
10	0.065344861	0.010561555			
11	-0.314416472	-0.010377558			
12	-0.028986451				
13	0.090980470				
14	-0.001525171				
15	0.005210085				
G_{TC}	3.4726	3.8163	1.5786	1.9429	3.2025
σ_A^2	0.174	0.0140	0.2006	0.1324	0.0487
$R_{LH}(0)$	0.0103	-0.0057	0.0000	0.0000	0.0000
mean	0.0000	0.0000	0.0000	0.0000	0.0000
E_p	0.0062	0.0009	0.0000	0.0000	0.000
E_s	8.4601	6.1696	1.7720	1.6005	1.4289

n	h(n) $\rho = 0.95$	h(n) $\rho = 0.85$	h(n) $\rho = 0.75$	h(n) $\rho = 0.5$
0	0.204212351	0.212661977	0.221143926	0.241189375
1	0.602581536	0.609547980	0.616246293	0.630923075
2	0.663204398	0.657327191	0.651243556	0.636196501
3	0.194273985	0.182280121	0.170522287	0.143871630
4	-0.235011082	-0.238168040	-0.240972596	-0.246239979
5	-0.151528819	-0.145729509	-0.139937253	-0.126439416
6	0.120055833	0.123102211	0.125939612	0.131810655
7	0.100225222	0.097266163	0.094287141	0.087264071
8	-0.075695486	-0.077797447	-0.079792850	-0.084076242
9	-0.060939689	-0.059502013	-0.058060644	-0.054691151
10	0.053731391	0.054992787	0.056219689	0.058988403
11	0.029632417	0.029236347	0.028856692	0.028029712
12	-0.038213006	-0.038988911	-0.039794727	-0.041822297
13	-0.002862284	-0.003393977	-0.003933441	-0.005213122
14	0.015950575	0.017449360	0.019022659	0.023014860
15	-0.005405583	-0.006087815	-0.006826404	-0.008798124
G_{TC}	3.9222	2.2494	1.7355	1.2351
σ_A^2	0.0056	0.0075	0.0113	0.0153
$R_{LH}(0)$	0.0063	-0.1575	-0.0069	-0.0160
mean	0.0022	0.0034	0.0060	0.0000
E_p	1.0616	1.0111	0.8542	1.2507
E_s	3.3553	2.5679	1.7441	1.3059

Table 7.9. A set of optimal PR-QMF filter coefficients and their performance. The optimality is based on energy compaction with different correlation functions.
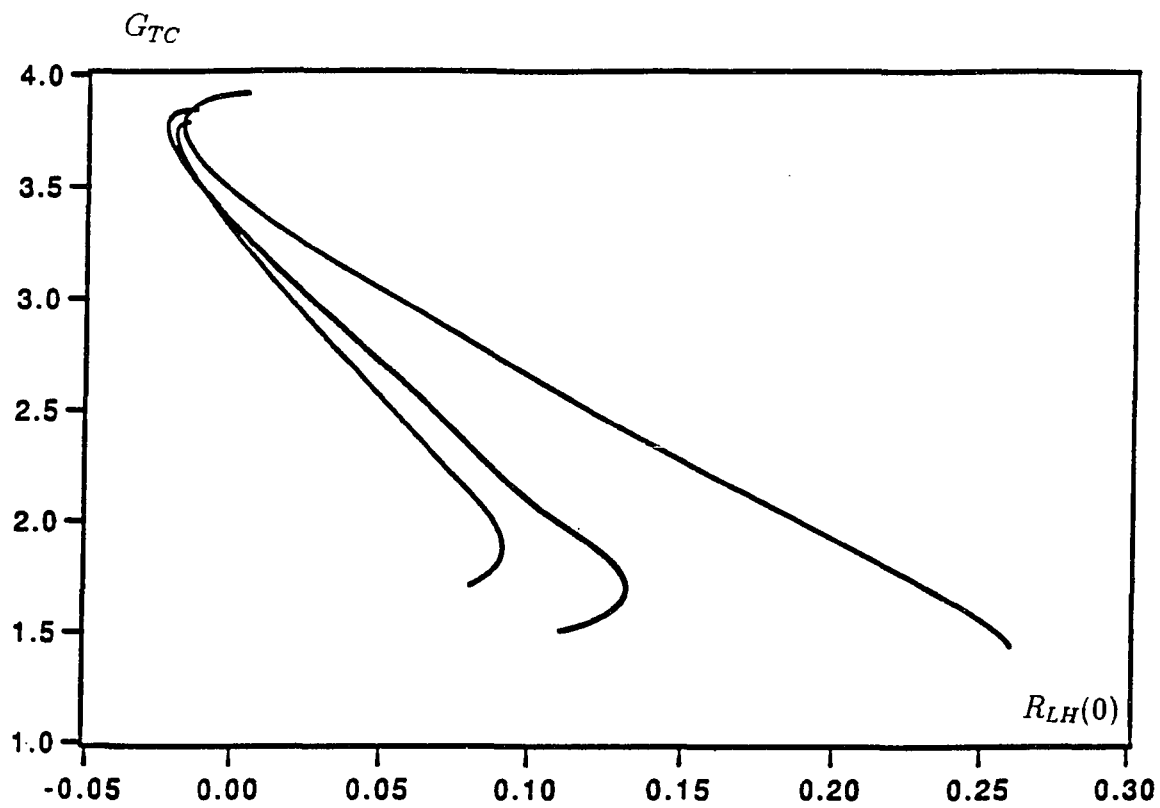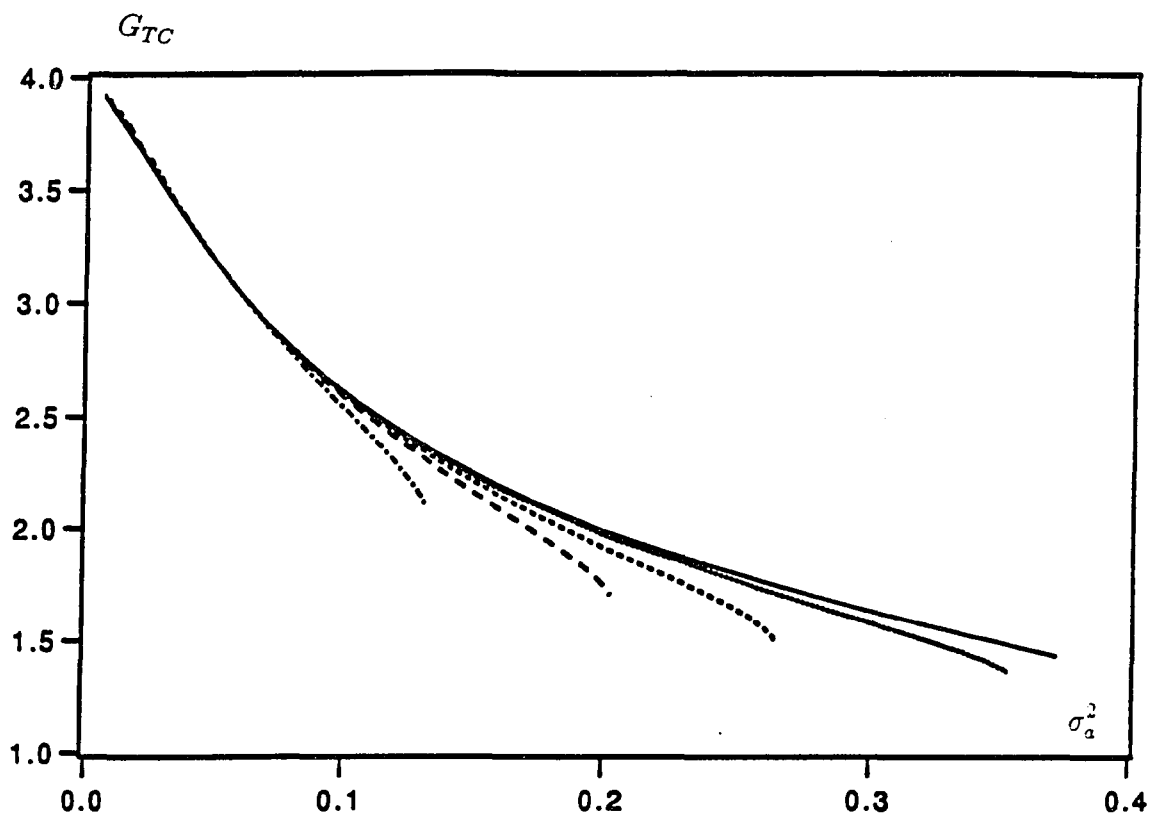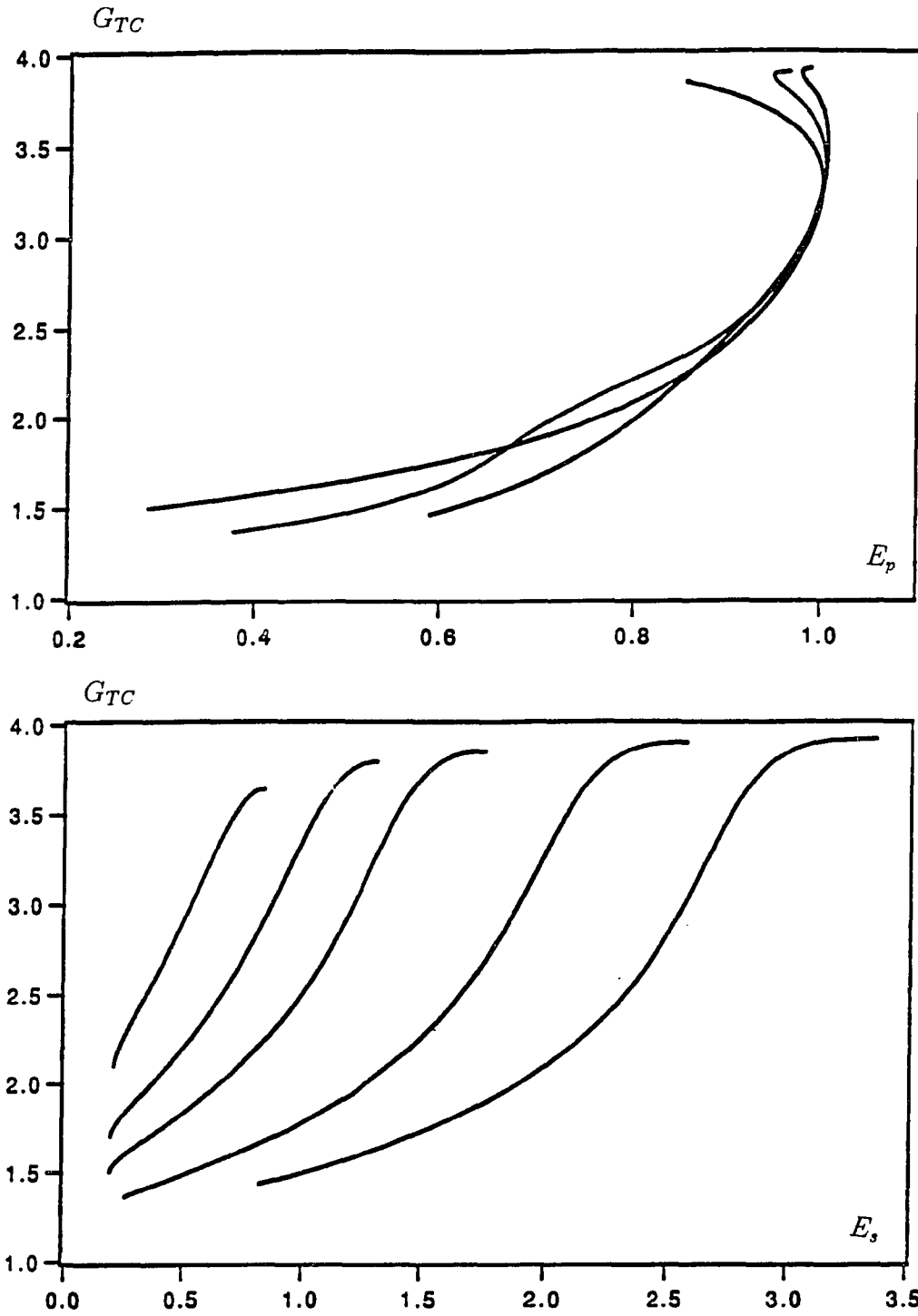
Fig. 7.1. The relations of a) G_{TC} vs σ_a^2 for $N = 16, 12, 8, 6, 4$ b) G_{TC} vs $R_{LH}(0)$

for $N = 16, 8, 6$ c) G_{TC} vs E_p for $N = 16, 12, 8$ d) G_{TC} vs E_s for $N = 16, 12, 8, 6, 4$

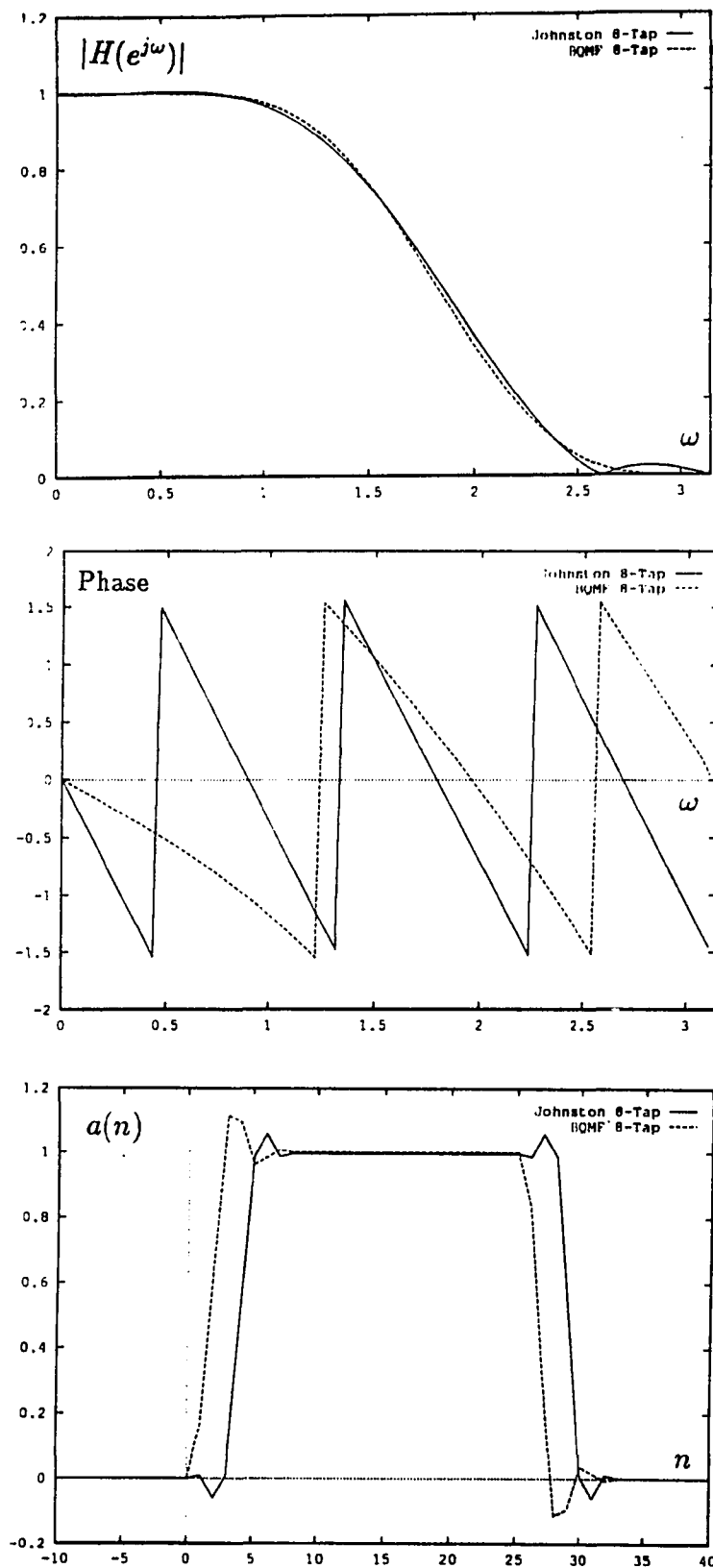of 8-tap 2 band PR-QMFs for AR(1), $\rho = 0.95$ source.

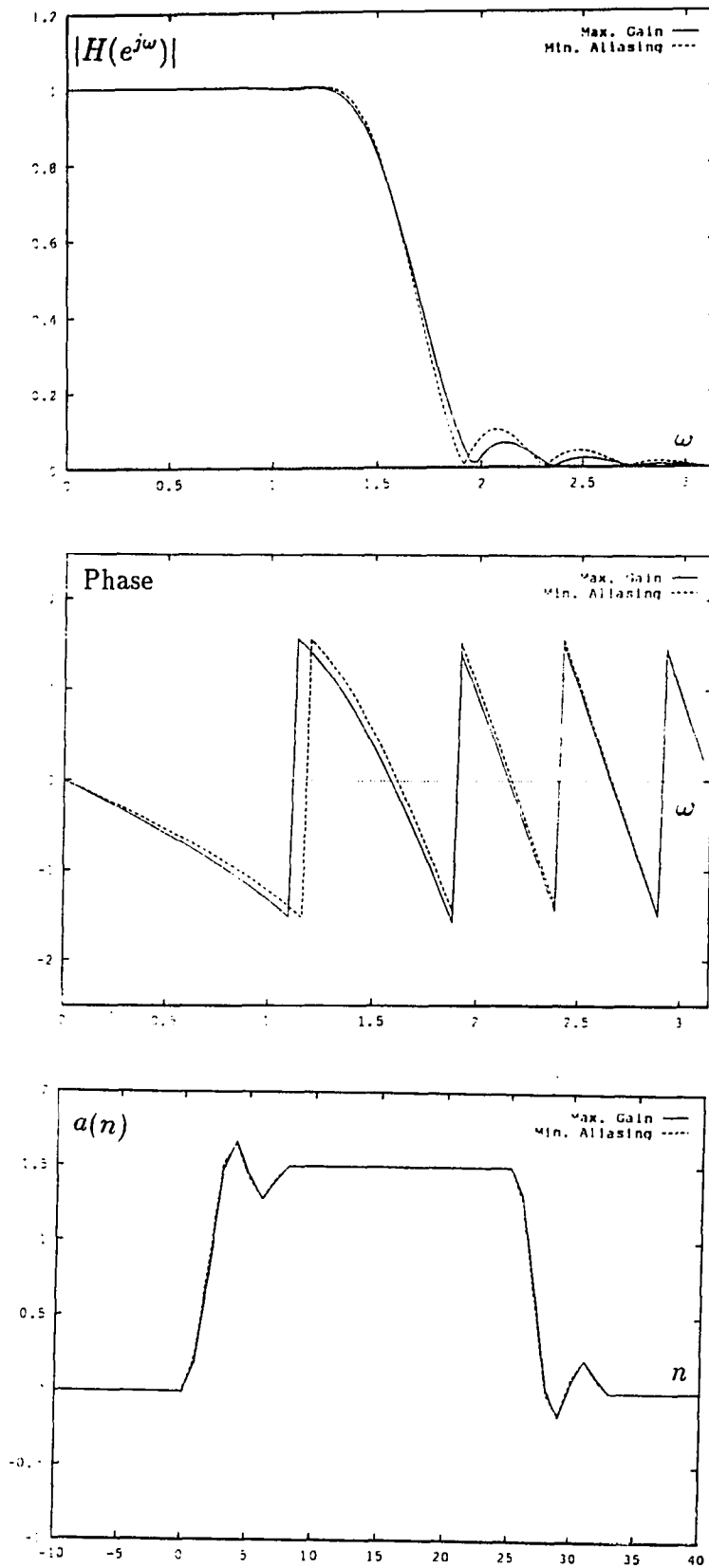Fig. 7.2 Magnitude, phase, and step responses of BQMF and Johnston's 8-tap

filters

Fig. 7.3 Magnitude, phase, and step responses of Max. Gain and Min. Aliasing solutions with zero mean high-pass filter constraintfor N=16.
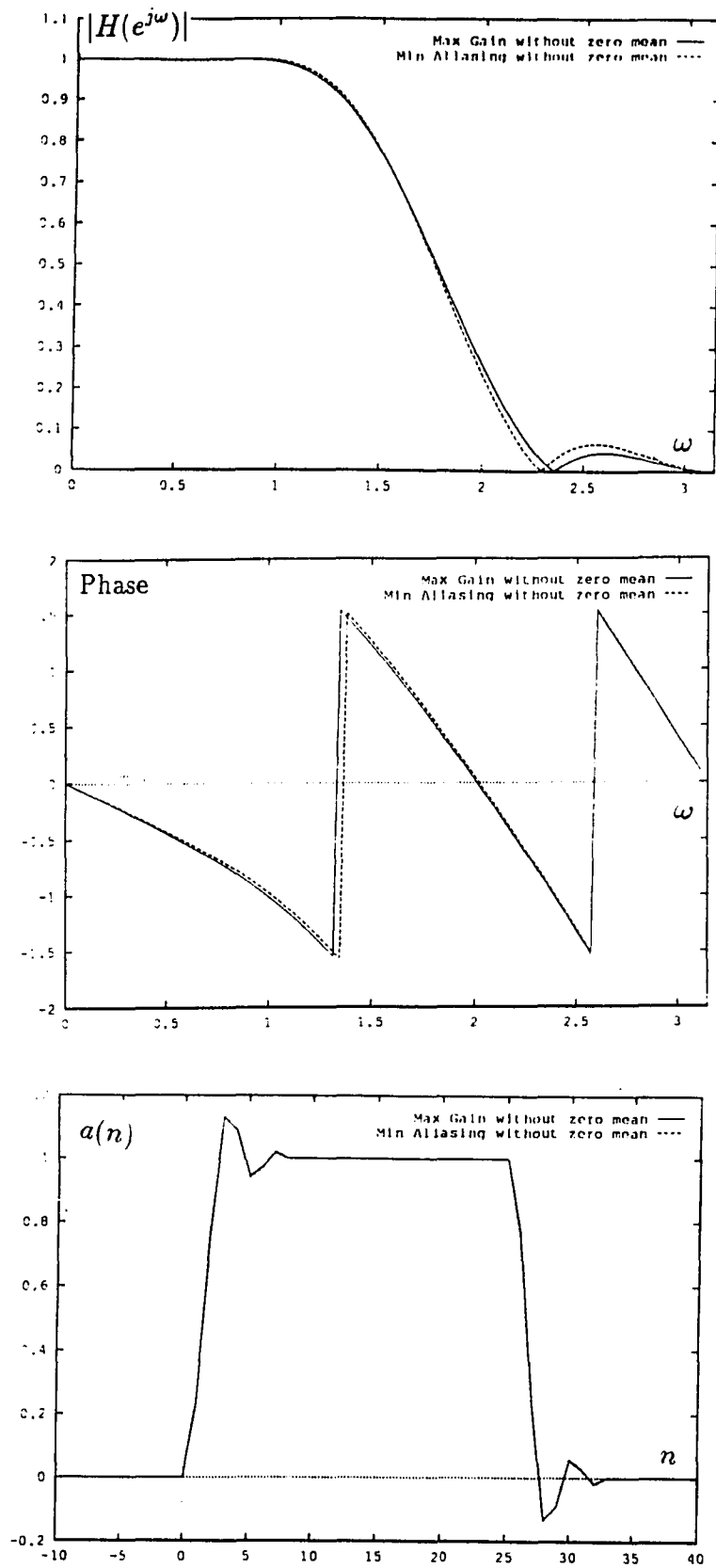
Fig. 7.4 Magnitude. phase. and step responses of Max. Gain and Min. Aliasing

solutions without zero mean high-pass filter constraint for N=8.

Chapter 8

Conclusions and Discussions for Future Research

The main contributions of this dissertation can be highlighted as the following :

- *Binomial-QMF:* The motivation of this study was simple, multiplier free structure of Binomial Network which was proposed by Haddad in 1971. We used the Binomial basis of smooth functions to design Perfect Reconstruction Quadrature Mirror Filter bank(PR-QMF). Interestingly enough, it is found that these filter are identical to the orthonormal wavelet transform inter scale coefficients or filters proposed by Daubechies. We have also shown first in the literature the connections of the celebrated works by Herrmann, 1971 and Daubechies 1988. It is shown that Binomial-QMF has the unique maximally flat function as its magnitude square.

- *2-band PR-QMF Bank Design Based on Bernstein Polynomial Approximation:* Our studies of Bernstein polynomials provided the insights about this smooth function family. We used this notion to generate smooth magnitude square functions of 2-band PR filter banks. This part of our studies introduced the old polynomial approximation concept into the PR filter bank design theory. This work yielded the connections of approximation parameters

and behavior of the designed filters. This is a generalized, parametric, filter bank design approach. As the specific examples of this technique, we have derived the popular wavelet filter proposed in the literature. This technique provides new insights for the design of filter bank and wavelet bases.

- *Non-Aliasing Energy Ration (NER):* The theoretical performance studies on orthonormal transforms predict that the performance increases, with the number of subbands or transform size. But, it is also well known that this prediction does not match with the applications performance. Therefore the practical merits of energy compaction measure should be examined more carefully. This observed mismatch has more than one reasons. We looked at the effects of aliasing energy in a multiresolution analysis/synthesis structure. Our results with this new performance measure, NER, follows the trend of experimental results. This new measure complements the commonly used energy compaction measure.

- *Optimal 2-band PR-QMF Design :* The block transforms have the duration of transform basis functions equal to the number of subbands or transform size. Therefore their freedom for tuning the basis is very limited. Indeed, The optimal block transforms KLT is a unique solutions of best possible energy compaction and uncorrelated coefficients for the given source statistics. The theory proves that general filter bank solution have many degrees of freedom available for the design purposes. Our motivation for this part of study is based on this simple concept. Therefore, we can considered the requirements of a meaningful basis or filter behaviors, in time as well as in frequency in the design procedure. We did not limit ourselves on the optimization of joint time-frequency localization. It is too abstract. We broke down that concept into its components which are considered simultaneously in the design of

176

filter banks. The interrelations of these components are displayed. The best possible 2-band PR-QMFs are derived for the given source and the measure. This work is the filter bank counterpart of KLT in block transforms. It is expected that this design approach will be heavily used for Image-Video processing applications in the near future.

- Our theoretical studies always supported with objective performance results to provide the merits of the present work. It is depicted that there are superior filter bank solutions over the existing block transforms based signal decomposition techniques like Discrete Cosine Transform (DCT).

Based on our studies and experience in the field of signal decomposition we will now address few possible extension of this dissertation for future research. We can summarize these as following:

- VLSI implementation of Binomial-QMF banks.

- Extension of Bernstein polynomial approximation based PR-QMF design to M equal and unequal bandwidth case.

- Connect the proposed parametric filter bank design technique with the design of orthonormal wavelet bases.

- Subjectively spectral splitting of image-video spectra to define the subband structure to be designed.

- More studies on the criteria employed in optimal PR-QMF bank design.

- More studies on the objective performance measure of signal decomposition techniques.

- Extensions of optimal 2-band PR-QMF approach to M-band case.

It should be concluded that the filter bank design problem should be related with the requirements of the applications side to yield practically superior solution to the industry standard block transforms.

Appendix A

Lemma 1.1 A set of functions $\phi(., -n)$ form an orthonormal family if and only if their Fourier transform satisfy[39],

$$\sum_k |\Phi(\Omega + 2\pi k)|^2 = 1 \tag{A.1}$$

Proof: Since $\{\phi(t - n); n \in Z\}$ is orthonormal family then they should satisfy

$$||f||^2 = \sum_n |\alpha(n)|^2 \tag{A.2}$$

then we can expand the $f(t)$ in orthogonal family as

$$f(t) = \sum_n \alpha(n)\phi(t - n) = \phi(t) * \sum_n \alpha(n)\delta(t - n) \tag{A.3}$$

this relation in Fourier domain becomes

$$F(\Omega) = \Phi(\Omega) \sum_n \alpha(n)e^{-j\Omega n} \tag{A.4}$$

by defining 2π periodic function

$$M(\Omega) = \sum_n \alpha(n)e^{-j\Omega n}$$

this relation becomes

$$F(\Omega) = \Phi(\Omega)M(\Omega) \tag{A.5}$$

Therefore from Parseval relation

$$\int_{-\infty}^{\infty} |f(t)|^2 dt = \frac{1}{2\pi} \int_{-\infty}^{\infty} |F(\Omega)|^2 d\Omega$$

179

$$= \frac{1}{2\pi} \int_{-\infty}^{\infty} |\Phi(\Omega)|^2 |M(\Omega)|^2 d\Omega$$

$$= \frac{1}{2\pi} \sum_{n=-\infty}^{\infty} \int_{2\pi n}^{2\pi(n-1)} |\Phi(\Omega)|^2 |M(\Omega)|^2 d\Omega$$

$$= \frac{1}{2\pi} \sum_{n=-\infty}^{\infty} \int_{0}^{2\pi} |M(\Omega)|^2 |\Phi(\Omega + 2\pi n)|^2 d\Omega$$

$$= \frac{1}{2\pi} \int_{0}^{2\pi} |M(\Omega)|^2 \sum_{n=-\infty}^{\infty} |\Phi(\Omega + 2\pi n)|^2 d\Omega \qquad (A.6)$$

From Eq.(A.2) we have

$$\int_{-\infty}^{\infty} |f(t)|^2 dt = \sum_{n} |\alpha(n)|^2$$

$$= \frac{1}{2\pi} \int_{0}^{2\pi} |M(\Omega)|^2 d\Omega$$

Therefore, $\phi(t)$ must satisfy

$$\sum_{n} |\Phi(\Omega + 2\pi n)|^2 = 1$$

Bibliography

[1] R. E. Crochiere, S.A.Weber, and J.L. Flanagan, *"Digital Coding of Speech Subbands,"* Bell Syst. Tech. J., Vol.55, pp.1069-1085, 1976.

[2] D. Esteban and C. Galand, *"Application of Quadrature Mirror Filters to Split-band Voice Coding Schemes,"* Proc. ICASSP, pp.191-195, May 1977.

[3] A. Croisier, D. Esteban, and C. Galand, *"Perfect Channel Splitting by use of Interpolation/Decimation/Tree Decomposition Techniques,"* Int'l Conf. on Information Sciences and Systems, Patras, 1976.

[4] M. Vetterli, *"Multi-dimensional Sub-band Coding: Some Theory and Algoithms,"* Signal Processing, pp.97-112, 1984

[5] J.W. Woods, S.D. O'Neil, *"Subband Coding of Images,"* IEEE Trans. ASSP, ASSP-34, No.5, Oct. 1986

[6] H. Gharavi and A. Tabatabai, *"Subband Coding of Digital Image Using Two-Dimensional Quadrature Mirror Filtering,"* Proc. SPIE, Vol.707, pp.51-61, Sept. 1986.

[7] N.S. Jayant and P. Noll, *"Digital Coding of Waveforms,"* Prentice Hall Inc., Englewood Cliffs, New Jersey, 1984.

[8] R.E. Crochiere and L.R. Rabiner, *"Interpolation and Decimation of Digital Signals: A Tutorial Review,"* Proc. IEEE, Vol.69, pp.300-331, Mar. 1981.

[9] R.E. Crochiere and L.R. Rabiner, *"Multirate Digital Signal Processing,"* Englewood Cliffs, NJ Prentice Hall, 1983.

[10] P.P. Vaidyanathan, *"Quadrature Mirror Filter Banks, M-Band Extensions and Perfect Reconstruction Techniques,"* IEEE ASSP pp.4-20 July 1987.

[11] P.P. Vaidyanathan, *"Multirate Digital Filters, Filter Banks, Polyphase Networks, and Applications: A Tutorial,"* Proc. of the IEEE Vol.78, No.1, pp.56-93, Jan. 1990.

[12] M. Bellanger, G. Bonnerot, and M. Coudreuse, *"Digital Filtering by Polyphase Network: Application to Sample Rate Alteration and Filter Banks,"* IEEE Trans. ASSP Vol.24, pp.109-114 Apr. 1976.

[13] M. Smith, and T.P. Barnwell, *"Exact Reconstruction Techniques for Tree-Structured Subband Coders,"* IEEE Trans. ASSP, pp.434-441, 1986.

[14] P.P. Vaidyanathan et. al., *"Improved Technique for Design of Perfect Reconstruction FIR QMF Banks with Lossless Polyhase Matrices,"* IEEE Trans. ASSP, pp.1042-1056, July 1989.

[15] F. Mintzer, *"Filters for Distortion-free Two-band Multirate Filter Banks,"* IEEE Trans. ASSP, vol.33, pp. 626-630, June, 1985.

[16] T.Q. Nguyen and P.P. Vaidyanathan *"Maximally Decimated Perfect Reconstruction FIR Filter Banks with Pairwise Mirror-Image Analysis and Synthesis Frequency Responses,"* IEEE Trans. in ASSP 36(5) pp.693-706 May 1988.

[17] A.N. Akansu, R.A. Haddad, and H. Caglar, *" The Binomial QMF-Wavelet Transform for Multiresolution Signal Decomposition,"* Submitted to IEEE Trans. ASSP.

[18] J.D. Johnston, "A Filter Family Designed for Use in Quadrature Mirror Filter Banks," in Proc. IEEE Int. Conf. ASSP, pp.291-294, Apr. 1980.

[19] V.K. Jain and R.E. Crochiere, " Quadrature Mirror Filter Design in the Time Domain," IEEE Trans. ASSP Proc., Vol.32, pp.353-361, Apr. 1984

[20] K. Swaminathan and P.P. Vaidyanathan, "Theory and Design of Uniform DFT, Parallel Quadrature Mirror Filter Banks," IEEE Trans. Circuits, Syst. Vol.33 pp.1170-1191, Dec. 1986.

[21] R. Ansari and B. Liu, "A Class of Low-Noise Computatinally Effecient Recursive Digital Filters with Applications to Sampling Rate Alterations," IEEE Trans. ASSP, Vol. pp.90-97 Feb. 1985.

[22] P.P. Vaidyanatan, P. Regalia and S.K. Mitra, "Design of Doubly Complementary IIR Digital Filters Using a Single Complex Allpass Filter, with Multirate Applications," IEEE Trans. on Circuits and Systems, Vol.34, Apr. 1987.

[23] T.A. Ramstad, "IIR Filter Bank for Subband Coding of Images," Proc. ISCAS, Helsinki, pp. 827-830, 1988.

[24] R. Ansari "Two Dimensional IIR Filters for Exact Reconstruction in Tree Structured Subband Decomposition", Electronics Letters, 23(12):633-634, June 1987.

[25] M. Vetterli, "Wavelets and Filter Banks for Discrete-Time Signal Processing," To appear in Wavelets and Their Applications, R. Coifman et al. ed., Jones and Bartlett 1991.

[26] M. Vetterli and C. Herley "Wavelet and Filter Banks: Relationships and New Results," in Proc. IEEE Int. Conf. ASSP, pp.1723-1726 May 1991.

[27] T.Q Nguyen and P.P. Vaidyanatan, *"Two Channel Perfect Reconstruction FIR QMF Structures Which Yield Linear Phase Analysis and Synthesis Filters,"* IEEE ASSP Vol.37, pp.676-690, May. 1989.

[28] R. Ansari, C. Guillemont, and J.F. Kaiser, *Wavelet construction Using Lagrange Halfband Filters,"* IEEE Trans. on Circuits and Systems, Vol.38, pp.1116-1118, Sept. 1991.

[29] M. Vetterli and C. Hertley, *"Wavelets and Filter Banks: Theory and Design,"* To appear IEEE Trans. on Signal Processing 1992

[30] P.P. Vaidyanathan, *"Robuts Digital Filters and Multirate Filter Banks"* To be pullished by Prentice Hall, 1991.

[31] P.P. Vaidyanathan and Z. Doganata, *"The Role of Lossless Systems in Modern Digital Signal Processing: A Tutorial,"* IEEE Trans. Education 32(3):181-197, August 1989.

[32] P.H. Westerink, *"Subband Coding of Images,"* Ph.D Thesis, Delft University, 1989.

[33] P.J. Burt, and E.H. Adelson, *"The Laplacian Pyramid as a Compact Image Code,"* IEEE Trans. Comm., pp.532-540, April 1983.

[34] R. Bracewell, "The Fourier Transform and Its Applications," Mc-Graw-Hill, New-York, 1965.

[35] D. Gabor, *"Theory of Communication,"* J. of the IEE Vol.29, pp.429-457

[36] C.W. Kim and R. Ansari, *"FIR/IIR Exact Reconstruction Filter Banks with Applications to Subband Coding of Images,* Proc. Midwest Circuits and Systems Symposium, May 1991.

[37] S.G. Mallat. "*A Theory for Multiresolution Signal Decomposition: The Wavelet Representation.*" MS-CIS-87-22. GRASP Lab.103. Univ. of Pennsylvania. May 1987.

[38] S.G. Mallat. "*Multifrequency Channel Decomposition of Images and Wavelet Models.*" IEEE Trans. ASSP. pp.2091-2110. Dec. 1989.

[39] S.G. Mallat. "*Time-Frequency Representation and Wavelet Transforms.*" Course Notes at NYU 1991.

[40] I. Daubechies. "*Orthonormal Bases of Compactly Supported Wavelets.*" Comm. on Pure and Applied Math.. vol. XLI. pp.909-996. 1988.

[41] I. Daubechies. "*The Wavelet Transform. Time-Frequency Localization and Signal Analysis.*" IEEE Trans. Information Theory. Vol.36. pp.961-1005. sept. 1990.

[42] J.O. Stromberg. "*A Modified Franklin System and Higher Order Spline Systems on R^n as Unconditional Bases for Hardy Spaces.*" Conf. in honor of A. Zygmund. Vol.II. pp.475-493. ed. W.Beckner.

[43] Y. Meyer. "*Principle Dincertitude. Bases Hilbertiennes et Algébres Dopérateurs.*" Séminaire Bourbaki 1985-1986.

[44] G. Battle. "*A Block Spin Construction of Ondelettes. Part:I Lemarié Functions.*" Comm. Math. Phsy. pp.601-615 1985.

[45] P.G. Lemarié. "*Une Nouvelle Base Dondelettes de $L^2(R^n)$*". To be published in J. de Math. Pures et Appl.

[46] I. Daubechies. "*Orthonormal Bases of Compactly Supported Wavelets. II. Variations on a Theme.*" preprint.

185

[47] A. Cohen and I. Daubechies, *"Orthonormal Bases of Compactly Supported Wavelets. III. Better Frequency Resolution,"* preprint.

[48] I. Daubechies, Private Communication.

[49] R.A. Gopinath *"The Wavelet Transform and Time-Scale Analysis of Signals,"* M.S. Thesis Rice University, Jan. 1990.

[50] J.M. Combes et al., ed., *"Wavelets, Time-Frequency Methods and Phase Space,"* New york NY, Springer-Verlag 1989. Lecture Notes on IPTI.

[51] M. Antonini, M. Barlaud, P. Mathieu, I. Daubechies, *"Image Coding Using Vector Quantization in the Wavelet Transform Domain,"* Proc. ICASSP, pp. 2297-2300, 1990

[52] R. Coifman and Y. Meyer, *"Orthonormal Wave Packet Bases",* Yale University preprint, 1990.

[53] O. Rioul, *"A Discrete-Time Multiresolution Theory Unifying Octave-band Filter Banks, Pyramid and Wavelet Transforms",* Submitted to IEEE Trans. ASSP 1990.

[54] R.A. Haddad, *"A Class of Orthogonal Nonrecursive Binomial Filters,"* IEEE Trans. Audio and Electroacoustics, pp.296-304, Dec. 1971.

[55] R.A. Haddad, and B. Nichol, *"Efficient Filtering of Images Using Binomial Sequences,"* Proc. ICASSP, 18.M4.7. May 1989.

[56] R. A. Haddad and A.N. Akansu, *"A New Orthogonal Transform for Signal Coding,"* IEEE Trans. ASSP, pp.1404-1411, Sept. 1988.

[57] G. Sansone, *"Orthogonal Functions,"* New York: Wiley-Interscience, 1959.

[58] R.A. Haddad and A.N. Akansu, "*A Class of Fast Gaussian Binomial Filters for Speech and Image Processing,*" To appear in IEEE Trans. ASSP.

[59] O. Herrmann, "*On the Approximation Problem in Nonrecursive Digital Filter Design,*" IEEE Trans. Circuit Theory, Vol.CT-18, No.3, pp. 411-413, May, 1971.

[60] P. J. Davis, "*Interpolation and Approximation,*" Ginn-Blaisdell, 1963.

[61] J.A. Miller, "*Maximally Flat Nonrecursive Digital Filters,*" Electronics Letters, Vol.8, No.6, pp.157-158, March 1972.

[62] L.R. Rajagopaland, S.C. Dutta Roy, "*Design of Maximally Flat FIR Filters Using the Bernstein Polynomial,*" IEEE Trans. Circuits and Systems, Vol.CAS-34, No.12, pp.1587-1590, Dec. 1987.

[63] H. Caglar and A. N. Akansu, "*Generalized, Parametric PR-QMF Design Technique Based on Berstein Polynomial Approximation,*" Submitted to IEEE Transactions on ASSP, June 1991.

[64] A.N. Akansu, and Y. Liu, "*On Signal Decomposition Techniques,*" Optical Engineering, pp. 912-920, July 1991.

[65] A.N. Akansu, H. Caglar, and Y. Liu, "*An Objective Performance Measure in Multiresolution Signal decomposition,*" Submitted to IEEE Trans. on Signal Processing.

[66] T. Kronader, "*Some Aspects of Perception Based Image Coding,*" Ph.D Thesis, Lipkoping University, 1989.

[67] F. Mintzer and B. Liu "*Aliasing Error in the Design of Multirate Filters'*" IEEE Trans. on ASSP, Vol.26 No.1, pp.76-88, Feb. 1978.

[68] H. Caglar, Y. Liu, and A. N. Akansu, "Optimal PR-QMF Design for Subband Image Coding," Submitted to Journal of Visual Communication and Image Representation, Sept. 1991.

[69] T. Caelli, and M. Hubner, "Coding Images in the Frequency Domain: Filter Design and Energy Processing Characteristics of the Human Visual System," IEEE Trans. on Systems, Man and Cybernetics, pp. 1018-1021, May 1980.

[70] R.J. Clarke, "Transform Coding of Images," London Academic Press, 1985.

APPROVAL SHEET

Title of Thesis: A Generalized, Parametric PR-QMF/Wavelet Transform
Design Approach for Multiresolution Signal Decomposition

Name of Candidate: Hakan Çağlar
Doctor of Philosophy, 1991

Thesis and Abstract Approved:_____Date _____
Dr. Ali N. Akansu
Assistant Professor
Department of Electrical and Computer Engineering

Signature of other members _____Date _____
of the thesis committee. Dr. Rashid Ansari
Bell Communications Research
Morristown, New Jersey

_____Date _____
Dr. Yeheskel Bar-Ness
Professor
Department of Electrical and Computer Engineering

_____Date _____
Dr. Erdal Panayırcı
Professor
Department of Electrical and Computer Engineering

_____Date _____

Dr. John Tavantzis
Professor
Mathematics Department

Hakan Çağlar

Objective: To obtain a tenure track academic position in the fields of Digital Signal Processing, Communications, and Digital Control.

Education: Ph.D. in Electrical Engineering, New Jersey Institute of Technology, Newark, NJ 07102 (expected graduation date: December, 1991)
Thesis Title : A Generalized, Parametric PR-QMF/Wavelet Transform Design Approach for Multiresolution Signal Decomposition.
Thesis Advisor : Prof. A. N. Akansu

M.S. in Electrical Engineering, Polytechnic University, Brooklyn, NY, 11201, January 1988.

B.S. in Electrical Engineering, Technical University of Istanbul, Turkey, June 1984.

Experience: January 1991 - Present: Instructor, New Jersey Institute of Technology, Newark, NJ, Teaching Undergraduate level Digital Signal Processing and Communications Courses.
January 1991 - Present: Co-Advisor, New Jersey Institute of Technology, Newark, NJ, guiding one M.S. level and two undergraduate senior projects in hardware implementation of few novel signal processing algoritms, Wavelet filters, on Texas Instruments TMS320C25 chip.
January 1989 - Present: Research Fellow, New Jersey Institute of Technology, Newark, NJ, performed research for several projects on Signal Decomposition Techniques, Wavelet Transforms, and Video Coding Techniques.
Jan.1988 - Jan. 1989: Teaching Fellow, New Jersey Institute of Technology, Newark, NJ, teaching undergraduate laboratory courses in Automatic Control.

Computer and Hardware skills: Languages : Fortran, C, Pascal, Motorola MC68000 family, Intel 8085-86, TI-TMS320 chips.
Operating systems : Unix, VAX/VMS, MS-DOS

Scholarships-Awards: Awarded for advanced studies in the US by the Turkish Paper Co. after a nationwide competitive examination.

Scholarships-Awards: Awarded for advanced studies in the US by the Turkish Paper Co. after a nationwide competitive examination.

Publications and Presentations:

- A. N. Akansu, R. A. Haddad, and H. Caglar, "Binomial QMF-Wavelet Transform for Image Coding," NSF/CBMS Conference on Wavelets, University of Lowell, MA, June 1990, Presentation only.
- A. N. Akansu, R. A. Haddad, and H. Caglar, "Binomial QMF-Wavelet Transform," IEEE, DSP workshop, pp. 6.10.1-2, Sept. 1990.
- A. N. Akansu, R. A. Haddad, and H. Caglar "Perfect Reconstruction Binomial QMF-Wavelet Transform," SPIE Visual Communications and Image Processing, Lausanne, Procedings Sept. 1990.
- A. N. Akansu, R. Haddad, H. Caglar " Binomial QMF-Wavelet Transform For Multiresolution Signal Decomposition," Submitted to IEEE Transactions on ASSP, May 1990.
- H. Caglar and A. N. Akansu, 'Generalized, Parametric PR-QMF Design Technique Based on Berstein Polynomial Approximation," Submitted to IEEE Transactions on Information Theory (special issue on Multiresolution Signal Representation/Wavelet Transforms), Jan. 1991.
- H. Caglar, Y. Liu, and A. N. Akansu, " Statistically Optimized PR-QMF Design," SPIE Visual Communications and Image Processing, Boston, November 1991, (to be presented).
- H. Caglar, A. N. Akansu, " A New Regular PR-QMF Design Technique," Submitted to IEEE Globecom, 1991.

References:

- Prof. A. N. Akansu, New Jersey Institute of Technology, Electrical and Computer Engineering Dept. Newark, NJ 07102.
  Tel: 201-596 5650
- Prof. R. A. Haddad, Polytechnic Universty, School of Electrical Engineering and Computer Science, Hawthorne, NY, 10532
  Tel: 914-347 6940
- Prof. Y. Bar-Ness, New Jersey Institute of Technology, Electrical and Computer Engineering Dept., Newark, NJ 07102.
  Tel: 201-596 3520
- Prof. E. Cohen, New Jersey Institute of Technology, Electrical and Computer Engineering Dept., Newark, NJ 07102.
  Tel: 201-596 3513
- Prof. E. Panayirci, New Jersey Institute of Technology, Electrical and Computer Engineering Dept., Newark, NJ 07102.
  Tel: 201-596 2440

Hakan Çağlar
NJIT, ECE Dept.
University Heights
Newark, NJ 07102 USA
Office: (201) 596 5659
email: hakan@faraday.njit.edu

3-Ekim-1991

Boğaziçi Üniversitesi, Elektrik Fakültesi Dekanlığına,

Doktara çalışmamı Aralık-1991 tarihinde tamamlayarak Boğaziçi Üniversitesi, Elektrik Fakültesine öğretim üyesi olarak Ocak-1992'den itibaren katılma arzusundayım.

Doktora çalışmam sayısal işaret işlemesi, kodlaması ve bunların görüntülü haberleşmeye uygulanması dallarında olup, özellikle video uygulamalarına ağırlık verilmektedir. Yaptığımız teorik çalışmaların başlıca uygulama alanları Sayısal TV, Video Kodek Dizaynı, Video-Telefon, ve Telekonferans konularında geniş olarak görülmektedir. Özgeçmişimi ve araştırma konularımla ilgili açıklamayı ilişikte ilginize sunuyorum.

1416 Sayılı kanuna göre Amerika Birleşik Devletlerine resmi burslu öğrenci olarak SEKA kurumu adına lisans üstü öğrenimi yapmak üzere 1985 yılında gönderildim. Burslu öğrenimime karşılık olan mecburi hizmet yükümlülüğümü Boğaziçi Üniversitesinde yerine getirmek arzusundayım.

Boğaziçi Üniversitesi, Elektrik Fakültesine yaptığım başvuru ile ilgili gerekli işlemlerin yapılmasını ve ayrıca üniversitenizin bursun devri işlemi konusundaki yaklaşımının tarafıma bildirilmesini arz ederim.

İlgileriniz için şimdiden teşekkür eder saygılarımı sunarım.

Hakan Çağlar